Dark Energy with Large-scale Inhomogeneities

Yue Nan

Supervisor :
Prof. Yasufumi Kojima

Department of Physical Science, Graduate School of Science,
Hiroshima University,
Higashi-Hiroshima 739-8526, Japan

Abstract

The successful standard ΛCDM model of cosmology takes several assumptions, and one of them is the cosmological principle assuming homogeneity and isotropy of the universe on large scales. Nevertheless, there are anomalies in large-scale observations, such as the low multipole anomalies in the cosmic microwave background (CMB) temperature power spectrum, implying possible phenomena breaking the cosmological principle.

In this thesis, models for dark energy with large-scale inhomogeneities are investigated based on ultralight-mass scalar fields to illuminate the nature of dark energy potentially related to these anomalies. Slightly breaking the cosmological principle, these models for dark energy can be implemented with ultralight scalar fields, which also relate the interests of this study to the axion-like particles (ALPs) predicted in the string landscape.

First, a dark energy model with nearly "frozen" dynamics and small spatial inhomogeneities is presented as a heuristic example. This is a specific model requiring a particular open inflationary scenario associated with the Coleman-De Luccia quantum tunneling. A canonical ultralight scalar field ϕ minimally coupled with the tunneling inflaton Ψ may possibly leave discrete non-normalizable modes as residual effects on the present open universe. These are superhorizon modes that fluctuate on scales far beyond the curvature scale and evolve most slowly in time, named supercurvature modes. The frozen expectation value of the supercurvature modes of ϕ observed within the present horizon can be interpreted as the dark energy density, with small spatial inhomogeneities sourced by quantum fluctuations predicted; this is the named the supercurvature-mode dark energy (ScmDE).

ScmDE setup for the inhomogeneous dark energy requires specific initial conditions associated with a particular inflationary scenario. The scope of application and the ability of prediction are also restricted by the random Gaussian field handling for ScmDE inhomogeneities. Hence, as a generalization to the ScmDE model, a general formulation for dynamical dark energy model with large-scale inhomogeneities sourced by a scalar field follows. By handling the dark energy inhomogeneities as cosmological perturbations on superhorizon scales on a flat universe background, the equations governing their evolution with the background are derived, following which predictions for the expansion rate and the dark energy equation of state (EoS) can be obtained under different model parameters subsequently.

The models with inhomogeneneous dynamical dark energy predict unique characteristic imprints on observations, such as contributions to CMB anisotropies through the late-time integrated Sachs-Wolfe (ISW) effect. Using the observational data of the CMB, constraints on the amplitudes of the perturbations related to model parameters are obtained. Further, as another example of the model application, possible corrections to the measurements of luminosity distance associated with light propagation with inhomogeneous dark energy is estimated utilizing the obtained constraints. The model predictions are potentially to be constrained tighter or falsified by current and future projects focusing on dark energy, such as Subaru PFS, DES, DESI, Euclid, RST, LSST-DESC, etc., together with increasing understandings of the systematics in cosmological observation.

This thesis is mainly based on the following publications/manuscripts:

- *Large-scale inhomogeneity of dark energy produced in the ancestor vacuum*
  Y. Nan, K. Yamamoto, H. Aoki, S. Iso, and D. Yamauchi
  Phys. Rev. D **99**, 103512 (2019)

- *Dark energy model with very large-scale inhomogeneity*
  Y. Nan and K. Yamamoto
  Submitted to Phys. Rev. D, under review (submission No. DD13014)

Acknowledgments

Firstly, I am sincerely grateful to my research supervisor, Professor Yasufumi Kojima, for his patient and kind guidance throughout the study and production upon this thesis. In the same time, I should never forget to thank Professor Kazuhiro Yamamoto at Kyushu University, the main collaborator of this research, whose academic instructions for me and inspirations shared with me are the essential cornerstones leading to the accomplishment of this thesis.

Secondly, I want to express my gratitude for Associate Professor Nobuhiro Okabe, not only for his guidance, but also for his perspective comments and innovative suggestions on my work. Assistant Professor Shota Kisaka also gave me beneficial advice in the methodology of presenting ideas and organizing information.

Special thanks go to all other researchers I have been working with in collaborations and academic discussions, for their contributions, helps, and insightful comments. Appreciations to all other former and present fellows in the research group shouldn't be left out, for their wits in the discussions and kindness in the daily life. Also, special appreciations ought to be paid to the Japan Society for the Promotion of Science (JSPS), as part of the research was supported by the DC2 program of the Research Fellowships for Young Scientists from JSPS.

Finally, I owe a debt of gratitude to my parents in my hometown Wuhan, and Jing Yang in Shijiazhuang, China, for their continuous understandings and persistent supports for me throughout my research and life. Especially, it is never easy to cope with all difficulties that one may face against the harsh winds of the COVID-19 pandemic. Nevertheless, I want to sincerely express that, in the vastness of space and the immensity of time, it is my pleasure to encounter all of you, and share a planet and an epoch with all of you.

Without all the help, support, and encouragement from all of you, the accomplishment of this thesis would not ever be possible.

Contents

List of Figures

List of Tables

1 Background

1.1 Introduction and motivation

With the successful applications of Einstein's theory of general relativity (GR) in cosmology in the past century, our knowledge of the universe has flourished as a productive outcome of the interplay between theories and observations. The acceleration in the cosmic expansion is one of the most intriguing puzzles observed in the past decades. The observations on the redshifts of the distant Type Ia supernovae implied the existence of an unknown repulsive effect, which is supposed to have accelerated the expansion of the universe in relatively late cosmological times [1, 2, 3, 4, 5]. Otherwise, the fact would possibly suggest the breakdown of GR on cosmological scales.

Nowadays, a well-accepted translation for the phenomena is that a component with potentially exotic properties, which is usually named the *dark energy*, dominates the expansion of the current universe. As the simplest and the most common model to explain the acceleration in expansion, dark energy as a negative pressure component whose equation of state (EoS) yields $w = p/\rho \simeq -1$ survives the tests from extensive observations as mentioned previously. Dark energy, which behaves in a similar way to the cosmological constant Λ hence is usually denoted by Λ, has become an essential content for standard cosmology to account for different observational results, such as the aforementioned accelerated expansion, the growth of fluctuations in matter distribution, the turnover scale of the matter power spectrum and so on since the late 1990s. In the age of precision cosmology in recent decades, the early analyses from supernovae were followed and enhanced by many consistent efforts from different observations, for instance, the galaxy clusters [6, 7], the large-scale structure (LSS) surveys [8, 9], the cosmic microwave background (CMB) with baryon acoustic oscillations (BAO) [10, 11, 12], the weak gravitational lensing shear [13, 14], as well as different aspects combined [7, 9, 14, 15, 16, 17].

In the standard cosmological model today, the density parameter Ω_i for a certain component of the universe denoted by "i" is widely adopted, which is defined as the ratio of the energy density of that component to the critical density for a flat universe at the present epoch. Recent observations suggest that the density parameter for dark energy yields $\Omega_\Lambda \sim 0.7$; in other words, Λ standing for the dark energy consists of about 70% of the total energy density in the universe. The matter component of total energy density is observed with $\Omega_m \sim 0.3$, and the contribution from radiation and curvature, Ω_r and Ω_K respectively, are negligible today. Within the matter

component Ω_m, only about 15% of the matter is in form of the ordinary baryonic matter denoted by Ω_b, and the left is composed of some unknown form of matter as the *cold dark matter* (CDM) [17]. Hence, this standard paradigm is often named the ΛCDM model.

Historically, the theoretical interest for cosmological constant Λ related to dark energy has been long. The early idea may trace back to Einstein's cosmological constant Λ to formulate a static universe. After discovering cosmic expansion in the early 20th century [18] suggesting a dynamical universe, the necessity of Λ seemed to have once become doubtful. However, even after the big-bang thermal history with an adiabatic expansion for the universe became a standard picture in cosmology, theoretical interests on Λ persisted. The developments in quantum field theories and cosmology had followed this interest on Λ, especially in lines such as vacuum energy and inflation, where theoretical frameworks had already been widely discussed.

The cosmological constant Λ revived when the community realized that observations addressed previously do not favour matter-dominant spatially flat Einstein-de Sitter model ($\Omega_m = 1$) for the universe, with $\Omega_m < 1$ constrained at relatively high confidence level. However, the fact that $\Omega_m \sim 0.3$ and $\Omega_\Lambda \sim 0.7$ also gave rise to the famous *cosmological constant problem* (CCP). There are different ways to make the statement of the problem, but one can briefly summarize two aspects potentially partly related to each other for CCP [19, 20]:

- *Vacuum energy problem* ("why so small"). As a natural realization of negative pressure for cosmological Λ-like dark energy, the naive estimation for total energies of vacuum fluctuations of quantum fields $\rho_{QFT} \sim 10^{71}\mathrm{GeV}^4$ deviates the observed dark energy density $\rho_{\Lambda 0} \sim 10^{-47}\mathrm{GeV}^4$ at about 120 orders of magnitudes, which is unnatural and extraordinary.

- *Coincidence problem* ("why now"). Present observed density for matter ρ_{m0} and dark energy $\rho_{\Lambda 0}$ yields $\rho_{m0}/\rho_{\Lambda 0} = \Omega_m/\Omega_\Lambda \sim \mathcal{O}(1)$. While ρ_Λ is generally considered nearly constant, ρ_m scales with the scale factor a of the universe as $\rho_m \propto a^{-3}$, and $\rho_m/\rho_\Lambda \sim \mathcal{O}(1)$ seems to have just taken place around $a \gtrsim 0.5$ with $a_0 \equiv 1$ for the present epoch. We seem to be coincidentally living in an epoch where the dark energy just began to show its importance *recently*.

In Sec. 2.1 more details will be addressed on this topic. Related to the CCP, either the possible break down of GR on cosmological scales, or the discrepancies between the predictions of quantum field theories against observed

expectations values, or some unknown material nature of dark energy, all these facts hopefully hints towards unknown new physical laws beneath the phenomena of dark energy.

Moreover, as $\rho_m \propto a^{-3}$ for the matter and $\rho_r \propto a^{-4}$ for the energy density of the radiation component, if $\rho_\Lambda \simeq$ const. a future de Sitter expansion for the universe is implied which behaves similarly to the primordial inflationary phase on totally different time and energy scale. As a result, dark energy is supposed to be vital for the evolution of the universe, especially in late times and in the future.

The answers to these problems are presumably related to the origin and nature of dark energy, which are of great interest to explore to understand the evolutionary history and the future fate of our universe.

Different theoretical models for the nature of dark energy have been proposed and discussed [19, 20]. Within them dynamical models for dark energy are very interesting [21, 22, 23, 24, 25, 26, 27, 28], which are related to the field theory associated with the primordial high-energy epoch of the universe, and other fields of interests for theoretical physics [19, 20, 29]. Particularly interesting ones are the dynamical models formulated on the basis of the quantum fluctuations from ultralight scalar fields, [22, 23, 24, 25, 26, 27, 28]; the ultralight scalar fields are expected in the string landscape [30, 31, 32, 33, 34, 35, 36], also revealing an interesting connection to the strong CP problem in the context of axion-like particles. As was addressed previously, in the parametrization of the ΛCDM model, in general models, dark energy has been considered as homogeneous, hence also isotropic when observed, most widely considered as the cosmological constant Λ with the EoS $w = -1$ following the cosmological principle. Nevertheless, since the late-time expansion of the universe is dominated by dark energy, some interesting outcomes may occur to affect cosmological observables if large-scale inhomogeneities and variable EoS arise for dark energy, which are expected to be tested by various observations [29, 37, 38, 39, 40, 41].

Additionally, in recent CMB observations, low multipole alignments corresponding to large angular scales of the CMB has been drawing attention [42, 43]. For example, among the low CMB multipoles, the dipole anomaly, sometimes phrased as the *hemispherical power asymmetry*, has long been a controversial topic related to the assumed CMB rest frame, while the accurate measurements on the dipole are sabotaged by the cosmic variance from various limitations on our ability for observations, such as the mere observing location near the earth at the present epoch. The general interpretation for the CMB dipole is to attribute the phenomenon to the peculiar motions towards an

assumed CMB rest frame where the hemispherical asymmetry is eliminated, sometimes interpreted as a dragging towards the Great Attractor in a celestial region, and at least part of the peculiar motions is interpreted as the evidence of gravitational bounding [44, 45]. However, these interpretations generally assume homogeneous dark energy background. Thanks to the improvements in observational instruments and analysis methods, our knowledge of the local environments of observations and the systematic errors is growing. If CMB dipole anomaly survive the cosmic variance after removing contributions from peculiar motions and other known effects, there remains the possibility for a physical origin of the anomaly, potentially as a clue for the physics beyond the standard cosmological model for dark energy. In the same time, a recent research on X-ray luminosity-temperature relation of the galaxy cluster over the sky seems to indicate anisotropy in the expansion rate of the universe [46]. Although there have been other alternatives to the explanation of these problems (e.g., Refs. [47, 48]), one motivation in this research is to propose that a dark energy model with large-scale inhomogeneities may serve as a possible solution.

Another intriguing problem of the cosmology today is the so-called Hubble tension problem. This tension has also been attracting attention along with the improved observations in the recent decade [49]. To brief, the present expansion rate H_0 locally measured from distance ladders calibrated by standard candles such as Type Ia supernovae [50], and the H_0 inferred from the CMB statistics with the physical sound horizon scale $r_s(\eta_d)$ at the epoch of photon decoupling as a standard ruler [51, 17] have shown nontrivial deviations from each other at a confidence level of 4σ–6σ. There have been many attempts to ease or explain this tension, and among them the possibility of new physics concerning dark energy beyond the standard ΛCDM breaking the cosmological principle exists [52].

Innovated by a previous work [53], the motivation of this research follows these veins. This thesis elaborate an attempt to shed light upon the previous problems potentially related to dark energy, by introducing inhomogeneities in dark energy model that breaks the cosmological principle on very large scales.

1.2 The structure of the thesis

Part of this thesis is based on a published paper as Ref. [54], where the authors introduced the large-scale inhomogeneities of the dark energy by handling them as the stochastic fluctuations, and the dark energy was the residual effect of some ultralight scalar field in an open universe associated with a specific inflationary scenario. Additionally

in this thesis, the development on the generalized dynamical model for dark energy with the large-scale fluctuations are presented based on a general scalar field ϕ, by handling them as cosmological perturbations to the metric analytically. These fluctuations will be translated into large-scale spatial inhomogeneities and time-dependent dark energy EoS in the evolution of the universe, which may introduce some observable effects on the anisotropies of the cosmological observations to address on the problems concerning dark energy property mentioned previously.

The remaining parts of this thesis are organized as follows. In Chapter 2, firstly, a review on the basic aspects for the ΛCDM model to characterized the background expansion, as well as the fundamental cosmological setups for dark energy in this framework. Then a brief review on dark energy by canonical scalar fields follows as an example of the implementation of general dynamical dark energy models, or quintessence models. Subsequently, as an modification to the quintessence models, a heuristic setup to implement an inhomogeneous dark energy model is addressed. Motivated by the ultralight scalar fields in the string landscape associated with open inflation. To qualitatively specify, the source of dark energy is interpreted as the the discrete mode of a ultralight scalar field in an almost flat open universe, named the supercurvature modes. The supercurvature modes of the ultralight scalar field fluctuates on superhorizon scales much larger than the curvature scale, so the associated dark energy is observed as almost "frozen" within the observable universe with mild large-scale spatial inhomogeneities. This model will be referred to as the supercurvature-mode dark energy (ScmDE) in the following parts.

Following on the heuristic setup of ScmDE, in Chapter 3, quantitative formulations for large-scale spatial inhomogeneities is considered by the Gaussian random field handling with "frozen" dynamics. Then, to extend the scope of application and ability of prediction from the inhomogeneities of the dark energy, a formulation for the inhomogeneities of dark energy is elaborated quantitatively, both from the view of stochastic fluctuations, and the view of cosmological perturbation on superhorizon scales.

In Chapter 4, the initial conditions and analytic approximation for the formulations will be considered to perform numerical evaluation on the dark energy inhomogeneities from the models formulated by Chapter 3. Subsequently, these numerical evaluation of the late-time evolution of the dark energy are presented showing characteristic behaviors of the background evolution and the perturbations of the systems. By calculating the imprints of these inhomogeneities on the CMB anisotropies, the constraints from observation are obtained with numerical solutions

under different model parameters. As the application of the generalized analytical formulation for inhomogeneities as superhorizon perturbations, the possible effect on luminosity distance measurements is evaluated.

Discussions on the results and conclusions drew from the model will follow in Chapter 5. Finally, miscellaneous technical details will be attached as the appendices.

2 The supercurvature-mode dark energy from ultralight scalar fields

The observations on CMB by experiments such as WMAP and Planck found that the order of the perturbations to the homogeneous background $\mathcal{O}(10^{-5})$, hence suggesting that the cosmological principle assuming a homogeneous background may only be violated to a slight extent in our universe. In order to formulated for the dark energy model with slight inhomogeneities allowed by observations, let us first start with a brief review on the background evolution and the accelerated expansion within the standard ΛCDM model framework.

2.1 A brief review on background expansion with standard cosmological model

One may adopt the natural unit convention of physical constants, where the velocity of light c, the reduced Planck constant $\hbar$, and the Boltzmann constant k_B are defined as unity reading

$$c = \hbar = k_B \equiv 1, \tag{2.1}$$

and take $(-,+,+,+)$ signature convention for the spacetime metric. Starting from the Hilbert-Einstein action with cosmological constant Λ and matter field $\mathcal{L}_M$

$$S = \int d^4x\sqrt{-g}\left[\frac{1}{16\pi G}(\mathcal{R} - 2\Lambda) + \mathcal{L}_M\right], \tag{2.2}$$

where $g \equiv det(g_{\mu\nu})$ is the determinant of the metric tensor $g_{\mu\nu}$, G is the Newton's gravitational constant, $\mathcal{R} \equiv g^{\mu\nu}R_{\mu\nu} = R^{\mu}{}_{\mu}$ is the Ricci scalar with $R_{\mu\nu}$ the Ricci tensor.

Operating the action variation principle $\delta S = 0$ on Eq. (2.2) will lead to the Einstein equation

$$R_{\mu\nu} - \frac{1}{2}\mathcal{R}g_{\mu\nu} + \Lambda g_{\mu\nu} = 8\pi G T_{\mu\nu}. \tag{2.3}$$

Here, $T_{\mu\nu}$ is the energy-momentum tensor (EMT) for the matter field source given schematically as

$$T_{\mu\nu} \equiv \mathcal{L}_M g_{\mu\nu} - 2\frac{\delta\mathcal{L}_M}{\delta g_{\mu\nu}}. \tag{2.4}$$

Following the cosmological principle that assumes a homogeneous and isotropic background universe, the line

element of the famous Friedmann-Lemaitre-Robertson-Walker (FLRW) metric reads

$$\begin{aligned} ds^2 &= g_{\mu\nu}dx^\mu dx^\nu \\ &= -dt^2 + a^2(t)\left(\frac{dr^2}{1-Kr^2} + r^2 d\Omega^2\right), \end{aligned} \tag{2.5}$$

with t representing the cosmic time, and K is the sign of shape for curvature, taking value from {-1,0,+1} for open, flat, closed universe respectively. In the comoving spherical coordinates (r, θ, ϕ), the element of solid angle writes

$$d\Omega^2 = d\theta^2 + \sin^2\theta d\phi^2. \tag{2.6}$$

$a(t)$ in Eq. (2.5) is the scale factor of the universe as a function of time characterizing the evolutionary history of the cosmic expansion. Observationally, with the existence of the cosmic expansion characterized by $a(t)$, the photons from distant objects receding from us will be observed with stretched wavelengths when received compared with when emitted. This wavelength stretch, as the cosmological version of the Doppler effect, is associated with a cosmological redshift z due to the cosmic expansion as

$$a(t) = \frac{1}{1+z} = \frac{\lambda_{\text{emit}}}{\lambda_{\text{obs}}}. \tag{2.7}$$

As a convention, the scale factor the of present epoch is defined as unity $a_0 \equiv 1$.

Now let us consider the geometry of the spacetime on the left hand side of Eq. (2.3). The Riemann tensor is defined as

$$R^\alpha_{\beta\mu\nu} = \partial_\mu\Gamma^\alpha_{\nu\beta} - \partial_\nu\Gamma^\alpha_{\mu\beta} + \Gamma^\alpha_{\mu\lambda}\Gamma^\lambda_{\nu\beta} - \Gamma^\alpha_{\nu\lambda}\Gamma^\lambda_{\mu\beta}, \tag{2.8}$$

with the metric connection, the Christoffel symbol written as

$$\Gamma^\alpha_{\mu\nu} = \frac{1}{2}g^{\alpha\beta}\left(\partial_\mu g_{\nu\beta} + \partial_\nu g_{\mu\beta} - \partial_\beta g_{\mu\nu}\right), \tag{2.9}$$

where the Einstein summation convention for summation over a same indice is already reposed. Given the metric in Eq. (2.5), the Ricci tensor and Ricci scalar can be consequently derived from tensor contraction

$$R_{\mu\nu} = R^\alpha_{\mu\alpha\nu}, \tag{2.10}$$

$$\mathcal{R} = g^{\mu\nu}R_{\mu\nu}. \tag{2.11}$$

The EMT $T_{\mu\nu}$ is specifically determined by the constituents of the universe. The perfect fluid treatment for energy components of the universe is a standard approach with the energy density ρ and pressure p related as

$$T_{\mu\nu} = (p+\rho)u_\mu u_\nu + p g_{\mu\nu}, \tag{2.12}$$

where the four velocity for the fluid yields $u^\mu u_\mu \equiv -1$. For the homogeneous background, this explictly leads to

$$T^\mu{}_\nu = \begin{pmatrix} -\rho & 0 & 0 & 0 \\ 0 & p & 0 & 0 \\ 0 & 0 & p & 0 \\ 0 & 0 & 0 & p \end{pmatrix}. \tag{2.13}$$

The definition for the EoS w (w_i) of a fluid (component "i") follows as

$$w_{(i)} = p_{(i)}/\rho_{(i)}. \tag{2.14}$$

For non-relativistic dust-like matter fluid, $p_m = 0$ hence $w_m = 0$, while for relativistic radiation $w_r = 1/3$.

With previous definition of the EMT tensor, the local conservation law associated with the geometry of the spacetime consequently writes

$$\nabla_\mu T^\mu{}_\nu \equiv \frac{\partial T^\mu{}_\nu}{\partial x^\nu} + \Gamma^\mu_{\alpha\mu} T^\alpha{}_\nu - \Gamma^\alpha_{\nu\mu} T^\mu{}_\alpha = 0. \tag{2.15}$$

Using Eq. (2.13) one can see the conservation law in the expanding background universe is

$$\frac{\partial \rho}{\partial t} + 3\frac{1}{a}\frac{\mathrm{d}a}{\mathrm{d}t}(\rho + p) = 0. \tag{2.16}$$

Now, with the right-hand side of the Einstein equation, Eq. (2.3), known in Eq. (2.12), the Friedmann equations characterizing the expansion of the universe can be reduced from the (0,0) component and the (i,i) component as below

$$\left(\frac{1}{a}\frac{\mathrm{d}a}{\mathrm{d}t}\right)^2 + \frac{K}{a^2} = \frac{8\pi G}{3}\rho + \frac{\Lambda}{3}, \tag{2.17}$$

$$\frac{1}{a}\frac{\mathrm{d}^2 a}{\mathrm{d}\,t^2} = -\frac{4\pi G}{3}\Big(\rho + 3p\Big) + \frac{\Lambda}{3}. \tag{2.18}$$

Eq. (2.17) characterize the evolution of the expansion rate of $a(t)$, while Eq. (2.18) describe the change rate in expansion rate of $a(t)$, as a function of proper time t. Though solutions of the Friedmann equations describes the dynamics of scale factor $a(t)$ and the evolution of the background, there are crucial cosmological parameters whose values can only be obtained from actual observations to fully determine the details of the predictions from the equations.

Conventionally, it is convenient to define the Hubble parameter for the expansion rate from the scale factor a of the universe as

$$H(t) \equiv \frac{1}{a}\frac{\mathrm{d}a}{\mathrm{d}t}. \tag{2.19}$$

As another convention, with the dimensionless cosmological parameter h, the current expansion rate, Hubble constant of the local present universe is defined as

$$\begin{aligned} H_0 &\equiv H(a=1) \\ &= 100h \quad \mathrm{km/s} \quad \mathrm{Mpc}^{-1}. \end{aligned} \tag{2.20}$$

In a universe without curvature component, the energy density exactly equal to the critical density ρ_{cr} to create a flat universe is known as

$$\rho_{cr} = \frac{3H_0^2}{8\pi G}, \tag{2.21}$$

which can be derived from the Friedmann equations and FLRW metric with curvature taken into consideration. It is also conventional to define the dimensionless density parameters in present epoch for different components of the universe as

$$\Omega_i \equiv \frac{\rho_{i,0}}{\rho_{cr}}, \tag{2.22}$$

$$\Omega_K \equiv -\frac{K}{H_0^2}, \tag{2.23}$$

where subscripts $i = m, r, \Lambda$ represents the different components, typically labelled as matter (including baryonic matter and dark matter), radiation, dark energy respectively, and K stands for the spatial curvature. Following the definition

$$\Omega_m + \Omega_r + \Omega_\Lambda + \Omega_K = 1 \tag{2.24}$$

generally holds. Notice that for the dark energy,

$$\rho_\Lambda \equiv \frac{\Lambda}{8\pi G} \tag{2.25}$$

is defined. On the other hand, looking back at Eq. (2.16) one can see that, for a component of a constant value Λ corresponding to a constant energy density ρ_Λ in the background, $\partial\rho_\Lambda/\partial t = 0$ leads to

$$3H(\rho_\Lambda + p_\Lambda) = 3H(1 + w_\Lambda) = 0. \tag{2.26}$$

The result is identical to the statement that a Λ-like dark energy component behaves as some unknown form of *negative pressure* as $p_\Lambda = -\rho_\Lambda$, whose EoS yields $w_\Lambda = -1$.

In the expanding universe, using subscript 0 to represents for today, from Friedmann equation Eq.(2.17) one can derive

$$H^2 = H_0^2\Big(\Omega_m a^{-3} + \Omega_\Lambda + \Omega_r a^{-4} + \Omega_K a^{-2}\Big). \tag{2.27}$$

Inserting parameters Ω_m, Ω_r, Ω_K and Ω_Λ calibrated by observations in Eq.(2.27), one can figure out the solution of scale factor a with respect to time t, hence the evolution of the background universe is basically determined. The Ω_Λ component corresponding to the cosmological constant Λ in Eq. (2.17) and Eq. (2.18) is then responsible for the explanation of the recent accelerated expansion found by observations, alternatively referred to as the dark energy.

To see this one may define the deceleration parameter q of cosmic expansion from Eq. (2.17) and (2.18) as

$$\begin{aligned} q &\equiv -\left(a\frac{\mathrm{d}^2 a}{\mathrm{d}t^2}\right) / \left(\frac{\mathrm{d}a}{\mathrm{d}t}\right)^2 \\ &= -\left(1 + \frac{1}{H^2}\frac{\mathrm{d}H}{\mathrm{d}t}\right) \\ &= \frac{\Omega_m a^{-3} - 2\Omega_\Lambda + 2\Omega_r a^{-4}}{2(\Omega_m a^{-3} + \Omega_r a^{-4} + \Omega_K a^{-2} + \Omega_\Lambda)}. \end{aligned} \tag{2.28}$$

Subsequently, the deceleration parameter q_0 for the present epoch when $a = a_0 \equiv 1$ is

$$q_0 = \frac{\Omega_m}{2} + \Omega_r - \Omega_\Lambda, \tag{2.29}$$

where condition Eq. (2.24) was understood. Note that a positive q suggest the deceleration in expansion, while a negative q indicates the acceleration in expansion. The sign of the Ω_Λ term in the right-hand sides of Eq. (2.29)

(or similarly, that of Λ term in Eq. (2.18)) implies although radiation with EoS $w_r = 1/3$ and matter with EoS $w_m = 0$ will eventually decelerate the expansion of the universe by decrease Hubble parameter H, the existence of a positive cosmological constant Λ may serve as the source of the acceleration in late-time expansion rate found by observations on Type Ia supernovae, which was also the motivation for reviving Λ in cosmology as a widely-accepted candidate for dark energy.

It is worth mentioning that, due to recent observations, the Ω_r for radiation is estimated to be generally negligible for the late-time expansion as $\Omega_r = \Omega_m a_{\rm eq} \sim \mathcal{O}(10^{-4})$, where $a_{\rm eq} \sim (1/3600)$ is the epoch of matter-radiation equality in the sense of energy density; on the other hand, the curvature component of the observable universe is also constrained to be small as $\Omega_K \lesssim \mathcal{O}(10^{-2})$ [17]. Following this, since the epoch of matter domination, especially in the late epochs when dark energy is believed to have become important for cosmic expansion, the parameterized Friedmann equation for expansion rate, i.e., Eq. (2.27), can usually be estimated as

$$\begin{aligned} H^2 &\simeq H_0^2\Big(\Omega_m a^{-3} + \Omega_\Lambda\Big) \\ &= H_0^2\Big(\Omega_m a^{-3} + 1 - \Omega_m\Big). \end{aligned} \tag{2.30}$$

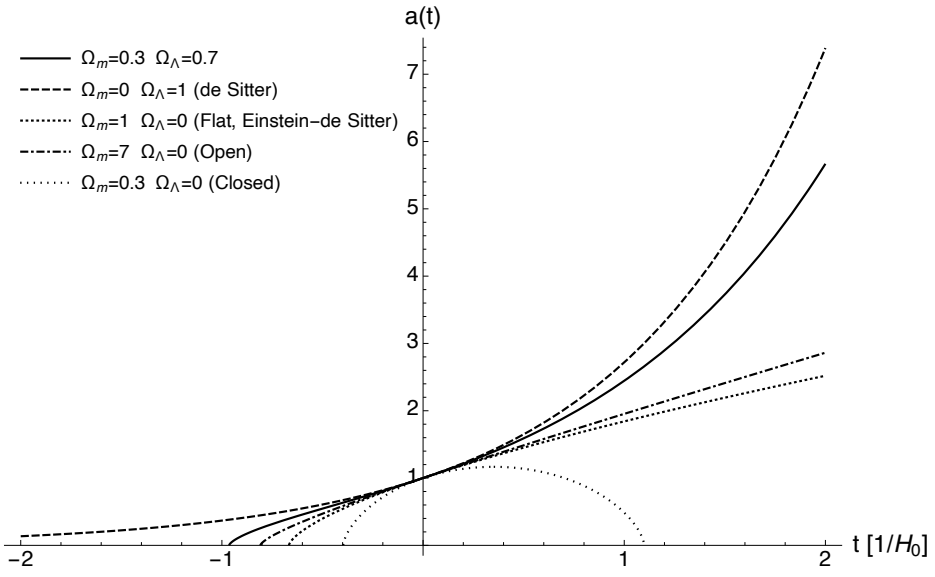

Figure 1: The evolution of the universe determined by solutions of Eq. (2.27) with different sets of cosmological parameters, where $\Omega_m = 0.3$, $\Omega_\Lambda = 0.7$ is a close approximation to the observable universe. Cosmic time $t = 0$ represents for today, and $t < 0$ is the "lookback" time representing for the history, and $t > 0$ stands for the future. In these solutions, the scale factor a of universe today follows the convention $a(0) = a_0 = 1$ with expansion rate today $H(a_0)$ set universally as the Hubble constant H_0.

As for the initial conditions of the background solution, generally a inflationary model is attached to the early universe before adiabatic expansion of the background. This inflationary scenario is to explain why the universe observed appears so homogeneous, even for regions with so large separations in the sky, that it seems causal interactions propagating lower than light speed should not have allowed these regions to "communicate" or interact with each other in order to keep them in similar states; this is sometimes phrased as the horizon problem. Inflation resolve this problem by assuming a rapid (mostly exponential) expansion in the spacetime itself in primordial universe, hence the regions greatly separated in the sky was actually causally contacted within the physical horizon in primordial universe. Also, the quantum fluctuations of the quantum fields in the inflationary epoch set seeds of the small perturbations to energy/matter distribution on the homogeneous background, later forming the structures observed in the universe today. Based on the background evolution reviewed previously, a standard approach named the standard perturbation theory can be developed to quantitatively understand the evolution of the perturbations on the homogeneous and isotropic background.

2.2 Dynamical dark energy with scalar field

Basically, it is in consensus of the community that the standard ΛCDM is a satisfactory model to describe the observable universe with several cosmological parameters calibrated from observations. But there are several concerns to address even for the background evolution, especially for the dark energy. Firstly, ΛCDM is a phenomenological parametrization both for the Λ component as dark energy and the dark matter, the knowledge of how Λ or dark energy was generated or is it natural for a cosmological constant Λ to emerge in (the action of) the universe Eq. (2.2) is still in the dark. On the other hand, as was addressed in Chapter 1, the observed energy scale of dark energy summarized as the CCP gave rise to the anthropic/coincidental concern for the observed status of the dark energy, that we seem to live in a special epoch of the universe.

Another perspective on the CCP is to look upon the energy level of the observed cosmological constant at present epoch, from dimensional analysis,

$$\epsilon_{\Lambda 0} \sim \rho_{\Lambda 0}^{1/4} \sim \mathcal{O}(10^{-3})\text{eV} \sim \mathcal{O}(1)\text{meV}. \tag{2.31}$$

This fact seems to suggest potential new physical phenomena related to the dark energy or cosmological constant at energy scale of chemical reactions, which is not likely to be true. But if the source of dark energy obeys some dynamics with ρ_Λ rolling to the zero value, the scenario will be more natural [19]. In this vein, alternative models to cosmological constant in attempts to resolve these concerns have been proposed and investigated [19, 20], and dynamical models are of natural interest to ease the CCP.

One interesting class of these solutions, is the dynamical dark energy models implemented by canonical scalar field weekly coupled to the gravitation denoted by spacetime metric, sometimes also referred to as the quintessence model [21].

The action of a canonical scalar field ϕ weakly coupled to the gravity represented by the spacetime metric $\sqrt{-g}$ can be written as

$$S_\phi = -\int d^4x\sqrt{-g}\left(\frac{1}{2}g^{\mu\nu}\partial_\mu\phi\partial_\nu\phi + V(\phi)\right) \tag{2.32}$$

in the $\{-,+,+,+\}$ notation system, sometimes also referred to as the minimal coupling model for scalar fields.

The equation of motion for the scalar field can by obtained by taking the action variation $\delta S_\phi = 0$, which reads

$$\frac{\mathrm{d}^2\phi}{\mathrm{d}t^2} + 3H\frac{\mathrm{d}\phi}{\mathrm{d}t} + \frac{\mathrm{d}V}{\mathrm{d}\phi} = 0, \tag{2.33}$$

where H is time-dependent Hubble parameter concerning the background expansion rate.

On the other hand, the EMT tensor of scalar field ϕ is defined as

$$T^{(\phi)\alpha}{}_{\beta} = g^{\alpha\nu}\frac{\partial\phi}{\partial x^\nu}\frac{\partial\phi}{\partial x^\beta} - g^{\alpha}{}_{\beta}\left[\frac{1}{2}g^{\mu\nu}\frac{\partial\phi}{\partial x^\mu}\frac{\partial\phi}{\partial x^\nu} + V(\phi)\right]. \tag{2.34}$$

where $V(\phi)$ is the potential for the field ϕ. The conservation law of the EMT tensor of the scalar field can also lead to the equation of motion identically, in a similar manner to Eq. (2.15). Inserting this EMT into the right-hand side of Einstein equations Eq. (2.3) with other cosmic components under a specific metric will give the background evolution of the field ϕ, which is associated with other species of the cosmic inventory in the expansion history. From Eq. (2.34), one can write the isotropic and homogeneous background part of the EMT for scalar field ϕ as

$$\rho_\phi = \frac{1}{2}\left(\frac{\mathrm{d}\phi}{\mathrm{d}t}\right)^2 + V(\phi), \tag{2.35}$$

$$p_\phi = \frac{1}{2}\left(\frac{\mathrm{d}\phi}{\mathrm{d}t}\right)^2 - V(\phi), \tag{2.36}$$

following which its EoS writes

$$w_\phi = \frac{p_\phi}{\rho_\phi} = \frac{(\mathrm{d}\phi/\,\mathrm{d}t)^2 - 2V(\phi)}{(\mathrm{d}\phi/\,\mathrm{d}t)^2 + 2V(\phi)}. \tag{2.37}$$

If the kinetic term $(\frac{\mathrm{d}\phi}{\mathrm{d}t})^2$ is small then in $w_\phi \simeq -1$ holds, which means ϕ behaves very similar to a cosmological constant, ϕ can be considered as the source of a dynamical dark energy.

Different classes of dynamical dark energy can be assumed by different types of scalar potential $V(\phi)$ and be constrained by observations (see Ref. [21]). However, it is worth noting that the potential $V(\phi)$ for a canonical free-field case is

$$V(\phi) = \frac{1}{2}m_\phi^2\phi^2 \tag{2.38}$$

with m_ϕ denoting the mass of the field ϕ, where there is only mass term in the potential without interacting terms. In this case, it follows Eq. (2.33) that the equation of motion for ϕ yields

$$\frac{\mathrm{d}^2\phi}{\mathrm{d}t^2} + 3H\frac{\mathrm{d}\phi}{\mathrm{d}t} + m_\phi^2\phi = 0. \tag{2.39}$$

This is the basic equation for the evolution of a scalar field ϕ in the homogeneous expanding background universe.

It would also be interesting to mention here that, the simplest inflationary models can also be implemented with a scalar field, in a similar formalism with Eq. (2.33)–(2.37), while its potential $V(\phi)$ is constrained by observations like Planck [17]. In this line, generally, the kinetic term $(\mathrm{d}\phi/\,\mathrm{d}t)^2$ is considered small as the slow-roll condition for an inflationary epoch long enough to resolve the horizon problem in observation. To see this, consider the case that universe is dominated by some form of energy density with almost constant value, whose EoS yielding $w \simeq -1$ was described in Eq. (2.26) and also in Eq. (2.37). Then the background expansion rate can be written as

$$H = \frac{1}{a}\frac{\mathrm{d}a}{\mathrm{d}t} \simeq \sqrt{\frac{\Lambda}{3}} \simeq \text{const.} \tag{2.40}$$

following Eq. (2.17). Here, if Λ is the cosmological constant, then the equality exactly holds. Following this one can easily obtain the de-Sitter exponential expansion of the scale factor $a(t)$

$$a(t) \propto \mathrm{e}^{Ht} \propto \mathrm{e}^{\sqrt{\frac{\Lambda}{3}}t} \tag{2.41}$$

assumed by general inflationary models.

2.3 The supercurvature-mode dark energy

This section will largely rely on the basis of the theoretical setup by a previous research in Ref. [53], where the so-called supercurvature-mode dark energy (ScmDE) was motivated. Additional details of the theoretical setups for review can be found in Appendix A.

Consider a scenario that our observable universe is an open universe patch created by a bubble nucleation due to the Coleman-De Luccia (CDL) quantum tunneling of a scalar field, the inflaton field ψ [55]. After the bubble nucleation, a primordial ordinary inflation occurred within the nucleated bubble, and then the big bang universe with negative spatial curvature has started to evolve into the observable universe one sees today. Then according to Ref. [53], consider another scalar field ϕ as a free field on the tunneling background, the supercurvature modes of ϕ can be generated during the bubble nucleation process. These modes can be translated as the dark energy observed in the universe today, which may be named the supercurvature-mode dark energy (ScmDE).

To start with this setup, one can denote Hubble parameter and mass of ϕ in the metastable de Sitter (ancestor) vacuum before the CDL tunneling by H_A and m_A respectively. Ordinary inflation follows the bubble nucleation

in the hyperbolic spatial geometry of H^{3*}. The Hubble parameter during the inflation is denoted by H_I. It should be noted that the Hubble parameters before and after the CDL quantum tunneling satisfy the relation $H_A > H_I$ (again, see Ref. [53]). The mass of the scalar field ϕ after the tunneling during ordinary inflationary phase is set as m_i, which could be different from m_A.

As a general approach, the CDL tunneling process can be considered on a Euclidean spacetime metric, If one assumes that the scalar field ϕ is minimally coupled with CDL instanton ψ via the Euclidean spacetime metric, in the free-field approximation, one can solve the equation of motion for the scalar field ϕ on the CDL background as a delta-function source. By expanding solutions in terms of the eigenfunctions of Laplacian ∇_S^2 on the 3-dimensional sphere slice S^3 with eigenvalues $-(k^2+1)$, the equation of motion becomes the eigen equation for the mode functions with a finite potential. The solution of the eigenfunctions on S^3 can classified into two types of modes. One type is the continuous modes with real wave numbers k while the other is a discrete mode with an imaginary wave number $k_B = i(1-\epsilon)$ correpsponding to the bound state contribution. The imaginary pole contribution from the bound state is normalizable on the global Cauchy surface in the Euclidean spacetime, thus should be included in the mode expansion of the quantum field ϕ in the complete basis. The discrete mode is called the supercurvature mode. Here ϵ is a small quantity related to the bound state energy, determined by the properties of the ancestor vacuum as

$$\epsilon = c_\epsilon \left(\frac{m_A}{H_A}\right)^2, \tag{2.42}$$

where c_ϵ is an order $\mathcal{O}(1)$ quantity that depends on the critical size of the bubble created in the ancestor vacuum, which can be calculated from the evolution of ϕ in the ancestor vacuum. Physically, the shift of small quantity ϵ arises from the ultralight but nonzero mass of scalar field ϕ as the perturbation to the zero-order bound state energy (which is zero) in the massless limit. Generally, to the mass m_A of the scalar field ϕ and the Hubble parameter H_A in the ancestor vacuum are assumed to follow the condition $m_A \ll H_A$ thus $\epsilon \ll 1$ holds as the supercurvature condition.

After operating the analytical continuation to the Lorentzian region in de Sitter space, the supercurvature mode becomes non-normalizable on the spatial slicing H^3 of the open universe and generate large-scale fluctuations,

*For convenience, one may define the geodesic distance as dimensionless quantities so that the spatial curvature is denoted by the sign of shape $|K| = 1$, and for open universe $K = -1$.

because the time-constant spatial slice in the open universe within the bubble is not the global Cauchy surface[†] needed for the normalization of the quantum modes. Unlike the continuous modes that decay as $e^{-\eta}$ in the conformal time η hence, the discrete supercurvature mode behaves as $e^{-\epsilon\eta}$ and decays remarkably slowly compared to the continuous modes providing ϵ is small enough. Hence, if the scalar field have ultralight mass at present epoch with $m_0 < H_0 \sim 10^{-33}$eV, the supercurvature mode can stay superhorizon and play the role of dark energy in the present universe. A candidate of such ultralight fields may appear as an axion-like particles (ALPs) arising from the string theory predictions [30, 31].

The supercurvature mode contributes to the correlation function of the scalar field $\phi(x)$ in the open universe within the bubble as [53]

$$\langle\phi(\eta,\boldsymbol{x})\phi(\eta',\boldsymbol{x}')\rangle = \varphi(\eta)\varphi(\eta')\frac{\sinh(1-\epsilon)R}{(1-\epsilon)\sinh R}, \tag{2.43}$$

where η is the conformal time, $\varphi(\eta)$ is the frozen expectation value of field ϕ. The explicit form of φ is given in Eq. (A.5).

R is the (dimensionless) geodesic distance on the 3-dimensional hyperbolic space H^3, normalized in terms of the curvature scale $L_c = 1/\sqrt{-K}$, and is given by

$$\cosh R \quad = \quad \cosh R_1 \cosh R_2 - \sinh R_1 \sinh R_2 \cos\psi. \tag{2.44}$$

R_1 and R_2 are the radial coordinates of the two points, $\boldsymbol{x}$ and $\boldsymbol{x}'$, and ψ is the included angle between them in the three-dimensional hyperbolic space (see Fig. 2). In the following parts, χ is widely used to denote the comoving radial coordinate distance with dimension of the length, with the relation $R = \sqrt{-K}\chi$. Thus the curvature radius is given by $R_c = \sqrt{-K}L_c = 1$.

If supercurvature mode of the scalar field ϕ stays frozen as almost constant until present as some form of substance pervading the background of the universe, it could play the role of the observed dark energy in the background as the ScmDE. However, due to the quantum fluctuation nature of the supercurvature mode of ϕ fluctuating on supercurvature scales, the large-scale inhomogeneities in the density of dark energy considered as ScmDE would be introduced as random fluctuations, which is to be discussed and formulated in detail in the next chapter.

[†]The global Cauchy surface exists in the Euclidean region of the spacetime.

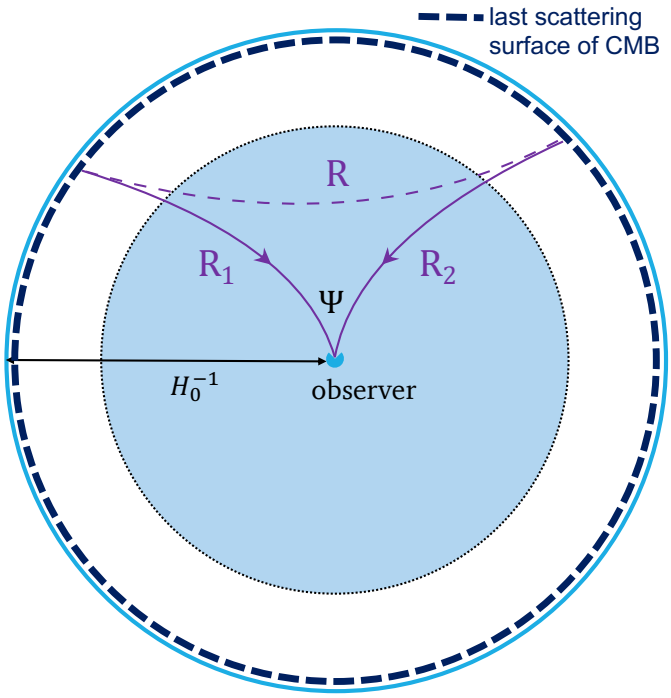

Figure 2: Schematic of the $\{R, R_1, R_2\}$ triplets in Eq. (2.44) associated with different line-of-sight directions for the two-point correlation function of scalar field ϕ. The shadowed region is a schematic of late-time domain, where dark energy is supposed to become important.

3 Formulation for the dark energy inhomogeneities

In this chapter, motivated by the supercurvature-mode dark energy, or ScmDE, discussed in the previous chapter, specific model formulation for the dark energy inhomogeneities which slightly breaks the cosmological principle's assumption for a homogeneous and isotropic background dark energy will be presented.

3.1 Stochastic field handling for Gaussian fluctuations of the ScmDE

The formulation for dark energy inhomogeneities will start with the ScmDE in this section. Following the ScmDE setups in Chapter 2 and supplements in Appendix A, the dark energy density at late-time matter-dominant era are vitally decided by the mass term contribution from the EMT of the supercurvature modes (see also period (ii) in Sec. V-C of Ref. [53] for a reference).

$$\rho_{\rm DE}(\eta,\boldsymbol{x}) \simeq \frac{m_0^2}{2}\phi^2(\eta,\boldsymbol{x}). \tag{3.45}$$

Note that there are random fluctuations in the value of ρ_{DE} due the quantum fluctuation nature. As for the inhomogeneities of the dark energy, one may define the density contrast of dark energy by

$$\delta(\eta,\boldsymbol{x}) = \frac{\rho_{\rm DE}(\eta,\boldsymbol{x}) - \langle\rho_{\rm DE}(\eta,\boldsymbol{x})\rangle}{\langle\rho_{\rm DE}(\eta,\boldsymbol{x})\rangle} \simeq \frac{\phi^2(\eta,\boldsymbol{x}) - \langle\phi^2(\eta,\boldsymbol{x})\rangle}{\langle\phi^2(\eta,\boldsymbol{x})\rangle}, \tag{3.46}$$

where the deviation from the statistical ensemble $\langle\rho_{\rm DE}\rangle$ can be comprehended as the dark energy inhomogeneities. Following this the two point correlation function of the density contrast will be calculated as

$$\langle\delta(\eta,\boldsymbol{x})\delta(\eta,\boldsymbol{y})\rangle \quad = \quad \frac{\langle\phi^2(\eta,\boldsymbol{x})\phi^2(\eta,\boldsymbol{y})\rangle - \langle\phi^2(\eta,\boldsymbol{x})\rangle\langle\phi^2(\eta,\boldsymbol{y})\rangle}{\langle\phi^2(\eta,\boldsymbol{x})\rangle^2}, \tag{3.47}$$

where $\langle\phi^2(\eta,\boldsymbol{x})\rangle = \langle\phi^2(\eta,\boldsymbol{y})\rangle$ is used because of the gaussian random field nature of the handling here. Furthermore, in the free field approximation with no interaction terms, one can decompose the four-point function of ϕ (two-point function of δ) into a product of two-point functions by using the Wick theorem:

$$\langle\phi^2(\eta,\boldsymbol{x})\phi^2(\eta,\boldsymbol{y})\rangle = \langle\phi^2(\eta,\boldsymbol{x})\rangle\langle\phi^2(\eta,\boldsymbol{y})\rangle + 2\langle\phi(\eta,\boldsymbol{x})\phi(\eta,\boldsymbol{y})\rangle^2. \tag{3.48}$$

Then, using Eq. (2.43), one will obtain

$$\begin{aligned}\xi(R) &\equiv \langle\delta(\eta,\boldsymbol{x})\delta(\eta,\boldsymbol{y})\rangle \\ &= \frac{2\langle\phi(\eta,\boldsymbol{x})\phi(\eta,\boldsymbol{y})\rangle^2}{\langle\phi^2(\eta,\boldsymbol{x})\rangle^2} \\ &= 2\left(\frac{\sinh(1-\epsilon)R}{(1-\epsilon)\sinh R}\right)^2,\end{aligned} \tag{3.49}$$

where $R=\sqrt{-K}|\boldsymbol{x}-\boldsymbol{y}|$. The correlation function $\xi(R)$ changes its behavior around the curvature scale $R_c=1$ as

$$\xi(R)\simeq 2\times\begin{cases}1 & (R\ll 1)\\ e^{-2\epsilon R} & (R\gg 1)\end{cases} \tag{3.50}$$

and diminishes at distances over the supercurvature scale $R_{sc}\equiv 1/\epsilon$. In physical length, R_{sc} corresponds to $L_{sc}=L_c/\epsilon$, which is much larger than the curvature radius L_c. The behavior of $\sqrt{\xi(R)}$ for $R\gg R_{sc}$ is depicted in Fig. 3. This indicates that the supercurvature-mode dark energy density varies considerably beyond the supercurvature scale R_{sc}. In Fig. 4, a schematic picture of the spatial variation of the ScmDE is demonstrated. At the horizon scale $H_0^{-1}(\ll L_c)$, one may take $R=\sqrt{-K}H_0^{-1}=\sqrt{\Omega_K}$, where the relation for the curvature component $\Omega_K=-K/H_0^2$ is used. For $\Omega_K\ll 1$ and $\epsilon\ll 1$, one has the estimation for the inhomogeneities expressed by the 2-point function of the ScmDE density, evaluated with respect to locations of the observer at $\boldsymbol{x}=0$ and that of the horizon $\boldsymbol{x}=H_0^{-1}$ as

$$\sqrt{\langle\delta^2(0)\rangle}-\sqrt{\langle\delta(0)\delta(1/H_0)\rangle}=\sqrt{2}-\sqrt{2}\frac{\sinh(1-\epsilon)\sqrt{\Omega_K}}{(1-\epsilon)\sinh\sqrt{\Omega_K}}\simeq\sqrt{2}\frac{\epsilon\Omega_K}{3}. \tag{3.51}$$

This extremely small quantity of $\mathcal{O}(\epsilon\Omega_K)$ within the current horizon shows the inhomogeneities in dark energy within the observable universe is small, and the background evolution is roughly isotropic.

However, small as it is, these inhomogeneities within the horizon may still give rise to observable effects on the anisotropies of the CMBtemperature power spectrum on the extremely large scales, as one shall see in the next section.

The previous results show that the density contrast $\xi(R)$ of the ScmDE has its inhomogeneities of $\mathcal{O}(1)$ over the scales of the supercurvature $R\gtrsim R_{sc}\gg 1$. This large-scale difference in the dark energy density is the characteristic feature of the dark energy model based on quantum fluctuations. For the large scales $R>R_{sc}$, the dark energy

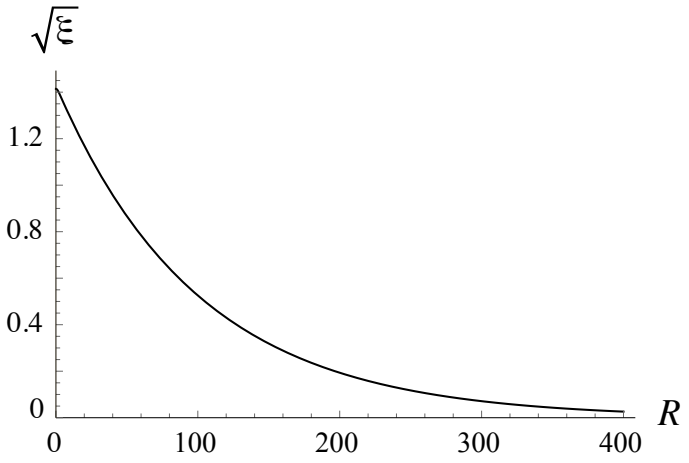

Figure 3: $\sqrt{\xi(R)}$ as a function of R, where $\epsilon = 0.01$ is adopted. The horizon scale at the present epoch is $R \sim \sqrt{-K}/H_0 = \sqrt{\Omega_K} \ll 1$, the curvature scale is $R_c = 1$, and the supercurvature scale is $R_{sc} = \epsilon^{-1} \gg 1$. The behavior of $\sqrt{\xi(R)}$ changes at the curvature scale following Eq. (3.50). The fact indicates that the order of magnitude for the spatial inhomogeneities of ScmDE within the present horizon (a very narrow domain near R=0 in the figure where $\sqrt{\xi(R)} \simeq \sqrt{2}$) is small.

density fluctuates greatly and can be treated as a classical Gaussian random variable with the properties of $\langle \phi_{sc} \rangle = 0$ and $\langle \phi_{sc}^2 \rangle = \varphi^2(\eta)$ (see Appendix A for the explicit expression of $\varphi(\eta)$). On the contrary, the dark energy density is nearly constant within the present horizon $H_0^{-1} (\ll L_c)$. The explicit form of the probability distribution function of the dark energy density is shown in Appendix A.1. The result demonstrates a wide distribution of probability of $\rho_{\rm DE}$ and the dark energy density parameter Ω_Λ at scales larger than the supercurvature scale R_{sc} even the parameter

$$\langle \rho_{\rm DE}(\boldsymbol{x}) \rangle = \frac{1}{2} m_0^2 \varphi^2(0) = 3H_0^2 \overline{\Omega}_\Lambda / 8\pi G \tag{3.52}$$

is fixed with $\overline{\Omega}_\Lambda = 0.7$. Thus the dark energy density has large spatial variation on the large scales $R > R_{sc}$. It may also be noted, that the spatial variations exist even within the horizon scale H_0^{-1}, although the order of magnitude is as small as Eq. (3.51). In the next section, CMB anisotropies caused by this spatial variations will be calculated in an exact way instead of order estimation, and observational constraints on the model parameters in the scenario will be given.

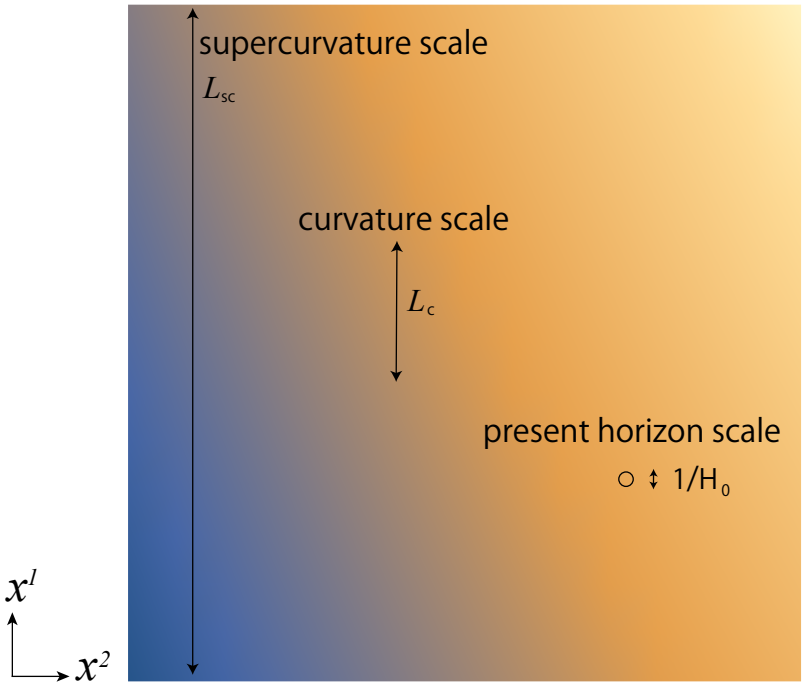

Figure 4: A schematic demonstration for the ScmDE density contrast, where the color scheme denotes the relative amplitude of the density contrast following Eq. (3.49). $x^1 = \boldsymbol{x}$ and $x^2 = \boldsymbol{y}$ are the coordinates for different spatial locations for two-point correlations in $R = \sqrt{-K}|\boldsymbol{x} - \boldsymbol{y}|$. The supercurvature scale is assumed to be $L_{sc} = 1/\epsilon\sqrt{-K}(= L_c/\epsilon)$ far beyond the curvature scale $L_c = 1/\sqrt{-K}$. Also, because the universe today is observed to be nearly flat, the curvature scale L_c is beyond the comoving horizon scale $1/H_0$, thus $1/H_0 \ll L_c \ll L_{sc}$.

3.1.1 Evolution of the stochastic fluctuations of ScmDE

To study the late-time evolution with the ScmDE inhomogeneities of in an open universe, one may adopt the line element under the conformal Newtonian gauge as

$$ds^2 = a^2(\eta)\left[-(1+2\Psi)d\eta^2 + (1+2\Phi)\gamma_{ij}dx^i dx^j\right], \tag{3.53}$$

where Ψ and Φ are the gravitational potential and the curvature potential, respectively, and γ_{ij} is the three-dimensional metric in the open universe, similar to a Kronecker delta as,

$$\gamma_{ij}dx^i dx^j = d\chi^2 + \left(\frac{\sinh\sqrt{-K}\chi}{\sqrt{-K}}\right)^2 (d\theta^2 + \sin^2\theta d\varphi^2). \tag{3.54}$$

Hereafter, one may use *dot* over a symbol to denote the differentiation with respect to the conformal time η,

$\dot{} \equiv \partial/\partial\eta$. In the following one may calculate the right-hand-side of Eq. (3.74) with the linear perturbative part of Einstein equation.

Using an overbar to represent the background average quantity, one can write out the 0-th order Einstein equations as [56],

$$\overline{G}^0{}_0 = -3\frac{1}{a^2}\left(\mathcal{H}^2 + K\right) = 8\pi G\overline{T}^0{}_0 = 8\pi G\left(\overline{T}^0{}_{0(\mathrm{m})} + \overline{T}^0{}_{0(\phi)}\right), \tag{3.55}$$

where (m) and (ϕ) denotes the matter and dark energy component, respectively, with $\mathcal{H} = \dot{a}/a = a_{,\eta}/a$ defined. A concrete definition of the overbar average will be presented later. The 1st-order perturbative parts of the Einstein equation will yied

$$\delta G^0{}_0 = 2\frac{1}{a^2}\left[3\mathcal{H}^2\Psi - 3\mathcal{H}\dot{\Phi} + (\nabla_H^2 + 3K)\Phi\right] = 8\pi G\delta T^0{}_0 = 8\pi G\left(\delta T^0{}_{0(\mathrm{m})} + \delta T^0{}_{0(\phi)}\right), \tag{3.56}$$

where ∇_H^2 is the Laplacian defined with respect to γ_{ij} in the open universe, as $\nabla_H^2 Q = \gamma^{ij}Q_{|ij}$ [56].

On the other hand, the EMT of the scalar field ϕ can be written as

$$T^0{}_{0(\phi)} = -\frac{1}{2a^2}\left((1-2\Psi)\dot{\phi}^2 + (1-2\Phi)\gamma^{ij}\nabla_i\phi\nabla_j\phi + m_0^2a^2\phi^2\right). \tag{3.57}$$

Following this, the spatial average of the scalar field EMT surrounding our horizon is defined as

$$\overline{T}^0{}_{0(\phi)} = -\frac{1}{2a^2}\left((1-2\Psi)\dot{\phi}^2 + (1-2\Phi)\gamma^{ij}\nabla_i\phi\nabla_j\phi + m_0^2a^2\phi^2\right)\Big|_{\mathrm{SA}\chi=0}, \tag{3.58}$$

where "SA" means"spatially average around" surrounding the present Hubble scale of the universe. Then one may consider the fluctuations of $T^0{}_{0(\phi)}$ around $\overline{T}^0{}_{0(\phi)}$ taking the background as this spatial average, which reads

$$\delta T^0{}_{0(\phi)} \equiv T^0{}_{0(\phi)} - \overline{T}^0{}_{0(\phi)}. \tag{3.59}$$

Since the supercurvature-mode dark energy ϕ has is almost frozen, which means it has almost constant value with tiny fluctuations within the Hubble scale, one may approximate the spatially averaged value of the ϕ by the value near the observer at $\chi = 0$. For example, one may set

$$\phi(\eta,\chi,\boldsymbol{\gamma})|_{\mathrm{SA}\chi=0} = \phi(\eta,\chi=0,\boldsymbol{\gamma}). \tag{3.60}$$

Of course, $\phi(\eta, \chi = 0, \boldsymbol{\gamma})$ does not depend on the direction of received photon denoted by line-of-sight direction $\boldsymbol{\gamma}$, hence one can simply write it as $\phi(\eta, \chi = 0)$.

As the ScmDE component fluctuates mildly both in space and time, the mass term in the EMT (3.57) dominantly contributes: ${T^0}_{0(\phi)} \simeq -\frac{1}{2}m_0^2\phi^2$. Then the background and the perturbation as spatial inhomogeneities of ${T^0}_0$ are given by

$$\overline{T}^0{}_{0(\phi)} = -\frac{1}{2}m_0^2\phi^2\Big|_{\mathrm{SA}\chi=0}\,, \qquad \delta T^0{}_{0(\phi)} = -\frac{1}{2}m_0^2\left(\phi^2 - \phi^2\Big|_{\mathrm{SA}\chi=0}\right), \tag{3.61}$$

respectively.

Since the interest here are the perturbations on the supercurvature scales, see Fig. 4, the metric perturbation in the late-time universe can be approximated as $\Psi + \Phi = 0$ and the spatial derivative term $(\nabla_H^2 + 3K)\Phi$ will be negligibly small. This will allow one to approximate Eq. (3.56) as

$$\delta G^0{}_0 = 2\frac{1}{a^2}\left[3\mathcal{H}^2\Psi + 3\mathcal{H}\dot{\Psi}\right] = 8\pi G\big(\delta T^0{}_{0(\phi)} + \delta T^0{}_{0(\mathrm{m})}\big). \tag{3.62}$$

The perturbed energy momentum tensor of the matter component is $\delta T^0{}_{0(\mathrm{m})} = -\delta_\mathrm{m}\rho_\mathrm{m}$, where δ_m is the density contrast of the matter component, which follows (e.g., [56])

$$\dot{\delta}_\mathrm{m} + kV_\mathrm{m} + 3\dot{\Phi} = 0, \tag{3.63}$$

$$\dot{V}_\mathrm{m} + \frac{\dot{a}}{a}V_\mathrm{m} - k\Psi = 0. \tag{3.64}$$

These equations follow the notations in Ref. [56] for the Fourier mode expansion formalism in an open universe. Therefore it should be noted that $k^2 = -K\epsilon$ for the supercurvature mode in the Fourier space. The equations writes

$$(a\dot{\delta}_\mathrm{m})\dot{} + k^2a\Psi + 3(a\dot{\Phi})\dot{} = 0, \tag{3.65}$$

where the term of the gravitational potential $k^2a\Psi$ may be omitted in the large-scale limit $k \ll \eta_0^{-1}$, as one is mainly interested of the supercurvature mode on superhorizon scales here. As a result, one writes

$$\delta_\mathrm{m}(\eta) + 3\Phi(\eta) = 0, \tag{3.66}$$

where the isocurvature initial conditions $\delta_{\rm m}(0) = \Phi(0) = 0$ for the supercurvature mode perturbations is assumed. With the general condition in an almost isotropic universe $\Psi + \Phi \approx 0$ (otherwise large quadrupole for energy or matter distribution would arise), Eq. (3.62) reduces to

$$6\frac{\mathcal{H}}{a^2}\dot{\Psi} + \left(6\frac{\mathcal{H}^2}{a^2} + 24\pi G\rho_m\right)\Psi = 8\pi G\delta T^0{}_{0(\phi)}. \tag{3.67}$$

Using Eqs. (3.61) and (3.67), one can write down the solution for Ψ as

$$\begin{aligned}\Psi(\eta,\chi,\boldsymbol{\gamma}) &= \frac{1}{F(\eta)}\int_{\eta_*}^{\eta} d\eta_1 \frac{8\pi G F(\eta_1)}{B(\eta_1)}\delta T^0{}_{0(\phi)}(\eta_1,\chi,\boldsymbol{\gamma}) \\ &\simeq -\frac{1}{F(\eta)}\int_0^{\eta} d\eta_1 \frac{4\pi G F(\eta_1)}{B(\eta_1)} m_0^2\left(\phi(\eta_1,\chi,\boldsymbol{\gamma})^2 - \phi(\eta_1,0)^2\right),\end{aligned} \tag{3.68}$$

where the approximation $\eta_*/\eta \ll 1$ hence $\eta_* \simeq 0$ was used, with functions defined as

$$F(\eta) = F_c \exp\left\{\int_0^{\eta} d\eta' \frac{A(\eta')}{B(\eta')}\right\}, \tag{3.69}$$

$$A(\eta) = 6\frac{\mathcal{H}^2}{a^2} + 24\pi G\rho_m \tag{3.70}$$

$$B(\eta) = 6\frac{\mathcal{H}}{a^2}, \tag{3.71}$$

with a constant F_c. Note that result of Eq. (3.68) is independent from constant F_c due to cancellation of the coefficient in the numerator and the denominator. The solution of Ψ in Eq. (3.68) denotes the perturbations to the metric caused by the inhomogeneities of ScmDE, which may be applied to the predictions of various observational effects in the universe.

3.1.2 CMB anisotropies from ScmDE

Following the solution for the perturbations to the metric caused by the inhomogeneities of ScmDE in the previous section, consequently, one may calculate the temperature fluctuation induced by the autocorrelation of the supercurvature-mode dark energy due to the spatial inhomogeneities. To find out, one calculates the impacts of inhomogeneous dark energy on the CMB anisotropies through the late-time integrated Sachs-Wolfe (ISW) effect. The evolution of the distribution function of CMB photons is described by the Boltzmann equation with the perturbed Planck distribution:

$$f(\eta,\boldsymbol{x},\boldsymbol{p}) = \frac{1}{\exp[p/(T(\eta)(1+\Theta(\eta,\boldsymbol{x},\boldsymbol{\gamma}))] - 1}, \tag{3.72}$$

where $\Theta(\eta, \boldsymbol{x}, \boldsymbol{\gamma})$ denotes the temperature fluctuation of photons. $\boldsymbol{\gamma}$ is the line-of-sight direction identical to the unit vector of the observed photon momentum $\boldsymbol{p}$, while p is its magnitude. Note that the temperature fluctuation $\Theta(\eta, \boldsymbol{x}, \boldsymbol{\gamma})$ depends on the photon's trajectory scattered from the past. It can be shown that the CMB anisotropy $\Theta(\eta, \boldsymbol{x}, \boldsymbol{\gamma})$ satisfies the equation [56]

$$\frac{d}{d\eta}(\Theta + \Psi) = \frac{\partial \Psi(\eta, \boldsymbol{x})}{\partial \eta} - \frac{\partial \Phi(\eta, \boldsymbol{x})}{\partial \eta} + C_{\mathrm{e}\gamma}, \tag{3.73}$$

where $C_{e\gamma}$ denotes the collision term for the Compton scattering, but it can be omitted in our investigation. Then, the integration yields the ISW contribution to the CMB anisotropies,

$$\frac{\Delta T}{T}(\boldsymbol{\gamma}) = \Theta(\eta_0, \boldsymbol{x}_0, \boldsymbol{\gamma}) + \Psi(\eta_0, \boldsymbol{x}_0) = \int_{\eta_*}^{\eta_0} d\eta \left(\frac{\partial \Psi(\eta, \chi, \boldsymbol{\gamma})}{\partial \eta} - \frac{\partial \Phi(\eta, \chi, \boldsymbol{\gamma})}{\partial \eta} \right)_{\chi = \eta_0 - \eta}. \tag{3.74}$$

Here, on the right-hand side, the spatial position $\boldsymbol{x}$ is represented by its radial coordinate and the angle as $\boldsymbol{x} = (\chi, \boldsymbol{\gamma})$. The direction of the photon, $\boldsymbol{\gamma}$, is fixed in this expression and the radial coordinate $\chi = \eta_0 - \eta$ denotes the position of the photon at the conformal time η. η_* stands for the conformal time of the CMB last scattering surface. Under the condition $\Phi + \Psi = 0$, Eq. (3.74) becomes

$$\frac{\Delta T}{T}(\boldsymbol{\gamma}) \simeq 2 \int_0^{\eta_0} d\eta \left(\frac{\partial \Psi(\eta, \chi, \boldsymbol{\gamma})}{\partial \eta} \right) \Big|_{\chi = \eta_0 - \eta}. \tag{3.75}$$

Thus using Eq. (3.68), the two-point correlation function of temperature fluctuations from the last scattering surface of the CMB is given by

$$\begin{aligned}
&\left\langle \frac{\Delta T}{T}(\boldsymbol{\gamma}) \frac{\Delta T}{T}(\boldsymbol{\gamma}') \right\rangle \\
&\quad = 4 \int_0^{\eta_0} d\eta_1 \int_0^{\eta_0} d\eta_2 \left[\frac{\partial}{\partial \eta_1} \frac{1}{F(\eta_1)} \int_0^{\eta_1} d\eta_3 \frac{4\pi G F(\eta_3)}{B(\eta_3)} m_0^2 \right] \left[\frac{\partial}{\partial \eta_2} \frac{1}{F(\eta_2)} \int_0^{\eta_2} d\eta_4 \frac{4\pi G F(\eta_4)}{B(\eta_4)} m_0^2 \right] \\
&\qquad \times \left\langle \left(\phi(\eta_3, \chi_3, \boldsymbol{\gamma})^2 - \phi(\eta_3, 0)^2 \right) \left(\phi(\eta_4, \chi_4, \boldsymbol{\gamma}')^2 - \phi(\eta_4, 0)^2 \right) \right\rangle \Big|_{\chi_3 = \eta_0 - \eta_3, \chi_4 = \eta_0 - \eta_4}.
\end{aligned} \tag{3.76}$$

In this way, the inhomogeneities by ScmDE is handled as Gaussian random fluctuations within the universe, and could be evaluated numerically.

3.2 Analytic formulation for dark energy inhomogeneities

The characteristic feature of the dark energy model previously proposed as the ScmDE is the spatial inhomogeneities of the dark energy density on the very large scales, which was originated from the vacuum fluctuations of the

supercurvature-modes of a scalar field during an open inflationary scenario [53, 57]. An ultralight scalar field ϕ with spatial fluctuations taking large amplitude on the supercurvature scales is responsible for the dark energy in the scenario. Because the horizon size of our universe is much smaller than the scales of the inhomogeneities of the dark energy, the breaking of the cosmological principle is small within the observable universe, which might enable us to escape from the observational constraints. One can formulate a phenomenological model of dark energy that slightly breaks the cosmological principle by mimicking the previous ScmDE.

However, the previous random field handling limits the predictive ability and application scope of the dark energy inhomogeneities, hence, in this part, as a generalization to the ScmDE setup, it is natural to consider an analytic formulation for dark energy inhomogeneities sourced by a scalar field that spatially varying on the superhorizon scales within a flat background universe. For simplicity, one may assume

$$ds^2 = a^2(\eta)\left[-(1+2\Psi)d\eta^2 + (1+2\Phi)\delta_{ij}dx^i dx^j\right], \tag{3.77}$$

where δ_{ij} is the Kronecker delta δ_{ij}, and $a(\eta)$ is the scale factor of the universe with the conformal time η, Ψ and Φ are the metric perturbations to be characterized later.

One can set the cosmological metric perturbation as Ψ, focusing on the large-scale superhorizon perturbations to be considered. In Ref. [54], it was discussed that the inhomogeneities induced by supercurvature fluctuations are dominated by dipole and quadrupole components ($\ell = 1, 2$) among all multipole contributions. Now, neglecting higher multipoles, one may explicitly write out the multipole expansion of the metric perturbations as

$$\Psi = \epsilon_1 \sum_{m=1}^{3} \Psi_{1(m)}(\eta) P_i^{(m)} x^i + \epsilon_2 \sum_{m=1}^{5} \Psi_{2(m)}(\eta) P_{ij}^{(m)} x^i x^j, \tag{3.78}$$

$$\Phi = \epsilon_1 \sum_{m=1}^{3} \Phi_{1(m)}(\eta) P_i^{(m)} x^i + \epsilon_2 \sum_{m=1}^{5} \Phi_{2(m)}(\eta) P_{ij}^{(m)} x^i x^j, \tag{3.79}$$

$$\phi = \phi_0(\eta) + \epsilon_1 \sum_{m=1}^{3} \phi_{1(m)}(\eta) P_i^{(m)} x^i + \epsilon_2 \sum_{m=1}^{5} \phi_{2(m)}(\eta) P_{ij}^{(m)} x^i x^j, \tag{3.80}$$

where $P_i^{(m)}$ and $P_{ij}^{(m)}$ are matrices related to the multipole expansion of the perturbations to the spatial basis and $P_{ij}^{(m)}$ are traceless. These matrices can be found explicitly in the Appendix C.

Considering standard CDM besides dark energy, and neglecting effects from baryonic matter here, The dark energy inhomogeneities will induce perturbations to the matter distribution via metric perturbations defined previ-

ously. Considering the matter component as a perfect fluid, in correspondence to the perturbations defined above, one may also define some scalar field perturbation $\overline{V}$ to the velocity potential of the fluid, expressed by its multipole contributions $V_{\ell(m)}$ in a similar way as

$$\overline{V} = \epsilon_1 \sum_{m=1}^{3} V_{1(m)}(\eta) P_i^{(m)} x^i + \epsilon_2 \sum_{m=1}^{5} V_{2(m)}(\eta) P_{ij}^{(m)} x^i x^j. \tag{3.81}$$

Following the definition of $\overline{V}$, perturbations to the matter distribution are

$$\rho = \rho_0(\eta) + \epsilon_1 \sum_{m=1}^{3} \rho_{1(m)}(\eta) P_i^{(m)} x^i + \epsilon_2 \sum_{m=1}^{5} \rho_{2(m)}(\eta) P_{ij}^{(m)} x^i x^j, \tag{3.82}$$

$$u_i \equiv \partial_i \overline{V}, \tag{3.83}$$

with constraints and conditions

$$u_\mu u^\mu = -1; \tag{3.84}$$

$$\boldsymbol{\nabla} \times \boldsymbol{v} = 0, \tag{3.85}$$

$$\boldsymbol{v} = \{u_1, u_2, u_3\}. \tag{3.86}$$

Here the monopole moment of distribution ρ is the matter density and the dipole moment u_μ is the fluid velocity.

Now, one may define the energy momentum tensors of the dark energy scalar field (ϕ) and the dark matter (DM) respectively as

$$T_{\mu\nu}^{(\phi)} = \partial_\mu \phi \partial_\nu \phi - g_{\mu\nu} \left(\frac{1}{2} g^{\alpha\beta} \partial_\alpha \phi \partial_\beta \phi + \frac{1}{2} m^2 \phi^2 \right), \tag{3.87}$$

$$T_{\mu\nu}^{(\mathrm{DM})} = \rho u_\mu u_\nu. \tag{3.88}$$

The previous definitions allow one to write out the Einstein equations as

$$G^\mu{}_\nu = 8\pi G \left(T^{(\phi)\mu}{}_\nu + T^{(\mathrm{DM})\mu}{}_\nu \right). \tag{3.89}$$

The equations of motion for scalar field ϕ reads

$$\frac{1}{\sqrt{-g}} \partial_\mu \left(\sqrt{-g} g^{\mu\nu} \partial_\nu \phi \right) - m^2 \phi = 0, \tag{3.90}$$

and the equations of motion for dark matter is

$$\nabla_\mu T^{(\mathrm{DM})\mu}{}_\nu = 0. \tag{3.91}$$

The EoS ω_ϕ of the dark energy field ϕ is an important quantity characterizing its property and evolution. From the standard scalar field formalism, taking the scalar potential $V(\phi) = m^2\phi^2/2$, one can obtain ω_ϕ as

$$\begin{aligned}\omega_\phi \equiv \frac{p_\phi}{\rho_\phi} &= \left(\frac{1}{2}\left(\frac{\mathrm{d}\phi}{\mathrm{d}t}\right)^2 - V(\phi)\right)\left(\frac{1}{2}\left(\frac{\mathrm{d}\phi}{\mathrm{d}t}\right)^2 + V(\phi)\right)^{-1} \\ &= -\frac{2a^2V(\phi) - \dot{\phi}^2}{2a^2V(\phi) + \dot{\phi}^2}\end{aligned} \tag{3.92}$$

The EoS depends on the dynamical evolution of ϕ, and is a concordant generalization to the Chevallier-Polarski-Linder (CPL) parametrization [58, 59].

3.2.1 Essence of the equations Governing the late-time evolution

The linear combination nature of Eqs. (3.78)–(3.80) ensures that Eqs. (3.89)–(3.91) give equations in the same form in essence, for each multipole component with indices $\ell = 1, 2$ and $m = 1, 2, 3, 4, 5$ and the summation over m. Indeed, the components with different ℓ indices, e.g., $\Psi_{\ell=1}$ and $\Psi_{\ell=2}$, have different dimensions to the order of length by definition. Baring this fact in mind, for simplicity of the notations, indices (m) in the following parts can be neglected for the simplicity of writing, and only the lower indices ℓ is used to denote the multipole components of these perturbations. As an additional convetion, in the following parts, lower indices 0 stands for the background quantities and ℓ stands for the perturbations.

Using the conformal Hubble parameter $\mathcal{H} = aH(a) = \dot{a}/a$ instead of Hubble parameter $H(a)$, Eq. (3.90) gives

$$\ddot{\phi}_0 + 2\mathcal{H}\dot{\phi}_0 + m^2a^2\phi_0 = 0, \tag{3.93}$$

$$\ddot{\phi}_\ell + 2\mathcal{H}\dot{\phi}_\ell + m^2a^2\phi_\ell + \dot{\phi}_0(3\dot{\Phi}_\ell - \dot{\Psi}_\ell - 4\mathcal{H}\Psi_\ell) - 2\ddot{\phi}_0\Psi_\ell = 0. \tag{3.94}$$

On the other hand, Eq. (3.91) leads to

$$3\mathcal{H}\rho_0 + \dot{\rho}_0 = 0, \tag{3.95}$$

$$3\mathcal{H}\rho_\ell + \dot{\rho}_\ell + 3\rho_0\dot{\Phi}_\ell = 0, \tag{3.96}$$

$$\dot{V}_\ell - a\Psi_\ell = 0. \tag{3.97}$$

By defining the density perturbation as $\rho_\ell \equiv \rho_0 \delta_\ell$, it is obvious to see Eqs. (3.95) and (3.96) are consistent with the general continuity equation and Eq. (25) in Ref. [54] in the large-scale limit, while it is worth mentioning that the velocity equation Eq. (3.97) is also consistent with the Eq. (26) in Ref. [54]. To see this, one may starting from Eq. (3.97), if one refines $\mathcal{V}_\ell$ with respect to V_ℓ as

$$\mathcal{V}_\ell \equiv \frac{k}{a} V_\ell, \tag{3.98}$$

with k denoting the wavenumber of the perturbations, one will have

$$\dot{V}_\ell - a\Psi_\ell = \frac{\dot{a}\mathcal{V}_\ell + a\dot{\mathcal{V}}_\ell}{k} - a\Psi_\ell = 0, \tag{3.99}$$

hence

$$\dot{\mathcal{V}}_\ell + \frac{\dot{a}}{a}\mathcal{V}_\ell - k\Psi_\ell = 0, \tag{3.100}$$

which is consistent with Eq. (26) in Ref. [54].

Define $M_{\rm pl}^{-2} \equiv 8\pi G$ for short, then the Einstein equations will be concluded as

$$-3\mathcal{H}^2 + M_{\rm pl}^{-2}(\frac{1}{2}m^2a^2\phi_0^2 + \frac{1}{2}\dot{\phi}_0^2 + a^2\rho_0) = 0, \tag{3.101}$$

$$\mathcal{H}^2 - 2\frac{\ddot{a}}{a} + M_{\rm pl}^{-2}(\frac{1}{2}m^2a^2\phi_0^2 - \frac{1}{2}\dot{\phi}_0^2) = 0, \tag{3.102}$$

$$-2(\mathcal{H}\Psi_\ell - \dot{\Phi}_\ell) + M_{\rm pl}^{-2}(a\rho_0 V_\ell + \dot{\phi}_0\phi_\ell) = 0, \tag{3.103}$$

$$6\mathcal{H}(\mathcal{H}\Psi_\ell - \dot{\Phi}_\ell) + M_{\rm pl}^{-2}\left(a^2\rho_\ell + m^2a^2\phi_0\phi_\ell - \dot{\phi}_0(\dot{\phi}_0\Psi_\ell - \dot{\phi}_\ell)\right) = 0, \tag{3.104}$$

$$(2\frac{\ddot{a}}{a} - \mathcal{H}^2)\Psi_\ell + \mathcal{H}\dot{\Psi}_\ell - 2\mathcal{H}\dot{\Phi}_\ell - \ddot{\Phi}_\ell + \frac{M_{\rm pl}^{-2}}{2}\left(m^2a^2\phi_0\phi_\ell + \dot{\phi}_0(\dot{\phi}_0\Psi_\ell - \dot{\phi}_\ell)\right) = 0. \tag{3.105}$$

These equations can be classified by the order of the perturbations, divided into the background equations that read

$$\dot{\rho}_0 + 3\mathcal{H}\rho_0 = 0, \tag{3.106}$$

$$\ddot{\phi}_0 + 2\mathcal{H}\dot{\phi}_0 + m^2a^2\phi_0 = 0, \tag{3.107}$$

$$-3\mathcal{H}^2 + M_{\rm pl}^{-2}(\frac{1}{2}m^2a^2\phi_0^2 + \frac{1}{2}\dot{\phi}_0^2 + a^2\rho_0) = 0, \tag{3.108}$$

$$\mathcal{H}^2 - 2\frac{\ddot{a}}{a} + M_{\rm pl}^{-2}(\frac{1}{2}m^2a^2\phi_0^2 - \frac{1}{2}\dot{\phi}_0^2) = 0, \tag{3.109}$$

and first-order perturbative equations relying on the background as follows

$$\dot{\rho}_\ell + 3\mathcal{H}\rho_\ell + 3\rho_0\dot{\Phi}_\ell = 0, \tag{3.110}$$

$$\ddot{\phi}_\ell + 2\mathcal{H}\dot{\phi}_\ell + m^2a^2\phi_\ell + \dot{\phi}_0(3\dot{\Phi}_\ell - \dot{\Psi}_\ell - 4\mathcal{H}\Psi_\ell) - 2\ddot{\phi}_0\Psi_\ell = 0, \tag{3.111}$$

$$\dot{V}_\ell - a\Psi_\ell = 0, \tag{3.112}$$

$$-2(\mathcal{H}\Psi_\ell - \dot{\Phi}_\ell) + M_{\rm pl}^{-2}(a\rho_0 V_\ell + \dot{\phi}_0\phi_\ell) = 0, \tag{3.113}$$

$$6\mathcal{H}(\mathcal{H}\Psi_\ell - \dot{\Phi}_\ell) + M_{\rm pl}^{-2}\left(a^2\rho_\ell + m^2a^2\phi_0\phi_\ell - \dot{\phi}_0(\dot{\phi}_0\Psi_\ell - \dot{\phi}_\ell)\right) = 0, \tag{3.114}$$

$$(2\frac{\ddot{a}}{a} - \mathcal{H}^2)\Psi_\ell + \mathcal{H}\dot{\Psi}_\ell - 2\mathcal{H}\dot{\Phi}_\ell - \ddot{\Phi}_\ell + \frac{M_{\rm pl}^{-2}}{2}\left(m^2a^2\phi_0\phi_\ell + \dot{\phi}_0(\dot{\phi}_0\Psi_\ell - \dot{\phi}_\ell)\right) = 0. \tag{3.115}$$

Solving the background, one is able to find out the evolution of large-scale perturbations related to the fluctuations of the dark energy field ϕ.

3.2.2 CMB anisotropies revisit

Through the integrated Sachs-Wolfe (ISW) effect [54, 56], the perturbations to the metric caused by the large-scale inhomogeneities of the dark energy ϕ would affect the observations of CMB anisotropies. Using the relation of comoving distance with respect to the conformal time $\chi = \eta_0 - \eta$ and recollecting the definition for the metric perturbations in Eq. (3.78), one can evaluate the ISW effect on the temperature fluctuations of the CMB as

$$\begin{aligned}\frac{\Delta T}{T} \simeq& 2\int_{\eta_d}^{\eta_0} \mathrm{d}\eta \left(\frac{\partial\Psi(\eta,\chi)}{\partial\eta}\right)\Bigg|_{\chi=\eta_0-\eta} \\ =& 2\int_{\eta_*}^{\eta_0} \mathrm{d}\eta \left(\epsilon_1\sum_{m=1}^{3}\frac{\partial\Psi_{1(m)}(\eta)}{\partial\eta}P_i^{(m)}x^i + \epsilon_2\sum_{m=1}^{5}\frac{\partial\Psi_{2(m)(\eta)}}{\partial\eta}P_{ij}^{(m)}x^ix^j\right)\Bigg|_{\chi=\eta_0-\eta} \\ =& 2\epsilon_1\int_{\eta_d}^{\eta_0} \mathrm{d}\eta \left(\frac{\partial\Psi_{1(m)}(\eta)}{\partial\eta}\sum_{m=1}^{3}P_i^{(m)}x^i\right)\Bigg|_{\chi=\eta_0-\eta} + 2\epsilon_2\int_{\eta_d}^{\eta_0} \mathrm{d}\eta \left(\frac{\partial\Psi_{2(m)}(\eta)}{\partial\eta}\sum_{m=1}^{5}P_{ij}^{(m)}x^ix^j\right)\Bigg|_{\chi=\eta_0-\eta}.\end{aligned} \tag{3.116}$$

Here η_d is used to denote the conformal time of epoch of the photon decoupling. Notice that $\Psi_{1(m)}$ and $\Psi_{2(m)}$ are unchanged for various ℓ and m component, and are only functions of the conformal time η as discussed in Sec. 3.2, thus one can use Ψ_ℓ again for short in the following lines. It can also be confirmed that the matrices P_{ij}^m and P_i^m introduced in Sec. 3.2 are actually related to the real basis spherical harmonics $Y_\ell^m(\theta,\varphi)$ (see Appendix C).

Utilizing the relation Eq. (C.10) and (C.11) it follows that

$$\begin{aligned}\frac{\Delta T}{T} &= 2\epsilon_1 \int_{\eta_d}^{\eta_0} \mathrm{d}\eta \left(\frac{\partial \Psi_\ell}{\partial \eta}\chi Y_{\ell=1}^{(m)}(\theta,\varphi)\right)\Bigg|_{\chi=\eta_0-\eta} + 2\epsilon_2 \int_{\eta_d}^{\eta_0} \mathrm{d}\eta \left(\frac{\partial \Psi_\ell}{\partial \eta}\chi^2 Y_{\ell=2}^{(m)}(\theta,\varphi)\right)\Bigg|_{\chi=\eta_0-\eta} \\ &= 2\epsilon_1 \left(\int_{\eta_d}^{\eta_0} \mathrm{d}\eta(\eta_0-\eta)\frac{\partial \Psi_\ell}{\partial \eta}\right) Y_{\ell=1}^{(m)}(\theta,\varphi) + 2\epsilon_2 \left(\int_{\eta_d}^{\eta_0} \mathrm{d}\eta(\eta_0-\eta)^2\frac{\partial \Psi_\ell}{\partial \eta}\right) Y_{\ell=2}^{(m)}(\theta,\varphi). \\ &\equiv 2\sum_{\ell=1}^{2} \epsilon_\ell Q_{\ell(m)} Y_\ell^{(m)}(\theta,\varphi), \end{aligned} \tag{3.117}$$

with integral

$$Q_{\ell(m)} \equiv Q_\ell \equiv \int_{\eta_d}^{\eta_0} \mathrm{d}\eta(\eta_0-\eta)^\ell \frac{\partial \Psi_\ell}{\partial \eta}. \tag{3.118}$$

Whereas the evolution of the perturbation Ψ_ℓ in the previous numerical solution have been obtained in Sec. 4.2, Q_ℓ is now numerically evaluable. On the other hand, the definition the temperature fluctuations can be written in the multipole expansion as [60]

$$\frac{\Delta T}{T} = \sum_\ell \sum_m A_{\ell m} Y_\ell^{(m)}(\theta,\varphi), \tag{3.119}$$

or, with θ dependence as

$$\frac{\Delta T}{T}(\cos\theta) = \sum_\ell A_{\ell m} Y_\ell^{(m)}(\theta,\varphi). \tag{3.120}$$

The angular power spectrum of CMB C_ℓ is defined by the ensemble of the squared expansion coefficients as

$$C_\ell \equiv \langle |A_{\ell m}|^2 \rangle. \tag{3.121}$$

Hence if one uses $\boldsymbol{\gamma}$ and $\boldsymbol{\gamma}'$ to represent for different unit line-of-sight directions with included angle θ, i.e. $\boldsymbol{\gamma}\cdot\boldsymbol{\gamma}' = \cos\theta$, the two-point correlation of the temperature fluctuations follow as

$$\begin{aligned}\langle \frac{\Delta T}{T}(\boldsymbol{\gamma}) \frac{\Delta T}{T}(\boldsymbol{\gamma}') \rangle &= \sum_\ell \langle |A_{\ell m}|^2 \rangle \int \mathrm{d}\phi |Y_\ell^{(m)}(\theta,\varphi)|^2 \\ &= \sum_\ell \frac{2\ell+1}{4\pi} C_\ell P_\ell(\cos\theta), \end{aligned} \tag{3.122}$$

where the $A_{\ell m}$ and $Y_\ell^{(m)}$ are taken as real functions.

By comparing Eq. (3.117) with (3.120) one will see that

$$A_{1m} = 2\epsilon_1 Q_1 = 2\epsilon_1 \left(\int_{\eta_d}^{\eta_0} \mathrm{d}\eta (\eta_0 - \eta) \frac{\partial \Psi_\ell}{\partial \eta} \right) \tag{3.123}$$

$$A_{2m} = 2\epsilon_2 Q_2 = 2\epsilon_2 \left(\int_{\eta_d}^{\eta_0} \mathrm{d}\eta (\eta_0 - \eta)^2 \frac{\partial \Psi_\ell}{\partial \eta} \right) \tag{3.124}$$

4 Numerical Evaluation and Applications

4.1 Evaluating CMB anisotorpies by stochastic fluctuations of ScmDE

The expectation value in (3.76) can be decomposed into products of two-point functions by using the Wick-theorem in Eq. (3.48) and calculated by using the two-point correlation function in Eq. (2.43). The details of the calculation are given can be referred in Appendix E, following which one obtains

$$\left\langle \frac{\Delta T}{T}(\boldsymbol{\gamma})\frac{\Delta T}{T}(\boldsymbol{\gamma}')\right\rangle = \int_0^1 da_j \int_0^1 da_{j'}\mathcal{I}(a_j)\mathcal{I}(a_{j'}) \times (-4\epsilon)\varphi^2(\eta_{j+2})\varphi^2(\eta_{j'+2})\left[-\frac{2}{3}R_jR_{j'}\cos\psi - \frac{2}{15}R_j^2R_{j'}^2\left(\frac{3}{2}\cos^2\psi - \frac{1}{2}\right)\right], \tag{4.125}$$

Here, $\mathcal{I}(a)$ are integration functions defined for simplicity of writing as

$$\mathcal{I}(a_j) \equiv 4\pi G m_0^2 \frac{\partial}{\partial a_j}\frac{1}{F(a_j)}\int_0^{a_j} da_{j+2}\frac{F(a_{j+2})}{3a_{j+2}H^2(a_{j+2})} \tag{4.126}$$

for $j = 1, 2$ (and generally $j \neq j'$), where $H(a)$ is the Hubble parameter. Moreover, the geodesic distances and $R_j = \sqrt{-K}(\eta_0 - \eta_{j+2})$, and $\eta_j(a_j)$ is a function of a_j, and its explicit form can be given by recollecting that, the conformal time η and scale factor a are related by

$$\frac{1}{a^2}\frac{da}{d\eta} = H(a), \tag{4.127}$$

where the evolution of the Hubble parameter obeys the Friedmann equation Eq. (2.27).

When the dark energy as ScmDE is considered to be close to the cosmological constant with small random spatial fluctuations, one may express the background expansion rate similar to standard ΛCDM model as

$$H(a) = \sqrt{\frac{8\pi G}{3}(\rho_m + \rho_{\rm DE}) - \frac{K}{a^2}} \equiv H_0\left(\frac{\Omega_m}{a^3} + \frac{\Omega_K}{a^2} + (1 - \Omega_m - \Omega_K)\right)^{1/2}. \tag{4.128}$$

If one assumes an open but nearly flat FLRW universe by adopting $\Omega_m \approx 0.3$, $\Omega_\Lambda \approx 0.7$, and $\Omega_K \approx 0$, the equation for late-time expansion of the interest here recovers Eq. (2.30). Given Eq. (4.127), the conformal time $\eta(a)$ is written as

$$\eta(a) = \int_0^a \frac{da'}{a'^2 H(a')} = H_0^{-1}\int_0^a \frac{da'}{a'^2(1 - \Omega_m + \Omega_m a'^{-3})^{1/2}}. \tag{4.129}$$

Following Sec. 3.1.2, the multipole expansion of two-point function of the CMB temperature fluctuation yields

$$\left\langle \frac{\Delta T}{T}(\boldsymbol{\gamma})\frac{\Delta T}{T}(\boldsymbol{\gamma}')\right\rangle = \frac{1}{4\pi}\sum_{\ell}(2\ell+1)C_\ell P_\ell(\cos\psi), \tag{4.130}$$

where $\cos\psi = \boldsymbol{\gamma}\cdot\boldsymbol{\gamma}'$ is the cosine angle included by different line-of-sights. Then, by comparing Eqs. (4.125) and (4.130), it is explicit to find

$$\frac{3}{4\pi}C_1 = S_1^2\frac{8}{3}\epsilon \sim \mathcal{O}(\epsilon\Omega_K), \tag{4.131}$$

$$\frac{5}{4\pi}C_2 = S_2^2\frac{8}{15}\epsilon \sim \mathcal{O}(\epsilon\Omega_K^2), \tag{4.132}$$

where the coefficients S_ℓ are defined as

$$S_\ell = \int_0^1 da\left(\sqrt{-K}(\eta_0-\eta(a))\right)^\ell \frac{\partial}{\partial a}\left(\frac{1}{F(a)}\int_0^a da'\frac{8\pi G\rho_{\rm DE}(a')F(a')}{3a'H^2(a')}\right), \tag{4.133}$$

where relation $\rho_{\rm DE}(a) = m_0^2\varphi^2/2$ is used for the dark energy density.

With $\eta(a)$ and $H(a)$ for ScmDE provided in Eq. (4.128) and Eq. (4.129), one can write S_ℓ defined by Eq. (4.133) more explicitly as

$$S_\ell = \int_0^1 da\left(\sqrt{-K}(\eta_0-\eta(a))\right)^\ell \frac{\partial}{\partial a}\left(\frac{G(a)}{F(a)}\right), \tag{4.134}$$

with

$$G(a) = \int_0^a da'\frac{8\pi G\rho_{\rm DE}(a')F(a')}{3a'H^2(a')} = \int_0^a da'\frac{(1-\Omega_m)a'^2F(a')}{\Omega_m+(1-\Omega_m)a'^3}, \tag{4.135}$$

where $F(a)$ is further defined as

$$F(a) = F_c\exp\left\{\int_0^a\frac{da'}{a'}\left(1+\frac{3\Omega_m}{2[\Omega_m+(1-\Omega_m)a'^3]}\right)\right\} \equiv \frac{F_c a^{5/2}}{\sqrt{\Omega_m+(1-\Omega_m)a^3}}. \tag{4.136}$$

An approximate expression for S_ℓ can be obtained by substituting Eqs. (4.135), (4.136) and (4.129) into Eq. (4.134), evaluate higher multipoles in a similar manner, which are approximately given by

$$C_\ell \sim \mathcal{O}(\epsilon\Omega_K^\ell). \tag{4.137}$$

These higher multipoles with $\ell \geq 3$ do not put tighter constraints compared to the dipole and the quadrupole as long as $\Omega_K \ll 1$. Thus, the dipole and the quadrupole are the most important, which is reflected by the property that the typical scales of the spatial variation are given by the supercurvature scale.

Now, one is able to evaluate the numerical integration over a and find out that numerical calculations of S_ℓ give the following results

$$S_1 \simeq 1.1 \times 10^{-1} \Omega_K^{1/2}, \tag{4.138}$$

$$S_2 \simeq 0.9 \times 10^{-1} \Omega_K, \tag{4.139}$$

where $\Omega_m = 0.3$ and $\Omega_K \ll 1$ are assumed.

The observed values of the dipole and the quadrupole in the CMB anisotropies are found in the literature. The dipole of the CMB is approximately expressed as

$$\frac{\delta T_{\rm dipole}}{T} = \frac{v}{c} \cos\theta, \tag{4.140}$$

where v is the peculiar velocity of the observer and $\cos\theta$ is the parameter related to the line-of-sight. The raw observational result gives $v \approx 370$km/s [61, 62]. From this observation, one may adopt the value of the dipole moment,

$$C_1^{\rm obs} \approx 6.3 \times 10^{-6} \tag{4.141}$$

using $3C_1/4\pi = (v/c)^2$. Comparing this with (4.131) and (4.138), one can obtain a preliminary constraint from the dipole

$$\epsilon \Omega_K \lesssim 4.9 \times 10^{-5}. \tag{4.142}$$

The observations on C_2 from the Planck Legacy Archive obtained by Planck experiment[‡] with 1σ error is

$$\frac{2 \times 3}{2\pi} C_2^{\rm obs} = 2.26^{+5.33}_{-1.32} \times \frac{10^2 \mu{\rm K}^2}{(2.725{\rm K})^2}. \tag{4.143}$$

By adopting the upper bound of the above observed value, taking the maximum advantage from the room by the observational error, one may constrain the quadrupole as

$$\frac{2 \times 3}{2\pi} C_2^{\rm obs} < 1.0 \times 10^{-10}. \tag{4.144}$$

[‡]Based on observations obtained with Planck (http://www.esa.int/Planck), an ESA science mission with instruments and contributions directly funded by ESA Member States, NASA, and Canada.

Then combining Eq. (4.144) with (4.132) and Eq. (4.139) leads to

$$\epsilon\Omega_K^2 < 1.0 \times 10^{-8}. \tag{4.145}$$

The constraints given by Eqs. (4.212) and (4.213) contain the parameter ϵ describing some properties of the ancestor vacuum Eq. (2.42) along with the curvature parameter Ω_K. The two parameters Ω_K and ϵ are coupled to each other in Eqs. (4.212) and (4.213), which are natural outcomes because this scenario connects the spatial curvature with the supercurvature-mode dark energy through the CDL tunneling inflation. Consequently, the constraint on the ancestor vacuum parameter ϵ is linked with the value of the spatial curvature Ω_K. The upper bound of the spatial curvature is given by $|\Omega_K| \lesssim 10^{-2} \sim 10^{-3}$ [16], and if one takes the possible value with BAO for $\Omega_K \sim 10^{-3}$, the parameter related to the ancestor vacuum in the open inflation scenario of ScmDE is constrained to satisfy the relation $\epsilon \lesssim 10^{-2}$. However, in the flat approximation limit where $\Omega_K \to 0$, there is only a very weak constraint on ϵ, and the conditions making supercurvature mode of ultralight scalar field ϕ to produce and to stay almost constant serving as ScmDE may need reconsideration, which also motivated the formulation of the dark energy with large-scale inhomogeneities in general cases.

4.2 Numerical solutions for the general dark energy with large-scale inhomogeneities

In this section, let us consider the concrete handling for solving the ϕ evolution of dark energy given in Sec. 3.2 next, both for the background and the perturbations. Since the late-time evolution after last-scattering of photons, or photon decoupling from the Compton scatterings with electrons during recombination epoch ($a_d \sim 1/1100$), is the interest here, one can find the analytic approximations in the matter-dominant epoch, and determine the initial conditions in epochs $1 \gg a_i \gtrsim a_d$ for numerical evaluations.

4.2.1 Equations governing the background

Firstly, one must solve the background evolution described by Eq. (3.106)–(3.109) of the system before considering about the perturbations. The solutions should basically yield the observational constraints that near-to-ΛCDM models are favored. Moreover, one must utilize the observed the value of Hubble expansion rate of present epoch to calibrate the value of dark energy density from scalar field ϕ.

4.2.1.1 As functions of the dimensionless time $\tilde{t}$

In order to parametrize and normalize the equations describing the cosmological evolution in the model, it will be beneficial to define the following quantities:

$$\tilde{t} \equiv H_0 t, \tag{4.146}$$

$$\widetilde{\phi}_0 \equiv \phi_0/\overline{\phi}_0, \tag{4.147}$$

$$\widetilde{r} \equiv \frac{1}{6}\left(\overline{\phi}_0/M_{\rm pl}\right)^2, \tag{4.148}$$

$$\widetilde{m} \equiv m_\phi/H_0. \tag{4.149}$$

Following this one can obtain ordinary differential equations for the background from equations given in Sec.3.2 using $\tilde{t}$ as variable as

$$\widetilde{r}\widetilde{m}^2\widetilde{\phi}_0^2(\tilde{t}) + \widetilde{r}\left(\frac{\mathrm{d}\widetilde{\phi}_0}{\mathrm{d}\tilde{t}}\right)^2 + \Omega_m a^{-3} = \left(\frac{1}{a}\frac{\mathrm{d}a}{\mathrm{d}\tilde{t}}\right)^2, \tag{4.150}$$

$$\frac{\mathrm{d}^2\widetilde{\phi}_0}{\mathrm{d}\tilde{t}^2} + 3\frac{1}{a}\frac{\mathrm{d}a}{\mathrm{d}\tilde{t}}\frac{\mathrm{d}\widetilde{\phi}_0}{\mathrm{d}\tilde{t}} + \widetilde{m}^2\widetilde{\phi}_0 = 0. \tag{4.151}$$

H_0 is the Hubble expansion rate today, the Hubble constant, and $\overline{\phi}_0$ is the average value of ϕ_0.

It is worth noting here that according to our definition in Eq. (4.146) to (4.149), there are actually two degrees of freedom for the parameters, namely $\widetilde{m}$ and $\widetilde{r}$, relating to the mass and energy scale of the dark energy field ϕ respectively. They correspond to the fact that the unknown component in our model, dark energy ϕ, can be fundamentally determined by two degrees of freedom to characterize the shape of its potential $V(\phi) = {m_\phi}^2\phi^2/2$, while the properties of other components (e.g. matter) are considered as known under the standard cosmological model.

Back to our focus on the solution, in search of initial conditions and the analytic approximations in the limit $a \ll 1$, Eq. (4.150) approaches to

$$\left(\frac{1}{a}\frac{\mathrm{d}a}{\mathrm{d}\tilde{t}}\right)^2 = \Omega_m a^{-3}, \tag{4.152}$$

which has the analytic solution

$$\tilde{t} = \frac{2}{3}\frac{a^{\frac{3}{2}}}{\sqrt{\Omega_m}} \qquad \text{or} \qquad a = \left(\frac{9}{4}\Omega_m\right)^{\frac{1}{3}}\tilde{t}^{\frac{2}{3}}. \tag{4.153}$$

Inserting this into Eq. (4.151) gives

$$\frac{\mathrm{d}^2\widetilde{\phi}_0}{\mathrm{d}\tilde{t}^2} + 2\frac{1}{\tilde{t}}(\frac{\mathrm{d}\widetilde{\phi}_0}{\mathrm{d}\tilde{t}}) + \widetilde{m^2}\widetilde{\phi}_0 = 0, \tag{4.154}$$

which has the general solution

$$\widetilde{\phi}_0(\tilde{t}) = C_1\frac{\sin(\widetilde{m}\tilde{t})}{\widetilde{m}\tilde{t}} + C_2\frac{\cos(\widetilde{m}\tilde{t})}{\widetilde{m}\tilde{t}}. \tag{4.155}$$

The cosine part diverges in the limit $a \ll 1$, which has to be abandoned in search of physical initial conditions, hence one writes

$$\widetilde{\phi}_0(\tilde{t}) = C_1\frac{\sin(\widetilde{m}\tilde{t})}{\widetilde{m}\tilde{t}}, \tag{4.156}$$

and understands

$$\widetilde{\phi}_0(\tilde{t}\to 0) = \lim_{\tilde{t}\to 0} C_1\frac{\sin(\widetilde{m}\tilde{t})}{\widetilde{m}\tilde{t}} = C_1 \tag{4.157}$$

is the initial condition.

However, the initial value of C_1 is not self-evident, and should be determined with the constraints on dark energy density of the present epoch inferred from the cosmological observations. The constraint by the present Hubble rate to fix $\tilde{t}_0$ by definitions is

$$a(\tilde{t}_0) = a(t_0) \equiv 1, \tag{4.158}$$

$$H(\tilde{t}_0) = H(t_0) \equiv H_0, \tag{4.159}$$

where t_0 is the proper cosmic time for the present epoch. Inserting this into Eq. (4.150) actually gives

$$1 - \Omega_m = \widetilde{r}\widetilde{m}^2\left(\widetilde{\phi}_0\Big|_{\tilde{t}=\tilde{t}_0}\right)^2 + \widetilde{r}\left(\frac{\mathrm{d}\widetilde{\phi}_0}{\mathrm{d}\tilde{t}}\Big|_{\tilde{t}=\tilde{t}_0}\right)^2. \tag{4.160}$$

Eq. (4.160) is the condition to calibrate the dark energy density observed today when solving the background. Together with Eq. (4.150) and (4.151) the system is now prepared for numerical evaluation to obtain the evolution of $a(\tilde{t})$ and $\widetilde{\phi}_0(\tilde{t})$. Note that one is mainly interested in the late-time evolution here, hence one may decide the initial value for independent variables $\tilde{t}$ or a (to be discussed later) manually as a typical value, for example

$a_i = a_d \approx 1/1100$ at the photon decoupling or the last scattering, by use of Eq. (4.153). These solutions are the background evolutions one must rely on in order to solve for the perturbations concerning $\ell = 1$ dipole component and $\ell = 2$ quadrupole component of the inhomogeneities that the dark energy ϕ produces.

It is worth mentioning that Eq. (4.160) also provides with a baseline to choose the parameters $\widetilde{m}$ and $\widetilde{r}$ from the various parameter space. In the case of cosmological constant Λ, $\mathrm{d}\widetilde{\phi}_0/\,\mathrm{d}\tilde{t}$ is always vanishing, leaving

$$1 - \Omega_m = \widetilde{r}\widetilde{m}^2 \left(\widetilde{\phi}_0 \Big|_{\tilde{t}=\tilde{t}_0} \right)^2. \tag{4.161}$$

Thus if one takes the dimensionless field in present epoch normalized as $\widetilde{\phi}_0(\tilde{t} = \tilde{t}_0) \sim \mathcal{O}(1) \equiv 1$, a special baseline for the choice of parameters approximating the ΛCDM model will writes

$$\widetilde{r}\widetilde{m}^2 = 1 - \Omega_m. \tag{4.162}$$

However, this condition for parameter choice is not a necessity to solve for the system, and the parameters may deviate from this baseline, showing possible interesting behaviors beyond standard ΛCDM cosmology.

4.2.1.2 As functions of the scale factor a

As the scale factor a of the universe is more commonly used than the dimensionless time $\tilde{t}$ defined in the preivous section, one can write out the dimensionless equations as functions of scale factor a, which may also serve as a reconfirmation of the previous subsection. The equations using a as variable are

$$\left[1 - \widetilde{r}a^2 \left(\frac{\mathrm{d}\widetilde{\phi}_0(a)}{\mathrm{d}a} \right)^2 \right] \widetilde{H}^2(a) = \widetilde{r}\widetilde{m}^2 \widetilde{\phi}_0^2(a) + \Omega_m a^{-3}, \tag{4.163}$$

$$a^2 \widetilde{H}^2 \frac{\mathrm{d}^2\widetilde{\phi}_0}{\mathrm{d}a^2} + a^2 \widetilde{H} \frac{\mathrm{d}\widetilde{H}}{\mathrm{d}a} \frac{\mathrm{d}\widetilde{\phi}_0}{\mathrm{d}a} + 4a\widetilde{H}^2 \frac{\mathrm{d}\widetilde{\phi}_0}{\mathrm{d}a} + \widetilde{m}^2 \widetilde{\phi}_0 = 0, \tag{4.164}$$

with

$$\widetilde{H}(a) \equiv \frac{H(a)}{H_0}. \tag{4.165}$$

From Eq. (4.163) the dimensionless expansion rate can be written as

$$\widetilde{H}(a) = \sqrt{\frac{\widetilde{r}\widetilde{m}^2 \widetilde{\phi}_0^2(a) + \Omega_m a^{-3}}{1 - \widetilde{r}a^2 \left(\mathrm{d}\widetilde{\phi}_0(a)/\,\mathrm{d}a \right)^2}}. \tag{4.166}$$

Defining notation for the derivative with respect to the scale factor a for simplicity

$$\frac{\partial(\quad)}{\partial a} \equiv (\quad)', \tag{4.167}$$

then the background equation Eq. (4.164) becomes

$$a^2\widetilde{H}^2\widetilde{\phi}_0'' + \left(4a\widetilde{H}^2 + a^2\widetilde{H}\widetilde{H}'\right)\widetilde{\phi}_0' + \widetilde{m}^2\widetilde{\phi}_0 = 0. \tag{4.168}$$

Insert Eq. (4.166) into Eq. (4.168) and simplify, the background equation to be solved is

$$\widetilde{m}^2a^2\widetilde{\phi}_0(1-\widetilde{r}a^2\widetilde{\phi}_0'^2) + \widetilde{m}^2\widetilde{r}a^3\widetilde{\phi}_0^2\left(4\widetilde{\phi}_0' - 3\widetilde{r}a^2\widetilde{\phi}_0'^3 + a\widetilde{\phi}_0''\right) + \frac{\Omega_m}{2}\left(5\widetilde{\phi}_0' - 3\widetilde{r}a^2\widetilde{\phi}_0'^3 + 2a\widetilde{\phi}_0''\right) = 0, \tag{4.169}$$

where initial conditions for $\widetilde{\phi}_0(a)$ is necessary to solve for $\widetilde{\phi}_0(a)$, and in turn for $\widetilde{H}(a)$.

Again, consider the analytic approximation for initial conditions. When $a \ll 1$, Eq. (4.166) simply approaches to

$$\widetilde{H} = \sqrt{\Omega_m}a^{-3/2}. \tag{4.170}$$

Inserting this into Eq. (4.168) and simplifying will lead to

$$a\widetilde{\phi}_0'' + \frac{5}{2}\widetilde{\phi}_0' + \widetilde{m}^2a^2\Omega_m^{-1}\widetilde{\phi}_0 = 0, \tag{4.171}$$

which can be solved analytically as

$$\widetilde{\phi}_0(a) = C_1\frac{3\sqrt{\Omega_m}}{2\widetilde{m}a^{3/2}}\sin\left(\frac{2\widetilde{m}a^{3/2}}{3\sqrt{\Omega_m}}\right), \tag{4.172}$$

which is actually identical to Eq. (4.156) by recalling Eq. (4.153).

Then one will be able to infer

$$\widetilde{\phi}_0(a \to 0) = \text{const.}, \tag{4.173}$$

$$\widetilde{\phi}_0'(a \to 0) = 0, \tag{4.174}$$

are the appropriate initial conditions for the system, which are virtually consistent with the equations using dimensionless time $\tilde{t}$ as the independent variable.

Now one can solve for $\widetilde{\phi}_0(a)$ numerically under two degrees of freedom for the choice of parameters $\widetilde{m}$ and $\widetilde{r}$. Examples of the solutions under the conditions that allow the recovery of the models close to the ΛCDM universe are presented in Figs. 1–8. To investigate the impact of parameter choices on the background solutions more specifically,other sets of parameters are also put into numerical calculations. Table 1 provides the parameter sets that have been investigated in the numerical evaluations.

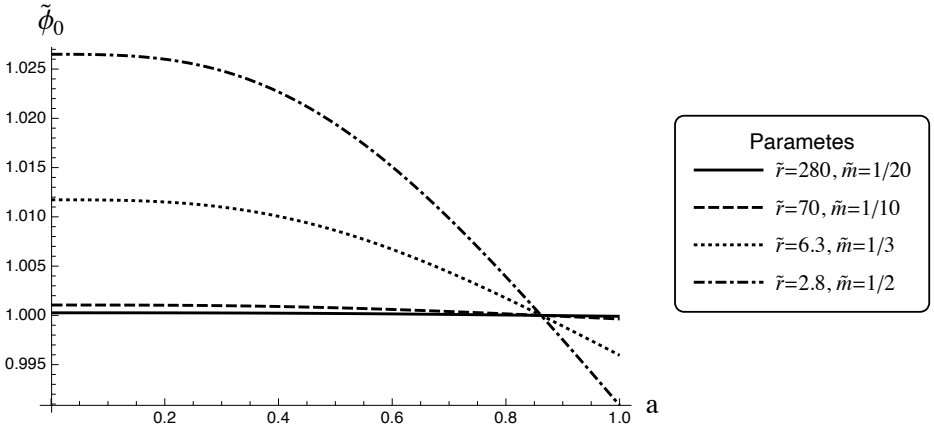

Figure 5: The evolution of the dark energy background $\tilde{\phi}_0(a)$ as a function of scale factor a under different conditions for $\widetilde{r}$ and $\widetilde{m}$ presented in the figure, which imitate ΛCDM universes under condition Eq. (4.162) with $\Omega_m = 0.3$ fixed. Moreover, in all following figures, unless specially specified, $\Omega_m = 0.3$ is assumed to be fixed (see also Table 1). Note that different models have different initial values for $\tilde{\phi}_0$ due to dark energy density fixing from the observed Hubble rate H_0 today. Since $\widetilde{m}$ is defined by the ratio of the mass of field today to the Hubble horizon today in Eq. (4.149), one can observe from the figure that the lighter field ϕ is, it appears to be more "frozen" in the evolutionary history of its energy density. Here the $\widetilde{m} = 1/20$, $\widetilde{r} = 280$ case is most similar to a cosmological constant Λ among the models.

Some typical figures showing how parameters $\widetilde{r}$, $\widetilde{m}$, and Ω_m can affect the evolution of the background solution and the equation of state as a function of a are presented as Figs. 5–8 and in Figs. 9–12, respectively.

Fig. 5 shows the impact of the parameter choice on the behavior of the solution for $\tilde{\phi}_0(a)$ in the cases following Eq. (4.162), where models close to the ΛCDM cosmologies are expected. Fig. 6 shows how the parameters $\widetilde{r}$ and $\widetilde{m}$ affect the behaviors of $\tilde{\phi}_0$, while Fig. 8 shows that for and $\widetilde{\Omega}_m$.

The behaviors of the $\widetilde{\phi}_0$ curves in these figures can be understood as follows: From Eqs. (4.150) and (4.160)

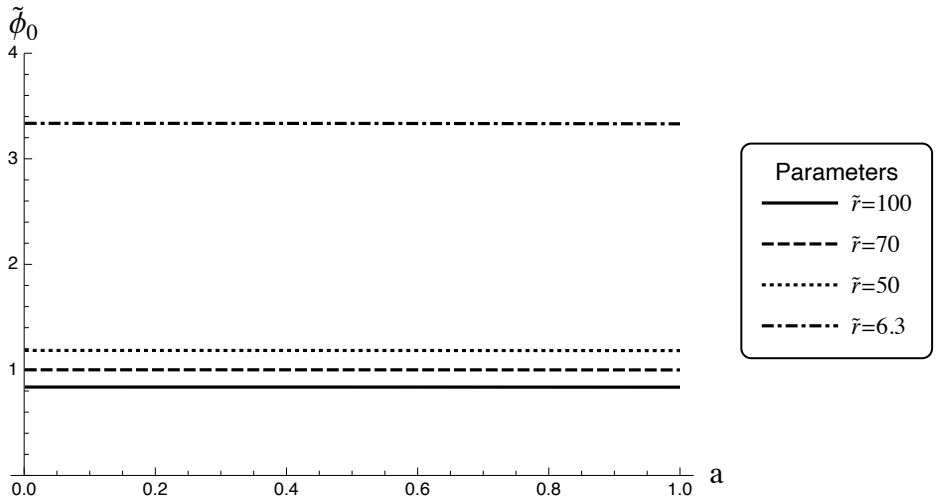

Figure 6: The impact of the value of $\widetilde{r}$ on the evolution of the background solution $\tilde{\phi}_0(a)$ as a function of a. According to Eq. (4.148), $\widetilde{r}$ is related to the energy scale of the scalar field ϕ. The figure shows the cases where the energy scale $\overline{\phi}$ of the scalar field ϕ is beyond the Planck scale, while even for $\widetilde{r} = 1/70$, hence $\overline{\phi} \sim M_{\rm pl}$, the behavior of the evolution is similar (almost constant) with a higher value.

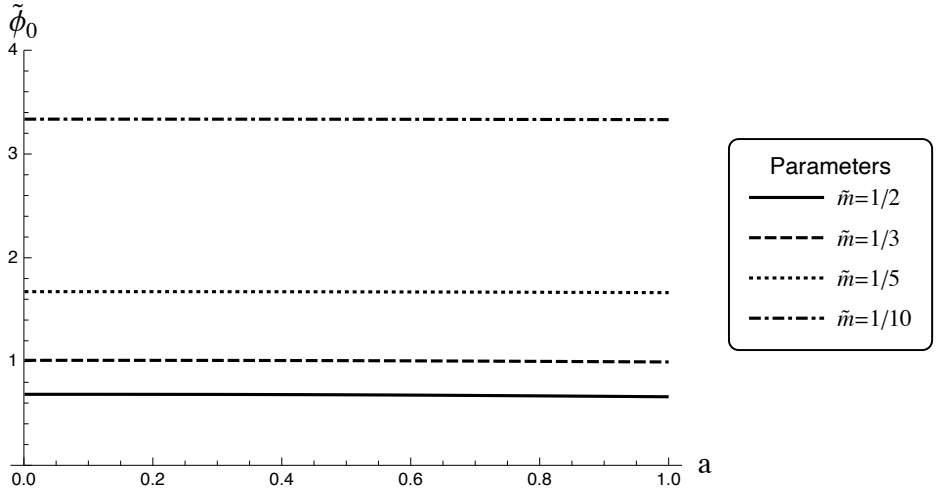

Figure 7: The impact of the value of $\widetilde{m}$ on the evolution of the background solution $\tilde{\phi}_0(a)$ as a function of a. Recalling Eq. (4.149), $\widetilde{m}$ is related to the field mass compared with the horizon scale today. Here $\tilde{r} = 6.3$ and $\Omega_m = 0.3$

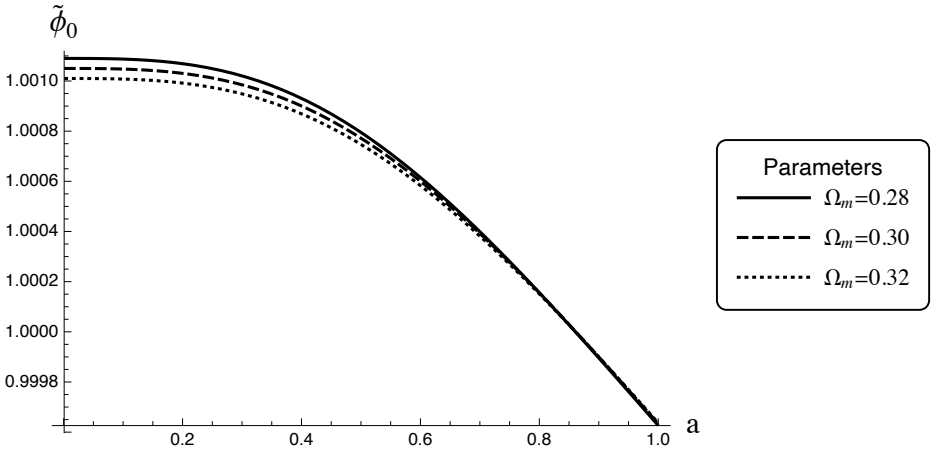

Figure 8: The impact of Ω_m on the evolution of the background solution $\tilde{\phi}_0(a)$. As expected, Ω_m only alter the evolution to a slight extent, hence suggesting that the model solutions are robust against changes in Ω_m calibration from observations. Herewhile fixing $\widetilde{m} = 1/10$, for $\Omega_m = 0.28$, $\tilde{r} = 72$ and for $\Omega_m = 0.32$, $\tilde{r} = 68$ holds respectively.

one can see that the parameter $\widetilde{r}$ can actually be absorbed into the amplitude of $\widetilde{\phi}_0$ as a rescaling factor, namely

$$\widetilde{m}^2(\sqrt{\widetilde{r}}\widetilde{\phi}_0)^2 + \left(\frac{\mathrm{d}(\sqrt{\widetilde{r}}\widetilde{\phi}_0)}{\mathrm{d}\tilde{t}}\right)^2 = \left(\frac{1}{a}\frac{\mathrm{d}a}{\mathrm{d}\tilde{t}}\right)^2 - \Omega_m a^{-3}, \tag{4.175}$$

with

$$1 - \Omega_m = \widetilde{m}^2(\sqrt{\widetilde{r}}\widetilde{\phi}_0\Big|_{a=1})^2 + (\sqrt{\widetilde{r}}\widetilde{\phi}_0'\Big|_{a=1})^2. \tag{4.176}$$

These two equations facilitates to understand why only changing $\widetilde{r}$ with other parameters fixed only alters the value of $\widetilde{\phi}_0$ without causing a nontrivial difference in the characteristic behaviors of the curves in Fig. 6.

Moreover, when one evaluates $\widetilde{\phi}_0$, choosing the condition in Eq. (4.162) close to the ΛCDM model as a baseline for the natural choices of the parameters, the condition

$$\frac{\mathrm{d}(\sqrt{\widetilde{r}}\widetilde{\phi}_0)}{\mathrm{d}\tilde{t}} \ll 1 \qquad \text{or} \qquad \sqrt{\widetilde{r}}\widetilde{\phi}_0' \ll 1 \tag{4.177}$$

always holds. Hence, it follows Eq. (4.175) that

$$(\sqrt{\widetilde{r}}\widetilde{m}\widetilde{\phi}_0)^2 \simeq \left(\frac{1}{a}\frac{\mathrm{d}a}{\mathrm{d}\tilde{t}}\right)^2 - \Omega_m a^{-3}. \tag{4.178}$$

Due to similar arguments on $\widetilde{r}$, it can be understood that, to some extent, $\widetilde{m}$ also works as a rescaling factor for the background $\widetilde{\phi}_0$, which explains the behavior of $\widetilde{\phi}_0$ in Fig. 6. At the same time, the appearance of Ω_m on the right-hand side of Eq. (4.178) explains the dependence of the background solution $\widetilde{\phi}_0$ on Ω_m in Fig. 8.

Now, let us discuss the parameter dependence of the dark energy EoS $\omega_\phi(a)$, as shown in Fig. 9 and Fig. 10. It may be concluded that the background dark energy EoS $\omega_\phi(a)$ is almost independent of $\widetilde{r}$; in contrast, $\widetilde{m}$ is the main influencing factor. There is also slight dependence on the cosmological parameter Ω_m, shown in Fig. 10. These behaviors can be understood using Eqs. (4.179)–(4.182) as an analogy to the CPL parametrization.

Following Eq. (3.92), one writes

$$\begin{aligned}\omega_\phi &= -\frac{m_\phi^2 a^2\phi^2 - \dot{\phi}^2}{m_\phi^2 a^2\phi^2 + \dot{\phi}^2} \\ &= -1 + \frac{2}{m_\phi^2 a^2(\phi/\dot{\phi})^2 + 1} \\ &\equiv -1 + 2W(a),\end{aligned} \tag{4.179}$$

where $'$ denotes the derivative of the scale factor a, $' \equiv \partial/\partial a$, where

$$W(a) \equiv \frac{1}{m_\phi^2 a^2(\phi/\dot{\phi})^2 + 1} = \frac{a^2}{(m_\phi/H)^2(\phi/\phi')^2 + a^2}. \tag{4.180}$$

At the background level assuming $\widetilde{\phi} \simeq \widetilde{\phi}_0$, one can further write

$$W(a) \simeq \frac{\widetilde{\phi}_0'^2 a^2 \widetilde{H}^2}{\widetilde{m}^2\widetilde{\phi}_0^2 + \widetilde{\phi}_0'^2 a^2 \widetilde{H}^2}. \tag{4.181}$$

Recall that $\widetilde{H}(a)$ is defined in Eq. (4.166), which depends on the values of $\widetilde{r}$, $\widetilde{m}$, and Ω_m. Because $\widetilde{m}^2$ is typically small in our model, using Eq. (4.166) and expanding to the order of $\mathcal{O}(\widetilde{m}^2)$, it follows that

$$\begin{aligned}W(a) &\simeq 1 - \frac{a\widetilde{m}^2}{\Omega_m}\left(\frac{\tilde{\phi}_0^2}{\tilde{\phi}_0'^2}\right)\left(1 - \widetilde{r}a^2\tilde{\phi}_0'^2\right) \\ &\simeq 1 - \frac{a\widetilde{m}^2}{\Omega_m}\left(\frac{\tilde{\phi}_0^2(a)}{\tilde{\phi}_0'^2(a)}\right),\end{aligned} \tag{4.182}$$

which can be numerically evaluated with $\widetilde{\phi}_0(a)$ and $\widetilde{\phi}_0'(a)$ as demonstrated in Sec. 4.2. The second line stands because $a^2\tilde{\phi}_0'^2$ is small and negligible for $0 < a < 1$ in almost all cases. Then, one can understand that $\widetilde{r}$ hardly affects the background EoS of the dark energy.

Fig. 11 shows a slight dependence on Ω_m for the expansion rate $\widetilde{H}(a)$ as a function of the scale factor for $0.5 < a < 1$, while Fig. 12 shows a possible impact on the future expansion rate from the mass parameter $\widetilde{m}$.

To explain these behaviors for $\widetilde{H}(a)$, let us consider the analytic approximation of $\widetilde{H}(a)$ starting from Eq. (4.166). For models close to the ΛCDM model, where $\widetilde{\phi}_0 \simeq$ const. and $\widetilde{\phi}_0' \simeq 0$ with Eq. (4.162), reading $\widetilde{r}\widetilde{m}^2 \simeq 1 - \Omega_m$ holds, one obtains

$$\widetilde{H}(a) \simeq \sqrt{(1-\Omega_m)\widetilde{\phi}_0^2 + \Omega_m a^{-3}}, \tag{4.183}$$

which is almost the same as the Hubble equation for the standard ΛCDM parametrization. Hence, it is obvious that Ω_m is the dominant parameter for the background expansion history when $0 < a < 1$.

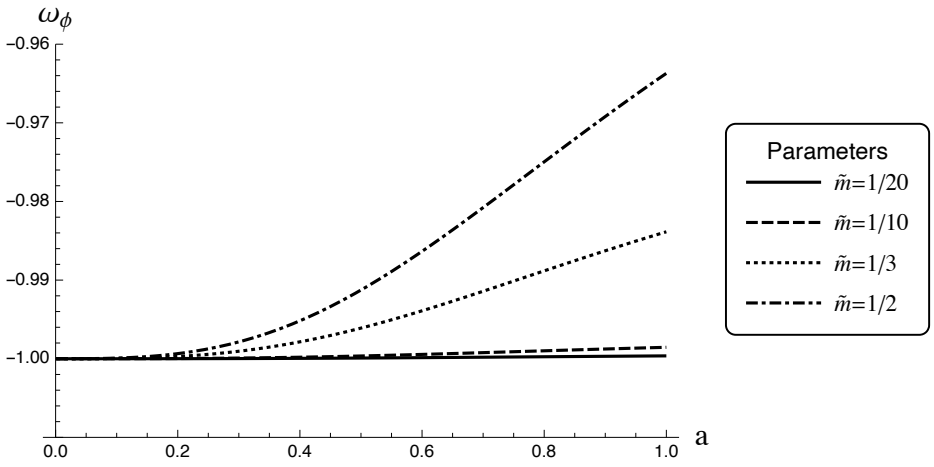

Figure 9: The evolution of the dark energy EoS $\omega_\phi(a)$ with the different sets of the parameters same with those in Fig. 5 are demonstrated here. According to Eq. (4.148), $\widetilde{r}$ is related to the value of the scalar field ϕ. And from Eq. (4.182), it is straightforward to see that $\widetilde{r}$ hardly affects the EoS of $\widetilde{\phi}_0$. The curves in this figure correspond to No. (1),(2),(7),(8) in Table 1, and the figure shows the influence of $\widetilde{m}$ on the EoS of $\widetilde{\phi}_0$ with fixed $\Omega_m = 0.3$.

4.2.2 Equations governing 1st order perturbations

Whereas the background has been solved, one is able to consider the numerical solution for the first-order equations characterizing the evolution of the perturbations in Eq. (3.110)–(3.115), where nonlinear coupling terms naturally arise as the effect of interactions of the perturbations with the background.

For the simplicity of notations, one may define the derivative with respect to the dimensionless time $\tilde{t}$ in

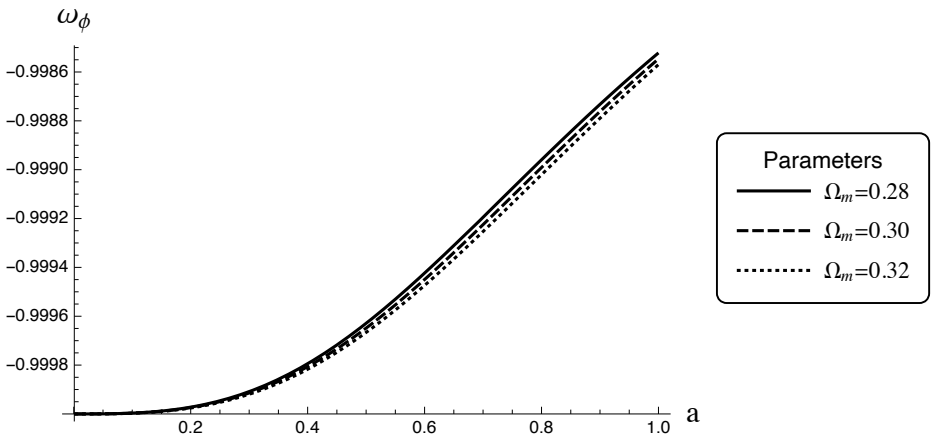

Figure 10: This figure demonstrates that for the EoS w_ϕ there is a weak dependence on cosmological parameter Ω_m, where $\widetilde{m} = 1/10$ and $\widetilde{r} = 70$ are fixed.

Eq. (4.146) as

$$\frac{\partial(\quad)}{\partial\tilde{t}} \equiv (\ \dot{}\ ) \qquad \text{and} \qquad \frac{\partial^2(\quad)}{\partial\tilde{t}^2} \equiv (\ \ddot{}\ ). \tag{4.184}$$

Moreover, define the perturbation to the matter density as

$$\rho_\ell \equiv \rho_0 \delta_\ell, \tag{4.185}$$

together with dimensionless quantity $\tilde{V}_\ell$ associated with the velocity as

$$\widetilde{V}_\ell \equiv H_0 V_\ell. \tag{4.186}$$

One may notice that the quantities without the over tilde notation are naturally dimensionless by definition, namely the density fluctuation δ_ℓ, and metric perturbations Ψ_ℓ, Φ_ℓ.

Subsequently, one may utilize the relations in Eqs. (3.110)–(3.115) to eliminate the quantities such as ρ_0 and ρ_ℓ, and use δ_ℓ to characterize the first-order matter perturbations as

$$\rho_0(a) = 3H_0^2 \Omega_m a^{-3} M_{\rm pl}^2, \tag{4.187}$$

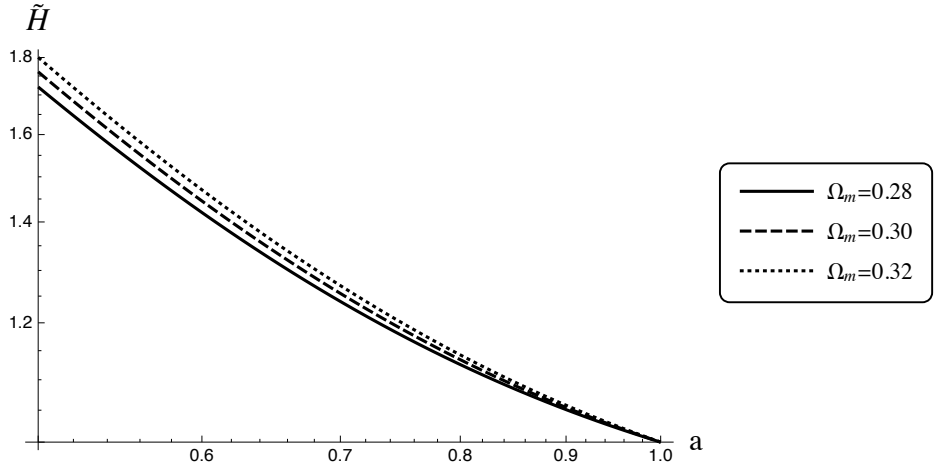

Figure 11: Examples of the late-time expansion history $\widetilde{H}(a)$ as a function of a for $0.5 \leq a \leq 1$ with different sets of Ω_m, $\widetilde{r} = 70$ and $\widetilde{m} = 1/10$ fixed. For the late-time expansion history in th past, only Ω_m is important.

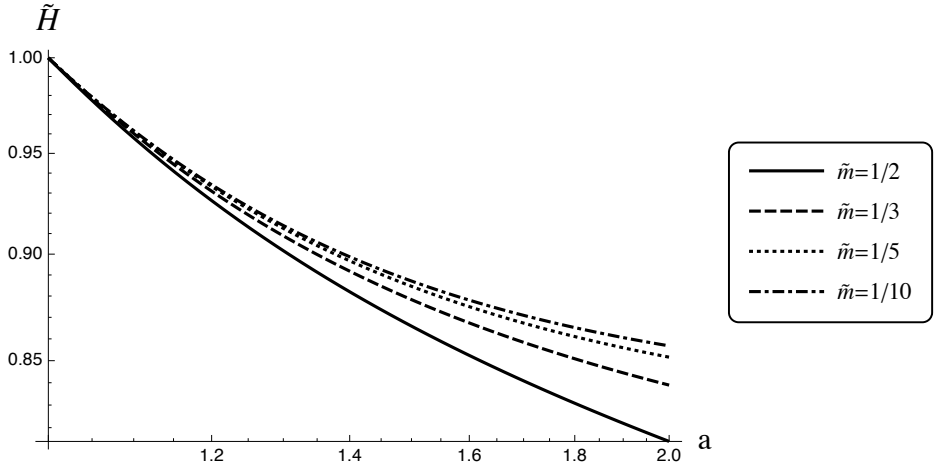

Figure 12: Future evolution of the expansion rate. The parameter $\tilde{m}$ is only important for future expansion when $1 \ll a$. The figure demonstrates examples of how the future expansion rate depends on $\widetilde{m}$ for $1 < a < 2$, where $\widetilde{r} = 6.3$ and $\Omega_m = 0.3$ are fixed.

thus the dimensionless differential equations as functions of $\tilde{t}$ will be

$$\check{\delta}_\ell + 3\check{\Phi}_\ell = 0, \tag{4.188}$$

$$\check{\widetilde{\phi}}_\ell + 3\frac{\check{a}}{a}\check{\widetilde{\phi}}_\ell + \widetilde{m}^2\widetilde{\phi}_\ell - 2\Psi_\ell\check{\widetilde{\phi}}_0 - 6\frac{\check{a}}{a}\check{\widetilde{\phi}}_0\Psi_\ell + (3\check{\Phi}_\ell - \check{\Psi}_\ell)\check{\widetilde{\phi}}_0 = 0, \tag{4.189}$$

$$\check{\widetilde{V}}_\ell - \Psi_\ell = 0, \tag{4.190}$$

$$-2\frac{\check{a}}{a}\Psi_\ell + 2\check{\Phi}_\ell + 3\widetilde{V}_\ell\Omega_m a^{-3} + 6\widetilde{r}\check{\widetilde{\phi}}_0\widetilde{\phi}_\ell = 0, \tag{4.191}$$

$$6(\frac{\check{a}}{a})^2\Psi_\ell - 6(\frac{\check{a}}{a})\check{\Psi}_\ell + 3\Omega_m a^{-3}\delta_\ell + 6\widetilde{r}\left(\widetilde{m}^2\widetilde{\phi}_0\widetilde{\phi}_\ell + \check{\widetilde{\phi}}_0\check{\widetilde{\phi}}_\ell - \Psi_\ell(\check{\widetilde{\phi}}_0)^2\right) = 0, \tag{4.192}$$

$$\left((\frac{\check{a}}{a})^2 + 2\frac{\check{\check{a}}}{a}\right)\Psi_\ell + \frac{\check{a}}{a}(\check{\Psi}_\ell - 3\check{\Phi}_\ell) - \check{\check{\Phi}}_\ell + 3\widetilde{r}\left(\widetilde{m}^2\widetilde{\phi}_0\widetilde{\phi}_\ell - \check{\widetilde{\phi}}_0\check{\widetilde{\phi}}_\ell + \Psi_\ell(\check{\widetilde{\phi}}_0)^2\right) = 0. \tag{4.193}$$

Notice that from Eq. (4.188)

$$\delta_\ell + 3\Phi_\ell = 0 \tag{4.194}$$

can be restored using the isocurvature initial conditions (see Appdendix B); additionally, if one assumes the general condition for the universe that the anisotropic stress is negligible, then

$$\Phi_\ell + \Psi_\ell \simeq 0. \tag{4.195}$$

Following this one can eliminate Φ_ℓ, Ψ_ℓ, as well as $\check{\widetilde{V}}_\ell$ using δ_ℓ with Eq. (4.190). Eventually, one may write two equations for δ_ℓ and $\tilde{\phi}_\ell$ to be solved explicitly, despite its subtly and triviality thus omitted here.

Again, one has to consider the initial conditions to solve for δ_ℓ and $\tilde{\phi}_\ell$. Firstly, recalling the definition in Eq. (3.80) and Eq. (4.147), one may generalized the dimensionless quantities as

$$\phi \equiv \overline{\phi}_0(\widetilde{\phi}_0 + \epsilon_1\widetilde{\phi}_1\sum_m P_i^{(m)}x^i + \epsilon_2\widetilde{\phi}_2\sum_m P_{ij}^{(m)}x^ix^j) \tag{4.196}$$

In the limit $a \ll 1$ (identically, $t \to 0, \widetilde{t} \to 0$), one may assume the power-law form for the time evolution of the perturbations as

$$\delta_\ell \equiv A_1\tilde{t}^\alpha, \tag{4.197}$$

$$\widetilde{\phi}_\ell \equiv \mathcal{D} + D_1\tilde{t}^\gamma. \tag{4.198}$$

Furthermore, Eq. (4.156) has already provided the initial condition for the background, that

$$\widetilde{\phi}_0(\tilde{t}) = C_1 \frac{\sin(\widetilde{m}\tilde{t})}{\widetilde{m}\tilde{t}} \approx C_1(1 - \frac{\widetilde{m}^2\tilde{t}^2}{6}) \equiv F(1 - \frac{\widetilde{m}^2\tilde{t}^2}{6}). \tag{4.199}$$

For a given $\widetilde{m}$ and $\widetilde{r}$, one may solve for the background and fix the value for C_1 or F in Sec. 4.2.1, hence F may be taken as a known quantity here. Another recollection of the relation is from Eq. (4.153), the background analytical approximation for the scale factor a,

$$a = \left(\frac{9}{4}\Omega_m\right)^{\frac{1}{3}} \tilde{t}^{\frac{2}{3}} \equiv B\tilde{t}^{\frac{2}{3}}, \quad \tilde{t} = \left(\frac{a}{B}\right)^{\frac{3}{2}}.$$

Inserting the ansatz Eqs. (4.197)–(4.199) into Eq. (4.189)–(4.193) will lead to equations as functions of a or $\tilde{t}$ relating the unknown coefficients α,γ,A_1,$\mathcal{D}$, D_1 that remain to be explored. For the early limit $a \to 0$ or $\tilde{t} \to 0$ (in matter dominant epoch), by examining the leading order terms of a for each equation, the following relation may be exploited:

$$\alpha = \gamma = 2, \tag{4.200}$$

$$D_1 = -\frac{1}{6}\widetilde{m}^2\mathcal{D}, \tag{4.201}$$

$$A_1 = -\frac{27}{22}\widetilde{m}^2\widetilde{r}F\mathcal{D}, \tag{4.202}$$

where $\mathcal{D}$ may be understood as the amplitude of each mode of the perturbations as ϵ_1 and ϵ_2, which will be constrained later with the observational data. For now, $\mathcal{D} = 1$ may be set for the interest of the numerical solution.

Further, the analytic approximations for the evolution of the perturbations in the limit $a \ll 1$ ($t \to 0, \widetilde{t} \to 0$) are found as

$$\delta_\ell \simeq -\frac{27}{22}\mathcal{D}\widetilde{m}^2\widetilde{r}F\tilde{t}^2 = -\frac{27}{22}\widetilde{m}^2\widetilde{r}F\tilde{t}^2, \tag{4.203}$$

$$\widetilde{\phi}_\ell \simeq \mathcal{D}\left(1 - \frac{1}{6}\widetilde{m}^2\tilde{t}^2\right) = 1 - \frac{1}{6}\widetilde{m}^2\tilde{t}^2, \tag{4.204}$$

allowing us to set the proper initial conditions for δ_ℓ and $\widetilde{\phi}_\ell$. The equations using a and $\tilde{t}$ as independent variables are mutually transformable using Eq. (4.153), as was done in Sec. 4.2.1. The analytic solutions of the first-order

equations in Eqs. (3.110)–(3.115) for the other quantities can also be found in a similar way as

$$\Phi_\ell \simeq -\Psi_\ell \simeq +\frac{9}{22}\mathcal{D}\widetilde{m}^2\widetilde{r}F\tilde{t}^2 = +\frac{9}{22}\widetilde{m}^2\widetilde{r}F\tilde{t}^2, \tag{4.205}$$

$$\widetilde{V}_\ell \simeq -\frac{3}{22}\mathcal{D}\widetilde{m}^2\widetilde{r}F\tilde{t}^3 = -\frac{3}{22}\widetilde{m}^2\widetilde{r}F\tilde{t}^3. \tag{4.206}$$

One may notice that δ_ℓ and Ψ_ℓ have negative values, corresponding to the positive values of $\widetilde{\phi}_\ell$ in Eq. (4.204). Physically, this implies that an increase in the dark energy ϕ and hence its density caused by isocurvature perturbations in primordial epochs will induce a negative perturbation δ_ℓ to the matter distribution (with associative positive curvature potentials Φ_ℓ).

The first-order equations Eqs. (3.110)–(3.115) can be solved in an exact manner using a numerical method. Examples of the numerical solutions for perturbations $\tilde{\phi}_\ell(a)$ and $\delta_\ell(a)$ are demonstrated in Fig. 13, where the amplitude(s) of the perturbations $\mathcal{D} = 1$ are adopted with the same typical values of parameters $\widetilde{r}$ and $\widetilde{m}$ chosen in Sec. 4.2.1. The consistency between the analytic approximations in Eq. (4.203) and (4.204) (dashed line) with the numerical results (solid line) is also demonstrated in Fig. 13.

Naturally, $\widetilde{m}$ affects the solution $\tilde{\phi}_\ell$ as shown in Fig. 14). It should be noted that there is a slight dependence on Ω_m for $\tilde{\phi}_\ell$, similar to the behavior of $\widetilde{\phi}_0$ in Fig. 8). The behaviors of $\tilde{\phi}_\ell$ can be roughly understood from Eq. (4.204), which is valid for $a \lesssim 0.5$. Here $\widetilde{m}$ is important for the evolution of $\tilde{\phi}_\ell$, whereas $\widetilde{r}$ is not. On the other hand, Eq. (3.111) indicates that the solution of $\tilde{\phi}_\ell$ depends on $\tilde{\phi}_0$; hence, it slightly depends on Ω_m, which can be understood by a discussion similar to that on the behavior of $\tilde{\phi}_0$ in Sec. 4.2.1.2 (see Eq. (4.178)).

The dependence on the parameters for δ_ℓ is shown in Fig. 11. From Eq. (4.203), one can conclude that $\widetilde{m}$ and $\widetilde{r}$ affect δ_ℓ, which is demonstrated in the upper left panel and the upper right panel of Fig. 11, respectively. However, for natural choices mimicking the standard ΛCDM scenario, satisfying Eq. (4.162), the coefficient F given by fixing the dark energy density today shows that $F \approx 1$ holds. It follows that $\delta_\ell \simeq -(27/22)(1-\Omega_m)\tilde{t}^2$, which explains the behavior of δ_ℓ in the lower panels of Fig. 11.

4.2.3 CMB revisit with the numerical solutions

The constraint on the model from the observational CMB power spectrum is

$$\ell(\ell+1)\langle|A_{\ell m}|^2\rangle \leqslant \ell(\ell+1)C_\ell^{\rm obs}, \tag{4.207}$$

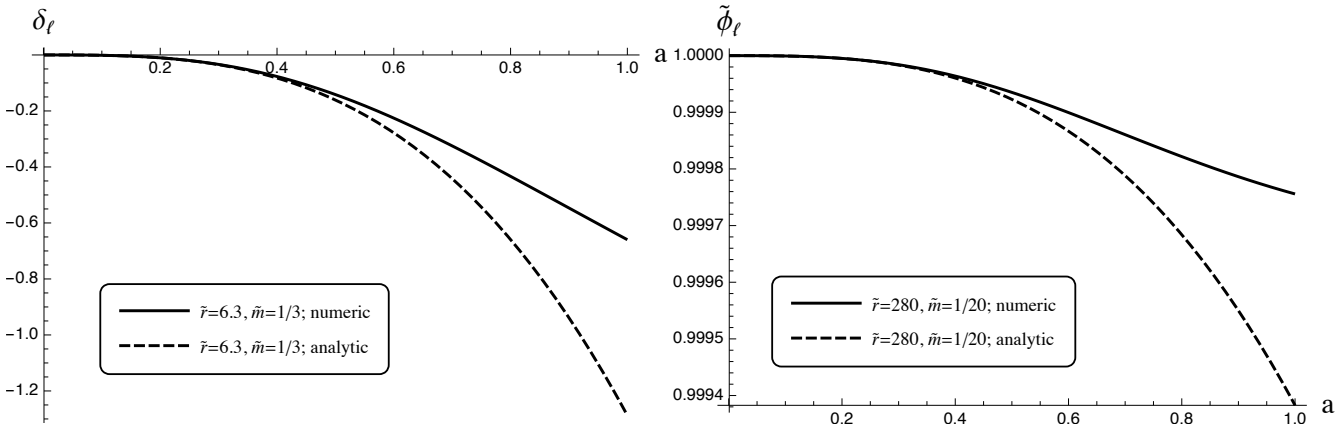

Figure 13: The validity of the analytic approximations in Eqs. (4.203) and (4.204) in the limit $a \ll 1$ in comparison with the exact numerical solutions, with the left panel showing the comparison for δ_ℓ and the right panel for $\tilde{\phi}_\ell$. Here$\widetilde{r} = 70$, $\widetilde{m} = 1/10$ for δ_ℓ, and $\widetilde{r} = 280$, $\widetilde{m} = 1/20$ for $\tilde{\phi}_\ell$ are taken as examples, while the approximations are also valid for other values of $\widetilde{m}$ and $\widetilde{r}$.

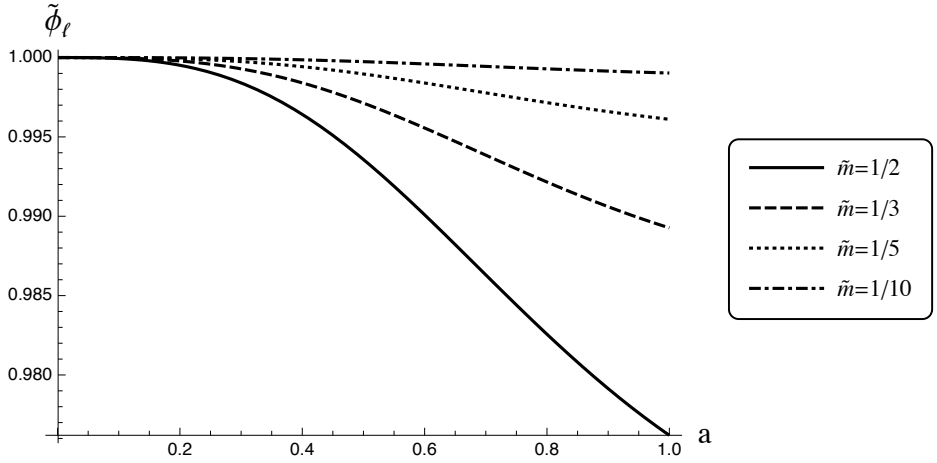

Figure 14: Numerical solutions for the perturbation to ϕ, namely $\tilde{\phi}_\ell(a)$, with the different values of parameter $\widetilde{m}$, where $\Omega_m = 0.3$ and $\widetilde{r} = 6.3$ are fixed.

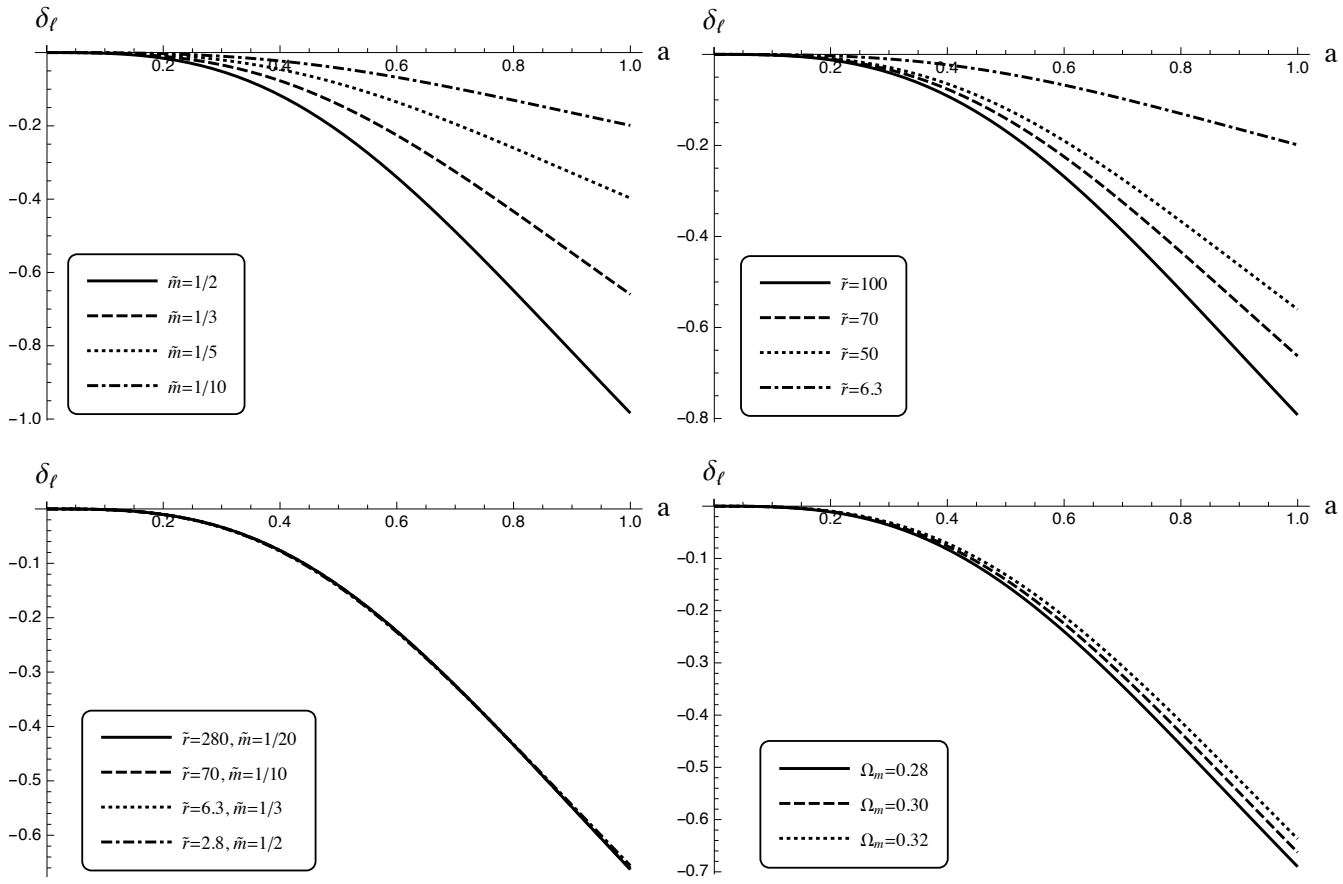

Figure 15: Numerical solutions for the matter perturbation δ_ℓ. The upper left and upper right panels demonstrate the dependence of δ_ℓ on $\widetilde{m}$ and $\widetilde{r}$, respectively. The lower left panel assumes the same value of $\Omega_m = 0.3$, while the lower right panel assumes slightly different values of Ω_m, where $\widetilde{r} = 70$ and $\widetilde{m} = 1/10$ are fixed. The lower panels show that δ_ℓ will be almost independent of $\widetilde{r}$ or $\widetilde{m}$ values, as long as they satisfy Eq. (4.162).

which means that the contribution by the large-scale mode perturbations to the CMB power spectrum multipoles should not exceed what is actually observed, since surely there may be other sources contributing to the anisotropies. Consequently one may obtain two constraints from the $\ell = 1$ dipole and the $\ell = 2$ quadrupole respectively as

$$4\epsilon_1^2 Q_1^2 \leqslant C_1^{\rm obs}, \tag{4.208}$$

$$4\epsilon_2^2 Q_2^2 \leqslant C_2^{\rm obs}. \tag{4.209}$$

Thanks to the Planck Legacy Archive, one can apply the upper limit of observational data as $C_1^{\rm obs} < 6.3 \times 10^{-6}$ and $C_2 < (2\pi/6) \times (1.0 \times 10^{-10})$ to put constraints on the magnitude of the perturbations ϵ_1 and ϵ_2.

For both parameter sets $(\widetilde{r} = 70, \widetilde{m} = 1/10)$ and $(\widetilde{r} = 6.3, \widetilde{m} = 1/3)$, by calculating Q_1 and Q_2 mutually consistent results are obtained as

$$Q_1 = -1.1 \times 10^{-1}, \tag{4.210}$$

$$Q_2 = -9.0 \times 10^{-2}. \tag{4.211}$$

following which the constraints will be

$$\epsilon_1 \leqslant 1.2 \times 10^{-2}, \tag{4.212}$$

$$\epsilon_2 \leqslant 5.7 \times 10^{-5}, \tag{4.213}$$

since both parameter sets mimic the cosmology close to a ΛCDM model to yield the observational constraints.

The results of the numerical evaluations with different parameter choices are presented in Table 1, where roughly same estimation for constraints on the order of magnitudes of ϵ_1 and ϵ_2 can be obtained.

4.2.4 Estimating perturbations to the luminosity distance caused by inhomogeneities

One may consider the perturbations to the luminosity distance introduced by the inhomogeneities of the dark energy on the basis of the metric perturbations formulated and solved previously as an example of further potential applications on observations. Following Refs. [63, 64], as the metric perturbations Ψ_ℓ associated with large-scale fluctuations of the dark energy have been solved, The perturbative correction to the luminosity distance in an

inhomogeneous universe is given as [63, 65]

$$I \equiv \frac{\delta d_L}{d_L} = \int_0^{\lambda_s} \mathrm{d}\lambda \frac{\lambda}{\lambda_s}(\lambda - \lambda_s)\left(\Delta^{(3)}\Psi - \left(\ddot{\Psi} + 2\frac{\mathrm{d}\dot{\Psi}}{\mathrm{d}\lambda}\right)\right), \tag{4.214}$$

where $\dot{\Psi} \equiv \frac{\partial\Psi(\eta,\chi)}{\partial\eta}$, and assume that the spatially flat universe. The traceless property of matrices $P_{ij}^{(m)}$ defined by Eq. (3.78) in Ψ ensures that $\Delta^{(3)}\Psi = 0$ (see Eq. (C.12)).

For the term containing differentiation with respect to the propagation parameter λ, one may write

$$\frac{\mathrm{d}}{\mathrm{d}\lambda} = \frac{\mathrm{d}\eta}{\mathrm{d}\lambda}\frac{\partial}{\partial\eta} + \frac{\mathrm{d}\chi}{\mathrm{d}\lambda}\frac{\partial}{\partial\chi}. \tag{4.215}$$

Here, let us take the parameter λ as the comoving distance χ; hence, $\lambda \equiv \chi = \eta_0 - \eta$ and $\lambda_s \equiv \chi_s = \eta_0 - \eta_s$ with an arbitrary light source indicated by lower index s, thus, one sees

$$I = \int_0^{\chi_s} \mathrm{d}\chi \frac{\chi}{\chi_s}(\chi - \chi_s)\left(\ddot{\Psi} - 2\frac{\partial\dot{\Psi}}{\partial\chi}\right). \tag{4.216}$$

One the other hand, starting from Eq. (4.214), while still taking the propagation parameter as $\lambda = \chi$, including the normal scalar mode fluctuations as $\Psi^{\mathrm{tot}} = \Psi^{\mathrm{norm}} + \Psi$, to the linear order, one obtains

$$I_{\mathrm{lin}}^{\mathrm{tot}} = \int_0^{\chi_s} \mathrm{d}\chi \frac{\chi}{\chi_s}(\chi - \chi_s)\Delta^{(3)}\Psi^{\mathrm{tot}}. \tag{4.217}$$

But recall Eq. (C.12) for Ψ here, the vanishing Laplacian suggests that only $\Psi^{\mathrm{norm}} + \Psi$ needs to be taken into consideration in the cosmological Poisson equation,

$$\Delta^{(3)}\Psi^{\mathrm{tot}} = \Delta^{(3)}\Psi^{\mathrm{norm}} = 4\pi G\overline{\rho}_m\delta_m a^2. \tag{4.218}$$

In gravitationally-bound local systems, for example, where objects such as Type Ia supernovae are located, the source term of the scalar perturbations from matter in the Friedmann equation simply reads

$$8\pi G\overline{\rho}_m = 3H^2 = 3H_0^2\Omega_m a^{-3}, \tag{4.219}$$

which is identical to Eq. (4.187), hence

$$I_{\mathrm{lin}}^{\mathrm{tot}} = -\frac{3H_0^2\Omega_m}{2}\int_0^{\chi_s} \mathrm{d}\chi \frac{\chi}{\chi_s}(\chi_s - \chi)a(\chi)^{-1}\delta_m(a(\chi), \boldsymbol{\gamma}). \tag{4.220}$$

Because $a^{-1} = 1 + z$ holds by definition between scale factor a and cosmological redshift z, if one only focuses on the contribution by the inhomogeneous background and neglect the peculiar motion terms, this result will be consistent with Eq. (6) in Ref. [64].

For the numerical evaluations of Eq. (4.216), a process similar to that of transforming Eq. (3.116) to Eq. (3.117) may be performed. With the definition of Ψ in Eq. (3.78) and Eqs. (C.10)–(C.11), I can be written as

$$\begin{aligned} I =& \int_0^{\chi_s} \mathrm{d}\chi(\chi - \chi_s)\frac{\chi}{\chi_s}\left[\left(\ddot{\Psi}_{\ell(m)} - 2\dot{\Psi}_{\ell(m)}\frac{\partial}{\partial\chi}\right)\left(\sum_{m=1}^{3}\chi Y_{\ell=1}^{(m)}(\theta,\varphi) + \sum_{m=1}^{5}\chi^2 Y_{\ell=2}^{(m)}(\theta,\varphi)\right)\right] \\ \equiv& \sum_{\ell=1}^{2}\sum_{m=1}^{2\ell+1} S_{\ell(m)} Y_\ell^{(m)}(\theta,\varphi), \end{aligned} \tag{4.221}$$

with the integral defined as

$$S_{\ell(m)} \equiv \int_0^{\chi_s} \mathrm{d}\chi \frac{\chi - \chi_s}{\chi_s}\left(\chi^{\ell+1}\ddot{\Psi}_{\ell(m)} - 2\ell\chi^\ell\dot{\Psi}_{\ell(m)}\right). \tag{4.222}$$

It is worth reminding again that $\Psi_{\ell(m)}(\eta)$ is only a function of η. $S_{\ell(m)}$ is the quantity that reflects the impact of accumulative corrections on the luminosity distance induced by the inhomogeneities of the dark energy, which can be evaluated numerically.

$S_{\ell(m)}$ due to the perturbations to Ψ caused by dark energy inhomogeneity can be evaluated at different epochs, with different a or cosmological redshift z, corresponding to the light sources from different epochs,

$$S_{\ell(m)}(a) = F_{S\ell(m)}(a)\mathcal{D}_{(\ell m)}. \tag{4.223}$$

Then it leads to

$$F_{S\ell(m)}(a) \equiv \int_{\eta_0}^{\eta_s(a)} \mathrm{d}\eta \left((\eta_0 - \eta)^{\ell+1}\frac{\partial^2\Psi_{\ell(m)}}{\partial\eta^2} - 2\ell(\eta_0 - \eta)^\ell\frac{\partial\Psi_{\ell(m)}}{\partial\eta}\right)\frac{\eta - \eta_s(a)}{\eta_0 - \eta_s(a)}, \tag{4.224}$$

in a more explicit manner for numerical evaluation as functions of a using a_1 as the variable of integration,

$$F_{S\ell(m)}(a) = -\int_a^1 \mathrm{d}a_1 \left[(\eta_0 - \eta(a_1))^{\ell+1}\frac{\partial}{\partial a_1}\left(a_1^2 H(a_1)\frac{\partial\Psi_{\ell(m)}}{\partial a_1}\right) - 2\ell\left(\eta_0 - \eta(a_1)\right)^\ell\frac{\partial\Psi_{\ell(m)}}{\partial a_1}\right]\frac{\eta(a_1) - \eta_s(a)}{\eta_0 - \eta_s(a)}. \tag{4.225}$$

The scale factor is related to the cosmological redshift by $z = a^{-1} - 1$, which is used to convert each other.

Since the evolution of the universe under the model as functions of the scale factor a has been solved in Sec. 4.2, $\Psi_\ell(a)$, $\eta(a)$, and $H(a)$, and the particle horizon η_0 can be considered already known for given parameters $\widetilde{r}$ and $\widetilde{m}$.

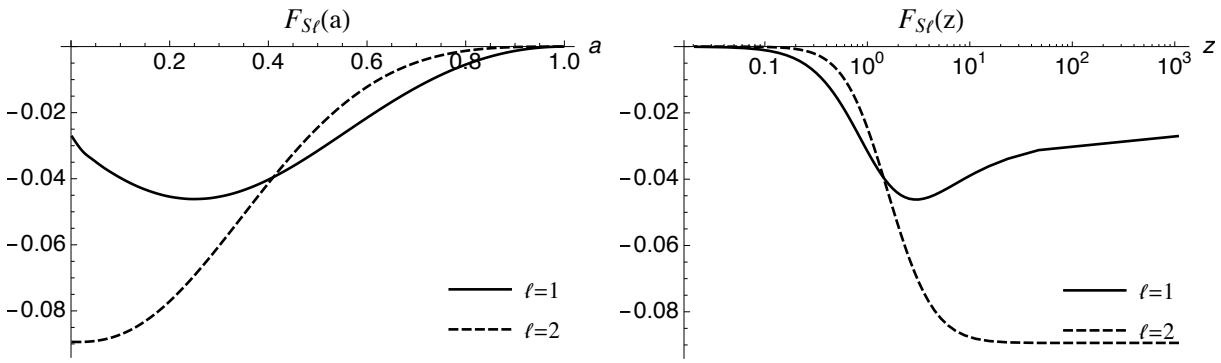

Figure 16: This figure shows the multipole components of the perturbations to the luminosity distance defined as $F_{S\ell(m)}(a;z)$ as a function of scale factor a (left panel) and redshift z (right panel). In each panel, the solid curve is the dipole, $\ell = 1$, and the dashed curve is the quadrupole $\ell = 2$. Here for the values of the parameters, those in model No. (1) in the Table 1 are adopted. The dipole $\ell = 1$ component contributes maximally to the change in luminosity distance around $z \approx 3$ or $a \approx 0.25$.

One may also transform these quantities using the conformal time η as an independent variable if necessary (see Appendix D). On the other hand, constraints on ε_1 and ε_2 were obtained in Sec. 3.2.2, thus one may evaluate the modification to the luminosity distance I with Eq. (4.221) by numerically evaluating $S_{\ell(m)}$ with the constraint on the amplitudes of dark energy multipole perturbations Eqs. (4.212) and (4.213). The numerical results of $F_{S\ell(m)}$ are demonstrated in Figure 16 as a function of a (left panel), and z (right panel), respectively.

It is interesting to note that $F_{S\ell(m)}(a)$ does not increase or decrease monotonically, whose typical behaviors are illustrated as a function of a or z in Fig. 16. This is due to the subtlety in the evolution of the contribution from $\ddot{\Psi}_{\ell(m)}$ and $\dot{\Psi}_{\ell(m)}$ terms in Eq. (4.222) with the expansion history scaled by a or z.

The specific parameters chosen for the different models corresponding to different numerical evaluations can be found in Table 1 again. $F_{S\ell(m)}(a)$ in the table are evaluated at $a = 0.25$, which corresponds to $z = 3$.

The multipole components of I, noted as I_ℓ, may then be estimated as

$$I_\ell \equiv \sum_{m=1}^{2\ell+1} S_{\ell(m)} \sim (2\ell+1) S_{\ell(m)}. \tag{4.226}$$

Allowed values of $\mathcal{D}_{(\ell m)} \sim \mathcal{O}(\varepsilon_\ell)$ $(\ell = 1, 2)$ were found in Sec. 3.2.2 (see Eqs. (4.212) and (4.213)), e.g., with $\varepsilon_1 < 1.2 \times 10^{-2}$ and $\varepsilon_2 < 5.7 \times 10^{-5}$, one can evaluate the modification to the luminosity distance caused by large-scale modes using Eq. (4.221), that the magnitude of the correction caused by the $\ell = 1$ component is $\mathcal{O}(10^{-3})$, whereas it is $\mathcal{O}(10^{-5})$ for the $\ell = 2$ component. Consistent results of modification to the luminosity distance I_ℓ

may be evaluated as

$$I_{\ell=1} \simeq -1.6 \times 10^{-3}, \tag{4.227}$$

$$I_{\ell=2} \simeq -2.0 \times 10^{-5}, \tag{4.228}$$

at the redshift $z = 3$ for all models in Table 1.

No.	$(\widetilde{r},\widetilde{m})$	Ω_m	$Q_{1(m)}$	$Q_{2(m)}$	$\varepsilon_1^{\max}$	$\varepsilon_2^{\max}$	$F_{S1(m)}(z=3)$	$F_{S2(m)}(z=3)$	$H_0\eta_0$
(1)	$(70, 1/10)$	0.30	-0.107	-0.0895	1.17×10^{-2}	5.72×10^{-5}	-0.0462	-0.0693	3.19
(2)	$(6.3, 1/3)$	0.30	-0.107	-0.0896	1.17×10^{-2}	5.71×10^{-5}	-0.0462	-0.0692	3.19
(3)	$(50, 1/10)$	0.30	-0.0904	-0.0757	1.39×10^{-2}	6.76×10^{-5}	-0.0390	-0.0586	3.19
(4)	$(100, 1/10)$	0.30	-0.128	-0.107	9.82×10^{-3}	4.78×10^{-5}	-0.0552	-0.0828	3.19
(5)	$(6.3, 1/5)$	0.30	-0.0642	-0.0537	1.96×10^{-2}	9.52×10^{-5}	-0.0277	-0.0416	3.19
(6)	$(6.3, 1/10)$	0.30	-0.0321	-0.0269	3.91×10^{-2}	1.91×10^{-4}	-0.0138	-0.0208	3.19
(7)	$(2.8, 1/2)$	0.30	-0.107	-0.0897	1.18×10^{-2}	5.70×10^{-5}	-0.0463	-0.0692	3.19
(8)	$(280, 1/20)$	0.30	-0.107	-0.0895	1.17×10^{-2}	5.72×10^{-5}	-0.0461	-0.0693	3.19
(9)	$(72, 1/10)$	0.28	-0.116	-0.100	1.08×10^{-2}	5.11×10^{-5}	-0.0503	-0.0770	3.28
(10)	$(68, 1/10)$	0.32	-0.0985	-0.0803	1.27×10^{-2}	6.37×10^{-5}	-0.0425	-0.0626	3.11
(11)	$(1/70, 1/10)$	0.30	-0.00153	-0.00128	8.21×10^{-1}	4.00×10^{-5}	-0.000659	-0.000990	3.19
(12)	$(6.3, 1/2)$	0.30	-0.160	-0.135	7.83×10^{-3}	3.80×10^{-5}	-0.0694	-0.104	3.19
(13)	$(70, 1/10)$	0.32	-0.100	-0.0815	1.25×10^{-2}	6.28×10^{-5}	-0.0431	-0.0635	3.11
(14)	$(70, 1/10)$	0.28	-0.115	-0.0988	1.09×10^{-2}	5.18×10^{-5}	-0.0496	-0.0759	3.28

Table 1: Numerical results for the setups in with different model parameters $(\widetilde{r},\widetilde{m})$ and cosmological parameter Ω_m. The models labeled as Nos. (1,2,7,8,9,10,13,14) are those close to the ΛCDM model. Furthermore, Nos. (1,2,7,8,9,10) within them satisfy the condition in Eq. (4.162) with the equality sign exactly holds. Note that, the values for the present comoving horizon η_0 also indicate that the background expansion is not sensitive to $\widetilde{r}$, whereas the matter component denoted by Ω_m does show its expected influence on the background evolution after matter dominance, related to η_0. To see this, one may focus on the comparison among the models Nos. (1,3,4,6,11), where different values of $\widetilde{r}$ rarely change η_0; on the other hand, a comparison among Nos. (1,13,14) shows a slight dependence of η_0 on Ω_m, as the matter should affect late-time evolution. Especially, No. (11) is a model extremely similar to the ΛCDM model, where the EoS of dark energy is almost constant $w_\phi \approx -1$, suggesting the future evolution of the universe quickly approaching the de Sitter expansion.

5 Discussions and Conclusions

The models of the dark energy with large-scale inhomogeneities have been formulated and investigated in this thesis, motivated by some crucial anomalous problems (see Chapter 1) in the standard ΛCDM paradigm of cosmology, implying the possibility of breaking the cosmological principle. The method of formulating dark energy with large-scale inhomogeneities associated with the late-time dynamics of some ultralight scalar field was developed on the basis of cosmic background expansion, and the evolution of the scalar field was briefly reviewed in Chapter 2. The formulation of the inhomogeneities was implemented by Gaussian random field handling for the ScmDE scenario, and was followed by a general model with superhorizon perturbations. The basic equations governing the evolution of the smooth background universe and the dark energy inhomogeneities, both under ScmDE and the general superhorizon model, were presented in Chapter 3. Subsequently, the numerical solutions for the equations were investigated in Chapter 4, by finding appropriate parameters and analytical approximates initiating from the matter-dominant epoch, which are compatible with near-to-ΛCDM cosmology indicated by various observations. Following the solutions, by evaluating possible observational imprints arising from the dark energy inhomogeneities, preliminary constraints on the model parameters and the magnitudes of the inhomogeneities were investigated, which facilitates further potential applications on observations in turn.

Based on these solutions, the dark energy inhomogeneities can be considered as the modifications to the smooth background slightly breaking the cosmological principle. Dark energy with large-scale inhomogeneities as superhorizon fluctuations predicts possible differences in the spatial distribution of dark energy density and deviation of EoS from the cosmological constant. Subsequently, unique characteristic imprints on observations induced by these inhomogeneities associated with the possible dynamics of ultralight scalar fields would arise, which were also formulated and investigated.

However, following the basic discussions on the behaviors of the solutions affected by these parameters in Chapter 4, there are several aspects within the models to discuss and address more.

Let us start from the comparison between the setups of the ScmDE and the general superhorizon perturbations.

- *The curvature of the universe*

In the heuristic scenario of ScmDE, where the contribution from the supercurvature mode of an ultralight scalar field ϕ on an open universe patch is considered as the dark energy, the density contrast $\delta_{\rm DE}(\phi^2)$ of the dark energy inhomogeneities becomes nontrivial on scales close to the supercurvature scale L_{sc}, which is much larger than the Hubble length H_0^{-1} in the present universe, hence $L_{sc} \gg H_0^{-1}$. This suggests that the spatial variation of dark energy density might be extremely small as $\mathcal{O}(\epsilon\Omega_K)$ within the present horizon scale H_0^{-1} (see Eq. (3.51)). Nevertheless, the calculations following this scenario indicate that the large-scale inhomogeneity of the dark energy density can be detected in the anisotropies of the CMB temperature spectrum via the late-time ISW effect. The detectable signatures are mainly imprinted on the low multipole components of the two-point correlation function of the CMB temperature fluctuation, especially, on the dipole and the quadrupole. Comparing the results with the current observations of the CMB multipoles, one can obtain the upper bounds for the curvature parameter Ω_K and the ancestor vacuum parameter ϵ, given in Eqs. (4.212) and (4.213), respectively. For instance, if one assumes that $\Omega_K \sim 10^{-3}$ as an upper limit from current observations for the spatial curvature, then for the ScmDE setup $\epsilon \lesssim 10^{-2}$ follows. For smaller values of Ω_K approaching a flat limit for the geometry of the universe, ϵ can be larger; hence the constraint may become looser.

The combinative fitting together with BAO measurements seems to imply a positive $\Omega_K \sim \mathcal{O}(10^{-3})$ with its deviation several times larger, $\delta\Omega_K \sim 4 \times 10^{-3}$ at 95% confidence level, however, suggesting the universe is nearly flat [17]. This also motivated the latter analytic formulation for the dark energy inhomogeneities as an extension and generalization of the ScmDE formulation in Sec. 3.1, where the inhomogeneities were considered as random fluctuations. The latter analytic formulation in Sec. 3.2 deals with the dark energy inhomogeneities sourced by a scalar field ϕ as superhorizon perturbations to the homogeneous background. Also, this model is capable of reproducing an observable universe that mimics the ΛCDM flat universe that seems to be favored by the observations, which is widely adopted as the baseline of fiducial models following ΛCDM paradigm in numerous cosmological analyses. Despite the possibility for disputes on the geometry of the universe, the generalized model in this thesis can be applied with the flat approximation even for an open/closed universe that is observed nearly flat within the surrounding Hubble patch.

- *The dark energy EoS and the late-time dynamics*

Although slightly complicated in its explicit form, Eqs. (4.179)–(4.182) can be considered as a natural extension of the CPL parametrization of the dark energy EoS [58, 59]. This is a manifestation of how the behaviors of the EoS of dark energy in the general model formulation are decided quantitatively by the parameters. If one includes the 1st-order perturbations $\widetilde{\phi}_\ell(a)$ in Eq. (4.179), and hence corrections to Eq. (4.182), one may evaluate the anisotropies of EoS $w_\phi(a)$ of the dark energy sourced by the inhomogeneities of ϕ, although these corrections to the isotropic background in Eq. (4.182) may be small because of the previous constraints on the amplitudes of ϵ_1 and ϵ_2 in Eqs. (4.212) and (4.213). Generally, $\omega_\phi(a) \simeq -1 + 2\left(1 - (a\widetilde{m}^2\tilde{\phi}_0^2)/(\Omega_m\tilde{\phi}_0'^2)\right)$ holds for almost all models; hence, $\widetilde{r}$ does not have an impact on ω_ϕ at the background level, while $\widetilde{m}$ and Ω_m do affect the dark energy EoS ω_ϕ .

As a comparison, in the ScmDE setup, it was required that the mass of ϕ at present epoch should be ultralight, i.e., $\widetilde{m} = m_{\phi 0}/H_0 \lesssim 1$, to allow the fluctuating scale of ϕ to be larger than the curvature scale as well as the hubble scale of the present, resulting in almost "frozen" dark energy density and EoS highly similar to a cosmological constant Λ. On the other hand, in the latter general case compared with ScmDE, although similar conditions should be met in a flat universe keeping fluctuations of ϕ on a superhorizon scale (see definition of $\widetilde{m}$ in Eq. (4.149)), the presumably dynamical EoS of dark energy only requires $w_0 \simeq -1$ at present to mimic a cosmological constant. It would be interesting to reintroduce negative or positive curvature into the formulation to investigate their influence on the evolution of general superhorizon perturbations in the latter part, where mild modifications to the results are expected.

Furthermore, in contrast to the superhorizon cases, there is a class of mathematical solutions in the models that $\widetilde{m} > 1$, hence the scale of fluctuations of interest may have re-entered the horizon, showing oscillating and decaying behaviors due to the expansion. But in those cases, the spatial gradient terms for the scalar field ϕ would become important in its equation of motion; hence the approximations for the metric Eq. (3.77) and the formulation for the perturbations Eqs. (3.78)–(3.83) may both require revisions and modifications to provide solutions with physical significance and insights, which can be considered in the scope of future investigations.

- *The amplitudes of the dark energy inhomogeneities and the imprints on observations*

The large-scale spatial inhomogeneities of the dark energy may introduce observable effects on the CMB

anisotropies reflected by the power spectrum of the temperature fluctuations, which gives us the clue to put constraints Eq. (4.212) and (4.213) on the amplitude of the fluctuations from the observational data by evaluating the ISW effect on the CMB temperature fluctuations from the last-scattering surface. The contribution from the large-scale inhomogeneities of the dark energy on the dipole of the CMB temperature power spectrum may accounts partly for the anomalies in the dipole and low multipoles of the CMB power spectra [43, 60].

On the other hand, these spatial inhomogeneities may introduce accumulative corrections to the calibration of the luminosity distance from distant objects such as Type Ia supernovae, since the expansion rate affected by dark energy density may have been altered along the photon geodesic of light propagating to the observer, us. The results of numerical evaluations in Eq. (4.227) and Eq. (4.228) suggest the maximum corrections to the luminosity distance are of magnitude $\mathcal{O}(10^{-3})$ from the dipole and $\mathcal{O}(10^{-5})$ from quadrupole component, which are sourced by the large-scale perturbations defined in Eqs. (3.78)–(3.80). For parameter choices in Table 1 including those following Eq. (4.162) (e.g. $(\widetilde{r} = 70, \widetilde{m} = 1/10)$ or $(\widetilde{r} = 6.3, \widetilde{m} = 1/3)$), naively, even later consideration for anisotropic expansion rate is introduced, the order of magnitudes of these corrections on luminosity suggests that the contribution from the dark enegy inhomogeneity seems too small to ease the Hubble tension. However, the possibility exists that the corrective effects caused by the anisotropies of dark energy do contribute to the divergence between the measurements on expansion rate, and it is also possible that these corrections become considerable under certain parameter choices. Another interesting aspect of the estimation on luminosity distance correction I_ℓ under this model is that the contribution from the dipole $\ell = 1$ is predicted by the numerical calculation to have a maximum value around $z \approx 3$, which may be an interesting scope for future cosmological surveys interested in or focused around this redshift.

This tension is becoming increasingly conspicuous between measurements via CMB and via standard candles like Type Ia supernovae addressed in Sec. 1.1. Related to these problems, recently there have been controversies on the model calibration for accelerated expansion represented by dark energy from analysis on Type Ia supernovae [66, 67, 68]. Nevertheless, contradictions on aforementioned arguments and reconfirmation of dark energy are given, with joint statistical analysis and the possible dependence of the luminosity of Type Ia supernovae on their environments [69, 70, 71]. On the other hand, due to the recent progress on gravitational wave detection by

running and future projects like aLIGO, VIRGO, KAGRA and LISA, the combinative detection of gravitational wave by compact binaries(BBH, NS-BH) mergers with associative electromagnetic observations as standard sirens for distance calibration have become increasingly realistic [72, 73, 74], which may help to account for this tension and to put tighter constraints on dark energy properties as well [75]. Furthermore, as a modification to the applications on the accumulative corrections to the luminosity distance, the general model formulation in this thesis has the potential to be utilized for the analytic formulation of anisotropic expansion rate or anisotropic EoS of dark energy (see Eq. (4.180) and (4.181)) of the universe, also having the potential to resolve or ease the Hubble tension problem, which will be left for a future job.

- *The parameters and the initial conditions*

Especially in the latter general formulation, for the numerical evaluations, the main interest of the model focus on the cases that restore a close-to-ΛCDM cosmology following Eq. (4.162) in a flat FLRW metric, for example, $(\widetilde{r} = 70, \widetilde{m} = 1/10)$ and $(\widetilde{r} = 6.3, \widetilde{m} = 1/3)$. However, it was shown that the model is robust against different parameter choices of $(\widetilde{r},\ \widetilde{m})$ in Table 1 in the numerical solutions presented in Sec. 4.2. It was also showed that slight changes in the calibration of Ω_m by other analyses or updates of the experiments are not likely to change the predictions of the model fundamentally. In the same time, even the parameter space for $\widetilde{r}$ and $\widetilde{m}$ to mimic the standard ΛCDM cosmology is also various. The observational constraints on cosmological parameters allow deviation from the standard ΛCDM scenario to some extent [38, 40], potentially suggesting that dynamical quintessence models for dark energy EoS are favored [71]. Hence it may be interesting and necessary to investigate into other domains in order to put constraints on the parameter space without violating substituent observational constraints from joint analysis.

The initial conditions for the background and the perturbations in Sec. 4.2 were found by considering the analytic approximations of the early matter-dominant limits after the last scattering, together with the calibration for H_0, the expansion rate of the present universe observed. This calibration is also subtlety related to the Hubble tension problem discussed previously. Although the specific value of H_0 or h is not directly a free parameter in the model, it does play an essential role in the model, for example, indirectly related with $\widetilde{m}$ via Eq. (4.149) and with the calibration of Ω_m. Although the disputes on H_0 tension are not fully explored at this stage. On the other hand,

as the source of dark energy, the initial conditions of scalar field ϕ naturally connect the interests of this work to that of the inflation in the primordial universe. There are two degrees of freedom ($\widetilde{r}$, $\widetilde{m}$) (see Eqs. (4.148) and Eq. (4.149)) in the model in this thesis related to the mass and energy scale of the dark energy field ϕ respectively. This corresponds to the fact that the potential shape $V(\phi) = ({m_\phi}^2\phi^2)/2$ of the field ϕ representing the dark energy can be fundamentally determined by 2 parameters. The 2 parameters relate the properties of scalar field ϕ to the inflationary phase that it underwent and are consistent with the cosmological parameter analysis for the degrees of freedom for dark energy parameters.

If one traces the initial conditions and primordial evolution the field ϕ back into the radiation and inflationary era similar to Refs. [27, 28, 53], more useful information or prediction from the model with dark energy inhomogeneities adopting ultralight scalar field as model may be extracted. Although for this aspect, the conclusion may be dependent on the origin of the field ϕ and the way ϕ interacts with and evolves on the background of the primordial epochs before the matter domination. The scenarios associated with open inflation as ScmDE [57], or those not necessarily coupled with the curvature for the general formulation were both possible and worth investigation. Hence, as a future outlook, it is also interesting to explore the primordial evolution of scalar field ϕ associated with conditions Eqs. (4.148) and (4.149) during the primordial ages, but this is out of the scope at this stage.

- **Concluding remarks and future outlooks**

Following the previous addressing on the initial conditions of the ultralight scalar field in the primordial universe, it is natural and necessary to mention that, although this work confines its interests on dark energy and late-time initial conditions after radiation domination with an ultralight scalar field, the scalar fields as the dominant component primordial epochs themselves are of great cosmological interests. For example, ultralight fields such as ALPs are not only interesting for the dark section of cosmology as dark energy, but also of great interest as cosmological candidates for and dark matter [36], linked with the strong CP problem and motivated by the string axiverse and the swampland conjecture [30, 31, 76]. String theory predicts the arising of multiple vacua associated with plenty of ALPs [31, 30] which are ultralight, in the vista of the string landscape. A recent research addressed on the string swampland criteria and its cosmological implications on dark energy [77].

Motivated partly by the CCP concern addressed in Chapter. 1, the dynamical EoS of dark energy in this

work (as well as in general dynamical dark energy models), is interesting and relevant for the future of our universe. Potentially, the predictions can be constrained or falsified by ongoing (SDSS-eBOSS, DES, DESI) and future generation observations (e.g. LSST [78], Euclid [79], WFIRST [80]) concerning this aspect [41], together with increasing understandings of the systematics sabotaging precise cosmological observations. Additionally, the neutral hydrogen cosmology from 21-cm spectrum survey planned by SKA [81] may link BAO with redshift-space distortions, also adding up to potential better understanding of dark energy. On the other hand, the impact of energy inhomogeneities on extremely large scales also give rise to observable effects, such as the ISW effect and the perturbations to luminosity distance evaluated in this thesis. Based on these solutions, the dark energy inhomogeneities can be considered as the modifications to the smooth background slightly breaking the cosmological principle.

Further applications of the model on other observational effects, e.g., structure growth and clustering of the matter, anisotropies in expansion rate, etc., may give more predictions to help examine the model and to provide possible explanation for some difficulties the standard ΛCDM cosmology faces while assuming homogeneity and isotropy, i.e., the cosmological principle. The coupling of the superhorizon-mode perturbations with the normal mode perturbations on matter may be further formulated following this model. Potentially observable effects may be induced in the distribution of the matter by this interaction, and the quantitative predictions on the statistics (e.g., growth factor of structure power spectrum and bispectrum) may be formulated, which are also worth investigating under the model in this thesis in the future.

References

[1] A. G. Riess et al., Astron. J. **116**, 1009 (1998).

[2] B. P. Schmidt et al., Astrophys. J. **507**, 46 (1998).

[3] S. Perlmutter et al., Astrophys. J. **517**, 565 (1999).

[4] J. R. Gott III, M. S. Vogeley, S. Podariu, and B. Ratra, Astrophys. J. **549**, 1 (2001).

[5] B. Leibundgut, Comput. Phys. Commun. **147** 459 (2002).

[6] S. W. Allen, R. W. Schmidt, H. Ebeling, A. C. Fabian, and L. Van Speybroeck, Mon. Not. R. Astron. Soc. 353, 457 (2004).

[7] D. Rapetti, S. W. Allen, and J. Weller, Mon. Not. R. Astron. Soc. 360, 555 (2005).

[8] K. Tegmark et al., (SDSS Collaboration), Phys. Rev. D 69, 103501, (2004).

[9] S. More, H. Miyatake, R. Mandelbaum, M. Takada, D. N. Spergel, J. R. Brownstein, and D. P. Schneider, Astrophys. J. 806, 2 (2015).

[10] D. Larson et al., Astrophys. J. Suppl. 192, 16, (2011).

[11] E. Komatsu et al. (WMAP Collaboration). Astrophys. J. Suppl. 192, 18, (2011).

[12] B. D. Sherwin et al., Phys. Rev. Lett. 107, 021302 (2011).

[13] M. Oguri and M. Takada, Phys. Rev. D 83, 023008 (2011).

[14] C. Hikage et al., Publ. Astron. Soc. Japan 71, 1 (2019).

[15] J.-W. Hu, R.-G. Cai, Z.-K. Guo, and B. Hu, JCAP 1405, 020 (2014).

[16] N. Aghanim et al. (Planck Collaboration), Astron. Astrophys. **641**, A1 (2020).

[17] N. Aghanim et al. (Planck Collaboration), Astron. Astrophys. **641**, A6 (2020).

[18] E. P. Hubble, Proc. Natl. Acad. Sci. USA **15**, 168 (1929).

[19] P. J. E. Peebles and B. Ratra, Rev. Mod. Phys. **75**, 559 (2003).

[20] S. Weinberg, Rev. Mod. Phys. **61**, 1 (1989).

[21] S. Tsujikawa, Class. Quant. Grav. **30**, 214003 (2013).

[22] C. Ringeval, T. Suyama, T. Takahashi, M. Yamaguchi, and S. Yokoyama, Phys. Rev. Lett. **105**, 121301 (2010).

[23] D. Glavan, T. Prokopec, and V. Prymidis, Phys. Rev. D **89**, 024024 (2014).

[24] D. Glavan, T. Prokopec, and D. C. van der Woude, Phys. Rev. D **91**, 024014 (2015).

[25] D. Glavan, T. Prokopec, and T. Takahashi, Phys. Rev. D **94**, 084053 (2016).

[26] D. Glavan, T. Prokopec, and A. A. Starobinsky, Eur. Phys. J. C **78**, 371 (2018).

[27] H. Aoki, S. Iso, and Y. Sekino, Phys. Rev. D **89**, 103536 (2014).

[28] H. Aoki and S. Iso, Prog. Theor. Exp. Phys. **2015**, 113E02 (2015).

[29] E. V. Linder, Phys. Rev. D **101**, 023506 (2020).

[30] P. Svrcek and E. Witten, J. High Energy Phys. 06 (2006) 015.

[31] A. Arvanitaki, S. Dimopoulos, S. Dubovsky, N. Kaloper, and J. March-Russell, Phys. Rev. D **81**, 123530 (2010).

[32] G. Obied, H. Ooguri, L. Spodyneiko, and C. Vafa, arXiv:1806.0836.

[33] P. Agrawal, G. Obied, P. J. Steinhardt, and C. Vafa, Phys. Lett. B **784**, 271 (2018).

[34] H. Ooguri, E. Palti, G. Shiu, and C. Vafa, Phys. Lett. B **788** 180 (2019).

[35] S. K. Garg, C. Krishnan and M. Zaid Zaz, J. High Energy Phys. 03 (2019) 029.

[36] L. Visinelli and S. Vagnozzi, Phys. Rev. D **99**, 063517 (2019).

[37] S. Appleby, R. Battye, and A. Moss, Phys. Rev. D **81**, 081301 (2010).

[38] A. Tripathia, A. Sangwana, and H. K. Jassala, J. Cosmol. Astropart. Phys. 06 (2017) 012.

[39] D. H. Weinberg, M. J. Mortonson, D. J. Eisenstein, C. Hirata, A. G. Riess, and E. Rozo, Phys. Rept. **530**, 87 (2013).

[40] H. K. Jassal, J. S. Bagla, and T. Padmanabhan, Mon. Not. R. Astron. Soc. **405**, 2639 (2010).

[41] D. Yamauchi, H. Aoki, S. Iso, D.-S. Lee, Y. Sekino, and C.-P. Yeh, J. Cosmol. Astropart. Phys. 05 (2019) 055.

[42] D. J. Schwarz, C. J. Copi, D. Huterer, and G. D. Starkman, Class. Quant. Grav. **33**, 184001 (2016).

[43] L. Polastri, A. Gruppuso, and P. Natoli, J. Cosmol. Astropart. Phys. 04 (2015) 018.

[44] R. B. Tully, E. J. Shaya, I. D. Karachentsev, H. M. Courtois, D. D. Kocevski, L. Rizzi, and A. Peel, Astrophys. J. **676**, 184 (2008).

[45] H. M. Courtois, D. Pomarède, R. B. Tully, Y. Hoffman, and D. Courtois, Astron. J. **146**, 69 (2013).

[46] K. Migkas, G. Schellenberger, T. H. Reiprich, F. Pacaud, M. E. Ramos-Ceja, and L. Lovisari, Astron. Astrophys. **636**, A15 (2020).

[47] C. Gordon, W. Hu, D. Huterer, and T. Crawford, Phys. Rev. D **72** 103002 (2005).

[48] P. da S. Ferreira and M. Quartin, arXiv:2011.08385.

[49] W. L. Freedman, Nature Astronomy, **1**, 0169 (2017)

[50] A. G. Riess, L. MacRi, S. Casertano, H. Lampeitl, H. C. Ferguson, A. V. Filippenko, S. W. Jha, W. Li, and R. Chornock, Astrophys. J. **730**, 119 (2011).

[51] C. L. Bennett et al., Astrophys. J. Suppl. Ser. **208**, 20 (2013).

[52] E. Mörtsell and S. Dhawan, J. Cosmol. Astropart. Phys. 09 (2018) 025.

[53] H. Aoki, S. Iso, D-S. Lee, Y. Sekino, and C-P. Yeh, Phys. Rev. D **97**, 043517 (2018).

[54] Y. Nan, K. Yamamoto, H. Aoki, S. Iso, and D. Yamauchi, Phys. Rev. D **99**, 103512 (2019).

[55] S. R. Coleman and F. De Luccia, Phys. Rev. D **21**, 3305 (1980).

[56] W. Hu, astro-ph/9508126.

[57] D. Yamauchi, A. Linde, A. Naruko, M. Sasaki, and T. Tanaka, Phys. Rev. D **84** 043513 (2011).

[58] M. Chevallier and D. Polarski, Int. J. Mod. Phys. D **10**, 213 (2001).

[59] E. V. Linder, Phys. Rev. Lett. **90**, 091301 (2003).

[60] P. Bielewicz, K. M. Górski, and A. J. Banday, Mon. Not. R. Astron. Soc. **355**, 1283 (2004).

[61] P. J. E. Peebles, Principles of Physical Cosmology (Princeton University Press, Princeton, New Jersey, 1993).

[62] N. Aghanim et al. (Planck Collaboration), Astron. Astrophys. **571**, A27 (2014).

[63] T. Futamase and M. Sasaki, Phys. Rev. D **40**, 2502 (1989).

[64] A. Agrawal, T. Okumura, and T. Futamase, Phys. Rev. D **100**, 063534 (2019).

[65] M. Sasaki, Mon. Not. R. Astron. Soc. **228**, 653 (1987).

[66] J. T. Nielsen, A. Guffanti, and S. Sarkar, Sci. Rep. **6**, 35596 (2016).

[67] R. Mohayaee, M. Rameez, and S. Sarkar, arXiv:2003.10420.

[68] J. Colin, R. Mohayaee, M. Rameez, and S. Sarkar, Astron. Astrophys. **631**, L13 (2019).

[69] D. Rubin and B. Hayden, Astrophys. J. **833**, L30 (2016).

[70] D. Rubin and J. Heitlauf, Astrophys. J. **894**, 68 (2020).

[71] E. Di Valentino, A. Melchiorri, O. Mena, and S. Vagnozzi, Phys. Rev. D **101**, 063502 (2020).

[72] D. E. Holz and S. A. Hughes, Astrophys. J. **629**, 15 (2005).

[73] N. Dalal, D. E. Holz, S. A. Hughes, and B. Jain, Phys. Rev. D **74**, 063006 (2006).

[74] S. Vitale and H. Y. Chen, Phys. Rev. Lett. **121**, 021303 (2018).

[75] X.-N. Zhang, L.-F. Wang, J.-F. Zhang, and X. Zhang, Phys. Rev. D **99**, 063510 (2019).

[76] S. Mizuno, S. Mukohyama, S. Pi, and Y.-L. Zhang, J. Cosmol. Astropart. Phys. 09 (2019) 072.

[77] L. Heisenberg, M. Bartelmann, R. Brandenberger, and A. Refregier, Phys. Rev. D **98**, 123502 (2018).

[78] P. A. Abell et al. [LSST Science Collaborations], arXiv:0912.0201.

[79] R. Laureijs et al. [EUCLID Collaboration], arXiv:1110.3193.

[80] D. Spergel et al. [WFIRST Collaboration], arXiv:1305.5422.

[81] D. J. Bacon et al. [SKA Collaboration], Publ. Astron. Soc. Austral. **37**, E007 2020.

[82] A. Linde, Particle physics and inflationary cosmology (CRC press, Boca Raton, Florida, 1990).

[83] S. Dodelson, Modern Cosmology (Academic Press, New York, 2003).

A Details for the dynamics of supercurvature mode

This part will largely rely on the basis of Ref. [53]. The formulation of ScmDE setup for inhomogeneous dark energy most importantly relies on and starts from the feature that, the supercurvature mode of an ultralight scalar field may exists and stays superhorizon with spatial fluctuations on the present universe, which was developed in Ref. [54]. However, this part may make for a better understanding of this setup. Consider an ultralight scalar field ϕ as a canonical free field on the CDL instanton geometry described by the Euclidean spacetime metric

$$ds^2_{\text{Euc.}} = a^2(X)(dX^2 + d\theta^2 + \sin^2\theta d\Omega_2^2), \tag{A.1}$$

whose symmetry of geometry is deformed by the different vacuum states before and after the quantum tunneling and the associative bubble wall, i.e., the tunneling wall, which is demonstrated in Fig. 17.

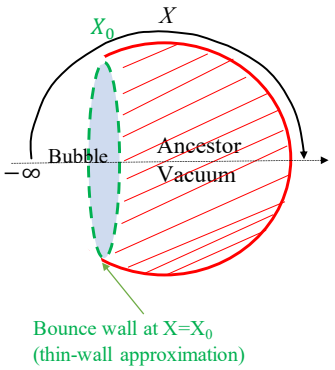

Figure 17: The figure shows a schematic picture of the CDL tunneling of instanton ψ and the related Euclidean spacetime. The true vacuum within the bubble nucleated after the CDL tunneling is S^3 denoted apparently by the S^1 surface, and the ancestor false vacuum with Swithin the deformed surface of S^2 in the figure. The dashed boundary of the bubble corresponds to the tunneling wall in the potential $V(\psi)$ with a thin-wall approximation.

The evolution of scale factor a in this spacetime is consequently a piecewise function determined by the deformation, giving a well in the potential term of ϕ in its equation of motions under certain circumstances of parameters related to the scale factor a, Hubble rate H in primordial epochs, mass $m_{(\phi)}$ of ultralight scalar ϕ.

After solving for perturbative bounce solution of the eigenfunctions for the mode expansion of ϕ in the complete basis in X coordinates, which is performable because the spatial coordinate along X is compact, the reflection and

transmission coefficients $\mathcal{R}(k)$ and $\mathcal{T}(k)$ of the mode functions, associated with the quantum tunneling probability from ancestor vacuum to the new vacuum can then be obtained. Subsequently, the contribution to correlation function from the eigenmode functions of field ϕ on the Lorentzian geometry

$$ds^2_{\text{Lor.}} = a^2(\eta)(-d\eta^2 + dR^2 + \sinh^2 R d\Omega_2^2), \tag{A.2}$$

where R and η are the time-constant spatial slice and conformal time of the open universe bubble that evolved into the observable universe today following Ref. [53]. Taking only the contributions from the supercurvature modes with $k = i(1-\epsilon)$, it is given as (Eq. (4.5) in Ref. [53])

$$\langle\phi(\eta, R)\phi(\eta', 0)\rangle^{(\text{scm})} = \frac{-2\pi i}{8\pi^2 a(\eta)a(\eta')} \cdot \text{Res}(i(1-\epsilon))\mathrm{e}^{(1-\epsilon)(\eta+\eta'+2\tilde{\eta}_1)} \frac{1}{\sin\epsilon\pi} \frac{\sinh(1-\epsilon)R}{\sinh R}, \tag{A.3}$$

where $a(\eta)$ is the scale factor. $\text{Res}(i(1-\epsilon))$ comes from the reflection coefficient $\mathcal{R}(k)$ of the eigen functions of modes at the pole $k_B = i(1-\epsilon)$ related to the bound state of energy arising from the pontential well mentioned previously, whose explicit form is also given in [53].

These bound states, shifted by the tiny but nonzero field mass m_ϕ of ϕ from $k_B = i$ pole with a small quantity ϵ, are vanishing at $X \to \infty$ in the Euclidean coordinates; hence they are normalizable and must be included in the mode expansion in the complete basis with respect to X coordinates. However, after applying the analytic continuation across the null infinity between the Euclidean spacetime and the open de Sitter chart of H^3 where our universe resides, these discrete modes became non-normalizable on the spatial slice and stay almost constant without decaying; the fluctuation scale is much larger than the curvature scale by factor ϵ^{-1}; hence these modes are named the supercurvature modes.

Let R be the radial coordinate parametrizing the spatial slice H^3. $\tilde{\eta}_1$ is a phase shift introduced for connecting the CDL and the open FLRW geometries smoothly expressed as

$$\mathrm{e}^{\tilde{\eta}_1} = \frac{H_A}{H_I}(1 + \mathrm{e}^{2\mathrm{X}_0}), \tag{A.4}$$

where X_0 is related to the size of the bubble ($X_0 \to -\infty$ corresponds to a small bubble limit). For small ϵ, Eq. (A.3) reduces to Eq. (2.43) with

$$\varphi(\eta) = c_*^{1/2} \frac{H_A^2}{m_A} \left(\frac{H_I}{H_A}\right)^{\epsilon} \varphi_*(\eta), \tag{A.5}$$

where c_* is an $\mathcal{O}(1)$ constant (Eq. (5.33) in [53]). $\varphi_*(\eta)$ represents the time evolution in the FLRW universe, and, for instance, in the periods (ii) and (iii) in Sec. V-C of Ref. [53], it is given by

$$\varphi_*(\eta) \simeq \frac{\sin m_0 t}{m_0 t}, \tag{A.6}$$

where t is the proper time in the FLRW universe. When $m_0 \lesssim H_0$ is satisfied, $m_0 t \lesssim 1$, hence one obtains $\varphi_*(\eta) \simeq 1$; the supercurvature mode is almost "frozen" in its dynamics. If more stringent condition $m_0 t \ll 1$ holds, then $\varphi(\eta) \simeq$ const. behaves extremely close to a cosmological constant.

With the frozen supercurvature modes, we can set, for example, $\eta = 0$ to evaluate the its energy density interpreted as dark energy. In the flat universe limit $\Omega_K \ll 1$, the supercurvature modes behave as the dark energy with the density

$$\frac{8\pi G}{3}\rho_{\rm DE} \simeq \frac{8\pi G}{3}\frac{m_0^2\varphi^2(0)}{2} = H_0^2\Omega_\Lambda. \tag{A.7}$$

An additional note in the massless limit $\epsilon \to 0$ is that, with a further assumption of small-bubble approximation as $X_0 \to -\infty$, the well-known result for the coincident-point correlation function in de Sitter spacetime [82]

$$\langle\phi^2\rangle = \varphi^2(0) = \frac{3}{8\pi^2}\frac{H_A^4}{m_A^2} \tag{A.8}$$

can be reproduced.

A.1 Probability distribution functions of ScmDE density

Following the setup of Eq. (A.7), the explicit form of the probability functions of the dark energy density and the density parameter from ScmDE can be demonstrated. For a *normalized* probability variable of the field, the distribution function is given by

$$P(\widetilde{\phi}(\boldsymbol{x})) = \frac{1}{\sqrt{2\pi}}\exp\left[-\frac{1}{2}\widetilde{\phi}^2(\boldsymbol{x})\right]. \tag{A.9}$$

Note that $\langle\widetilde{\phi}^2(\boldsymbol{x})\rangle = 1$. Using $\widetilde{\phi}(\boldsymbol{x})$, one may write the scalar field as $\phi(\eta,\boldsymbol{x}) = \varphi(\eta)\,\widetilde{\phi}(\boldsymbol{x})$, where $\varphi(0)$ is defined in Appendix A. One will find the for the supercurvature-mode dark energy, the probability density function its density is given by

$$\rho_{\rm DE}(\boldsymbol{x}) = \frac{1}{2}m_0^2\phi^2(\eta_0,\boldsymbol{x}) \approx \frac{1}{2}m_0^2\varphi^2(0)\widetilde{\phi}^2(\boldsymbol{x}). \tag{A.10}$$

On the large scales $R > R_{sc}$, the spatial variation is significant, however, as long as we consider a region of the present Hubble horizon, which is much smaller than the scale R_{sc}, $\rho_{\rm DE}(\boldsymbol{x})$ can be regarded as a probability variable through $\widetilde{\phi}$ by Eq. (A.10). Following the conservation of the probability,

$$d\widetilde{\phi}(\boldsymbol{x})P(\widetilde{\phi}(\boldsymbol{x})) = d\rho_{\rm DE}\, f(\rho_{\rm DE}), \tag{A.11}$$

we define the probability density function of $\rho_{\rm DE}(\boldsymbol{x})$

$$f(\rho_{\rm DE}) = \int d\widetilde{\phi}(\boldsymbol{x})\delta(\rho_{\rm DE} - \rho_{\rm DE}(\boldsymbol{x}))P(\widetilde{\phi}(\boldsymbol{x})). \tag{A.12}$$

It can be analytically calculated as

$$f(\rho_{\rm DE}) = \frac{1}{\sqrt{4\pi}m_0^2\varphi^2(0)}\frac{\exp\left(-\rho_{\rm DE}/m_0^2\varphi^2(0)\right)}{\sqrt{\rho_{\rm DE}/m_0^2\varphi^2(0)}}, \tag{A.13}$$

which is plotted in left panel Figire 18. This figure shows the a wide range for the probability distribution of $\rho_{\rm DE}$ at scales larger than the supercurvature scale R_{sc} even when we fix the parameter as Eq. (3.52).

For scales within the horizon, one can also discuss the probability distribution function of the density parameter for dark energy defined by

$$\Omega_\Lambda(\boldsymbol{x}) \equiv \frac{\rho_{\rm DE}(\boldsymbol{x})}{\rho_{\rm DE}(\boldsymbol{x}) + \rho_m} = \frac{\overline{\Omega}_\Lambda\widetilde{\phi}^2(\boldsymbol{x})}{1 - \overline{\Omega}_\Lambda + \overline{\Omega}_\Lambda\widetilde{\phi}^2(\boldsymbol{x})}, \tag{A.14}$$

where ρ_m is the dark matter energy density. In a similar way to the case for the dark energy density, we can find the probability density function of Ω_Λ as

$$f(\Omega_\Lambda) = \int d\widetilde{\phi}\delta(\Omega_\Lambda - \Omega_\Lambda(\boldsymbol{x}))P(\widetilde{\phi}(\boldsymbol{x})). \tag{A.15}$$

It can be analytically calculated as

$$f(\Omega_\Lambda) \;=\; \frac{1}{2\sqrt{2\pi}\Omega_\Lambda(1-\Omega_\Lambda)}\sqrt{\frac{\Omega_\Lambda(1-\overline{\Omega}_\Lambda)}{\overline{\Omega}_\Lambda(1-\Omega_\Lambda)}}\exp\left(-\frac{\Omega_\Lambda(1-\overline{\Omega}_\Lambda)}{2\overline{\Omega}_\Lambda(1-\Omega_\Lambda)}\right). \tag{A.16}$$

The right panel of Fig. 18 plots the function $f(\Omega_\Lambda)$ assuming $\overline{\Omega}_\Lambda = 0.7$ in Eq. (A.16). $f(\Omega_\Lambda)$ has a peak at a point of Ω_Λ slightly larger than $\overline{\Omega}_\Lambda = 0.7$, but this figure demonstrates a wide distribution of probability of Ω_Λ at scales larger than the supercurvature scale R_{sc}.

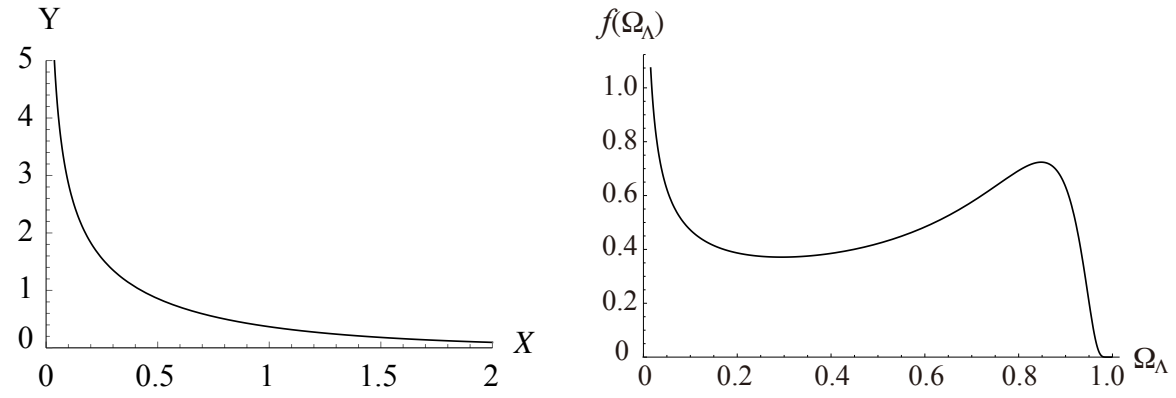

Figure 18: The left panel shows the probability density distribution $f(\rho_{\rm DE})$ as a function of $\rho_{\rm DE}$ in Eq. (A.13). The horizontal axis is $X = \rho_{\rm DE}/m_0^2\varphi^2(0)$, and the vertical axis is $Y = \sqrt{4\pi}m_0^2\varphi^2(0)f(\rho_{\rm DE})$. The right panel shows the probability density distribution $f(\Omega_\Lambda)$ for Ω_Λ in Eq. (A.16), with its expectation value fixed as $\overline{\Omega_\Lambda} = 0.7$.

B Isocurvature and adiabatic initial conditions

This appendix is devoted to the explanation of isocurvature initial conditions used for the superhorizon perturbations of ϕ representing dark energy.

The adiabatic (curvature) perturbations are defined as those inherited from the initial perturbations of some decayed background (e.g., some scalar field), leaving the relative particle number density n_X and n_Y of different species (e.g., matter and radiation) unchanged

$$\delta\mathcal{R} \equiv \frac{\delta n_X}{n_X} = \frac{\delta n_Y}{n_Y} \propto \delta t, \tag{B.1}$$

or

$$\delta\left(\frac{n_X}{n_Y}\right) = 0, \tag{B.2}$$

where the entropy related to the EoS of the system of X and Y is conserved. The perturbations in form of this kind perturbs the energy density related to particle number density in the system, inducing spatial curvature Φ (specifically, $4k^2\Phi/a^2$ in Fourier representation in wavenumber k) related to the energy density enclosed in the spacetime at a fixed time, hence are sometimes called the curvature perturbations as well.

However, it is also reasonable to consider initial perturbations that are *orthogonal* to the adiabatic perturbations, resulting in perturbations to the entropy, not changing the total energy density of the system but changing the (local) EoS of the system, hence

$$\frac{\delta n_X}{n_X} \neq \frac{\delta n_Y}{n_Y}, \tag{B.3}$$

or

$$\delta\mathcal{S} \equiv \frac{\delta n_X}{n_X} - \frac{\delta n_Y}{n_Y}, \tag{B.4}$$

which is the definition of entropy perturbation. The isocurvature perturbations are defined as *orthogonal* to hence independent from the perturbations to energy density and curvature by adiabatic perturbations discussed previously, hence is called the *isocurvature* perturbations as well.

The Boltzmann equations for the first moment (monopole) of the perturbations to photon distribution and matter distribution are [56, 83]

$$\dot{\Theta}_0 + \dot{\Phi} = 0, \tag{B.5}$$

$$\dot{\delta} + 3\dot{\Phi} = 0, \tag{B.6}$$

respectively.

From the previous definition of isocurvature perturbations, consequently the isocurvature initial condition reads

$$\Theta_0^{\rm iso}(0) = -\Phi^{\rm iso}(0) = 0 = \Psi^{\rm iso}(0), \tag{B.7}$$

$$\delta^{\rm iso}(0) + 3\Phi^{\rm iso}(0) = 0. \tag{B.8}$$

Eq. (B.8) corresponds to the initial conditions for Eq. (3.66) and Eq. (4.195). From Eq. (B.5) one obtains

$$\Theta_0^{\rm iso}(\eta_d) = -\Phi^{\rm iso}(\eta_d) + \Phi^{\rm iso}(0) + \Theta_0^{\rm iso}(0), \tag{B.9}$$

hence inserting Eq. (B.7) one will see for the isocurvature initial condition

$$\Theta_0^{\rm iso}(\eta_d) = -\Phi^{\rm iso}(\eta_d) = \Psi^{\rm iso}(\eta_d). \tag{B.10}$$

Then one can evaluate the ISW effect contribution from the isocurvature modes as

$$[\Theta_0 + \Psi]^{\rm iso}(\eta) \sim 2\Psi^{\rm iso}. \tag{B.11}$$

The prefactor 2 here is nontrivial, and can referred to in Eq. (3.75). On the contrary, for the adiabatic perturbations, the prefactor is 1/3 in matter dominant epoch.

C Multipole Expansion Matrices

The matrices $P_i^{(m)}$ utilized in the definitions of the perturbations in Sec. 3 are simply written as

$$P_i^{(m=1)} = \sqrt{\frac{3}{4\pi}} \begin{pmatrix} 1 \\ 0 \\ 0 \end{pmatrix}, \tag{C.1}$$

$$P_i^{(m=2)} = \sqrt{\frac{3}{4\pi}} \begin{pmatrix} 0 \\ 1 \\ 0 \end{pmatrix}, \tag{C.2}$$

$$P_i^{(m=3)} = \sqrt{\frac{3}{4\pi}} \begin{pmatrix} 0 \\ 0 \\ 1 \end{pmatrix}, \tag{C.3}$$

while $P_{ij}^{(m)}$ are traceless matrices related to the multipole expansion of the perturbations, listed as following

$$P_{ij}^{(m=1)} = \sqrt{\frac{15}{16\pi}} \begin{pmatrix} 0 & 1 & 0 \\ 1 & 0 & 0 \\ 0 & 0 & 0 \end{pmatrix}, \tag{C.4}$$

$$P_{ij}^{(m=2)} = \sqrt{\frac{15}{16\pi}} \begin{pmatrix} 0 & 0 & 0 \\ 0 & 0 & 1 \\ 0 & 1 & 0 \end{pmatrix}, \tag{C.5}$$

$$P_{ij}^{(m=3)} = \sqrt{\frac{15}{16\pi}} \begin{pmatrix} 0 & 0 & 1 \\ 0 & 0 & 0 \\ 1 & 0 & 0 \end{pmatrix}, \tag{C.6}$$

$$P_{ij}^{(m=4)} = \sqrt{\frac{15}{16\pi}} \begin{pmatrix} 1 & 0 & 0 \\ 0 & -1 & 0 \\ 0 & 0 & 0 \end{pmatrix}, \tag{C.7}$$

$$P_{ij}^{(m=5)} = \sqrt{\frac{15}{16\pi}} \begin{pmatrix} -1 & 0 & 0 \\ 0 & -1 & 0 \\ 0 & 0 & 2 \end{pmatrix}. \tag{C.8}$$

Eq. (3.78)–(3.80) are by virtue of the multipole expansion of the inhomogeneous perturbations under the real spherical harmonics in the space up to $\ell = 2$, the quadrupole component, with the $\ell = 0$ component standing for the homogeneous background as the monopole.

Using θ and φ to denote the polar angle and azimuthal angle in the spherical coordinates respectively, taking

spatial basis

$$x^1 = \chi \sin\theta \cos\varphi,$$
$$x^2 = \chi \sin\theta \sin\varphi,$$
$$x^3 = \chi \cos\theta, \tag{C.9}$$

the relation between these matrices and the spherical harmonics can be understood as

$$Y^{(m)}_{\ell=1}(\theta,\varphi) \equiv P^{(m)}_i x^i/\chi, \tag{C.10}$$
$$Y^{(m)}_{\ell=2}(\theta,\varphi) \equiv P^{(m)}_{ij} x^i x^j/\chi^2, \tag{C.11}$$

with integer $m \in [1, 2\ell+1]$ instead of $m \in [-\ell, \ell]$, corresponding to the three matrices for $\ell = 1$ and five matrices for $\ell = 2$ previously.

Notice that the traceless property for the matrices is in correspondence to the conclusion that the large-scale modes make no source term contribution additional to the scalar modes as its Laplacian vanishes

$$\begin{aligned}\Delta^{(3)}\Psi = \nabla^2\Psi &= \Psi_{1(m)}\nabla^2 P^{(m)}_i x^i + \Psi_{2(m)}\nabla^2 P^{(m)}_{ij} x^i x^j \\ &= 0 + \mathrm{Tr}P^{(m)}_{ij}\Psi_{2(m)}\nabla^2\chi^2 \\ &= 0.\end{aligned} \tag{C.12}$$

D Some Useful Transformation Relations

In this appendix, some useful relations to help transform equations quickly between forms as functions of $\tilde{t}$, a, or η are provided. As the dimensionless quantities was defined in Eqs. (4.146) and (4.165),

$$\tilde{t} = H_0 t,$$
$$\widetilde{H} = H/H_0,$$

with

$$H = \frac{1}{a}\frac{\mathrm{d}a}{\mathrm{d}t} \tag{D.1}$$

as a usual convention. Hence, recalling $'$ is the derivative with respect to a and overdot $\dot{}$ indicates that with respect to η, for arbitrary function $\mathcal{A}$ one has

$$\frac{\partial \mathcal{A}}{\partial \tilde{t}} = \frac{\partial \mathcal{A}}{H_0 \partial t} = a\frac{H}{H_0}\frac{\partial \mathcal{A}}{\partial a} = a\widetilde{H}\mathcal{A}', \tag{D.2}$$

as well as

$$\frac{\partial \mathcal{A}}{\partial \tilde{t}} = \frac{\partial \mathcal{A}}{H_0 \partial t} = \frac{1}{aH_0}\frac{\partial \mathcal{A}}{\partial \eta} = \frac{\widetilde{H}}{aH}\frac{\partial \mathcal{A}}{\partial \eta} = \frac{\widetilde{H}}{\mathcal{H}}\dot{\mathcal{A}}. \tag{D.3}$$

These will help to transform equations quickly. Consequently, one sees

$$\begin{aligned}\frac{\partial^2 \mathcal{A}}{\partial \tilde{t}^2} &= a\widetilde{H}\frac{\partial}{\partial a}\left(a\widetilde{H}\frac{\partial \mathcal{A}}{\partial a}\right) \\ &= a^2\widetilde{H}^2\mathcal{A}'' + (a^2\widetilde{H}\widetilde{H}' + a\widetilde{H}^2)\mathcal{A}'\end{aligned} \tag{D.4}$$

and

$$\frac{1}{a}\frac{\partial a}{\partial \tilde{t}} = \frac{1}{H_0}\frac{1}{a}\frac{\partial a}{\partial t} = H/H_0 = \widetilde{H}. \tag{D.5}$$

Finally it is worth noting that a universal relation widely used reads

$$\dot{\mathcal{A}} = a^2 H \mathcal{A}'. \tag{D.6}$$

E Details of the correlation function for random field ϕ

The expectation value in (3.76) can be decomposed into products of two-point functions by using the Wick-theorem in Eq. (3.48):

$$\langle(\phi^2(X)-\phi^2(0))(\phi^2(X')-\phi^2(0'))\rangle = 2\left(\langle\phi(X)\phi(X')\rangle^2-\langle\phi(X)\phi(0')\rangle^2-\langle\phi(0)\phi(X')\rangle^2+\langle\phi(0)\phi(0')\rangle^2\right). \quad \text{(E.1)}$$

Here, $X, X', 0, 0'$ are used to denote $(\eta,\chi,\boldsymbol{\gamma})$, $(\eta',\chi',\boldsymbol{\gamma}')$, $(\eta,0,\gamma)$, and $(\eta',0,\gamma')$, respectively for clarity and simplicity of writing. Then, using the two-point correlation function given in Eq. (2.43) (c.f. Eq. (3.49)), one finds that Eq. (E.1) can be evaluated as

$$\begin{aligned}
&\langle(\phi^2(X)-\phi^2(0))(\phi^2(X')-\phi^2(0'))\rangle \\
&\quad= 2\varphi^2(\eta)\varphi^2(\eta')\left(\frac{\sinh^2(1-\epsilon)R}{(1-\epsilon)^2\sinh^2 R}-\frac{\sinh^2(1-\epsilon)R_1}{(1-\epsilon)^2\sinh^2 R_1}-\frac{\sinh^2(1-\epsilon)R_2}{(1-\epsilon)^2\sinh^2 R_2}+1\right) \\
&\quad= -4\varphi^2(\eta)\varphi^2(\eta')\left(R\coth R-R_1\coth R_1-R_2\coth R_2+1\right)\epsilon+\mathcal{O}(\epsilon^2) \\
&\quad\simeq -4\epsilon\times\varphi^2(\eta)\varphi^2(\eta')\left(\frac{1}{3}\left(R^2-R_1^2-R_2^2\right)+\frac{1}{45}\left(-R^4+R_1^4+R_2^4\right)+\mathcal{O}\left(R^6\right)\right),
\end{aligned} \quad \text{(E.2)}$$

where $R_i=\sqrt{-K}\chi_i$ for $i=1,2$. The schematic relation of R, R_1, and R_2 is presented in Fig. 2. In the expansion of $\coth(R_i)$, one understands that $R_1=\sqrt{-K}\chi_1\ll 1$ and $R_2=\sqrt{-K}\chi_2\ll 1$.

Using the relation of Eq. (2.44), one can verify the mathematical property of term in the bracket that

$$\begin{aligned}
&\frac{1}{3}\left(R^2-R_1^2-R_2^2\right)+\frac{1}{45}\left(-R^4+R_1^4+R_2^4\right) \\
&\simeq -\frac{2}{3}R_1R_2\left(1-\frac{2}{15}\left(R_1^2+R_2^2\right)\right)\cos\psi-\frac{2}{15}R_1^2R_2^2\left(\frac{3}{2}\cos^2\psi-\frac{1}{2}\right) \\
&\simeq -\frac{2}{3}R_1R_2\cos\psi-\frac{2}{15}R_1^2R_2^2\left(\frac{3}{2}\cos^2\psi-\frac{1}{2}\right).
\end{aligned} \quad \text{(E.3)}$$

Substituting Eqs. (E.2) and (E.3) into Eq. (3.76), Eq. (4.125) can be obtained.

F Frequently used abbreviations

Abbreviations	Full spellings
ALPs	**A**xion-**L**ike **P**articles
BAO	**B**aryon **A**coustic **O**scillations
CCP	**C**osmological **C**onstant **P**roblem
CDL	***C**oleman-**D**e **L**uccia*
CPL	***C**hevallier-**P**olarski-**L**inder*
CDM	**C**old **D**ark **M**atter
CMB	**C**osmic **M**icrowave **B**ackground
EoS	**E**quation **o**f **S**tate
EMT	**E**nergy-**M**omentum **T**ensor
FLRW	***F**riedmann-**L**emaitre-**R**obertson-**W**alker*
GR	**G**eneral **R**elativity
ISW effect	**I**ntegrated ***S**achs-**W**olfe effect*
LSS	**L**arge-**S**cale **S**tructure
RSD	**R**edshift **S**pace **D**istortions
ScmDE	**S**uper**c**urvature-**m**ode **D**ark **E**nergy
SPT	**S**tandard **P**erturbation **T**heory